
Unterschrift des Betreuers



TECHNISCHE
UNIVERSITÄT
WIEN
Vienna University of Technology

DIPLOMARBEIT

**HYPERSPECTRAL IMAGING OF HYPHAE AND SPORES
OF *PENICILLIUM CHRYSOGENUM* USING CONFOCAL
RAMAN (MICRO-)SPECTROSCOPY**

ausgeführt am

Institut für Chemische Technologien und Analytik

der Technischen Universität Wien

unter der Leitung von

Ao. Univ. Prof. Dr. Bernhard Lendl

und

Dipl. Ing. Cosima Koch

durch

Karin Wieland

Mörtelsdorf 87, A-5580 Tamsweg

Datum

Unterschrift (Student)

*”... par hasard, diriez-vous peut-être, mais souvenez-vous que dans les champs
de l’observation le hasard ne favorise que les esprits préparés.”*

*“... by chance, you might say, but remember that in the fields of observation chance only favors
the prepared minds.”*

(Louis Pasteur, Université de Lille 1854)

Content

| | | |
|---------|---------------------------------------------------------|----|
| I. | Abstract | 9 |
| II. | Zusammenfassung | 11 |
| III. | Acknowledgement | 13 |
| IV. | Introduction | 15 |
| IV.1. | Confocal Raman spectroscopy | 15 |
| IV.1.1. | Surface enhanced Raman spectroscopy (SERS) | 19 |
| IV.2. | Fluorescent stains | 25 |
| IV.2.1. | Fluorescein diacetate (FDA) | 27 |
| IV.2.2. | Propidium iodide (PI) | 28 |
| IV.2.3. | 4',6-diamidin-2-phenylindol (DAPI) | 29 |
| IV.3. | <i>Penicillium chrysogenum</i> | 31 |
| IV.4. | Chemometrics | 32 |
| IV.4.1. | Hierarchical cluster analysis (HCA) ²⁷ | 32 |
| IV.4.2. | Principal component analysis (PCA) ²⁷ | 33 |
| V. | Experimental | 35 |
| V.1. | Equipment | 35 |
| V.1.1. | Horiba Jobin-Yvon LabRAM 800HR | 35 |
| V.1.2. | Renishaw inVia Raman Microscope | 35 |
| V.1.3. | Thermo Scientific DXR Raman Microscope | 35 |
| V.2. | Set-up characterization | 35 |
| V.2.1. | Laser power | 35 |
| V.2.2. | Laser spot size ²⁹ | 37 |
| V.2.3. | Spatial resolution ²⁹ | 39 |
| V.3. | Sample preparation | 40 |
| V.4. | Data analysis | 40 |
| VI. | Hyphae of <i>P. chrysogenum</i> | 41 |
| VI.1. | Raman spectroscopy of fungal hyphae | 41 |

| | | |
|---------------|-------------------------------------------------------------------------------------------------|----|
| VI.2. | Device settings | 41 |
| VI.3. | First Raman mappings | 46 |
| VI.3.1. | Small scale mapping | 47 |
| VI.3.2. | Large scale mapping | 58 |
| VI.4. | Raman spectra of stained fungal hyphae | 69 |
| VI.4.1. | Fluorescein diacetate (FDA)..... | 69 |
| VI.4.2. | Propidium iodide (PI)..... | 71 |
| VI.4.3. | Fluorescein diacetate (FDA), propidium iodide (PI) and 4',6 diamidin-2-phenylindol (DAPI) | 72 |
| VI.5. | Conclusion | 74 |
| VII. | Spores of <i>P. chrysogenum</i> | 77 |
| VII.1. | Raman spectroscopy of fungal spores..... | 77 |
| VII.2. | Device settings..... | 78 |
| VII.2.1. | 532 nm Raman laser | 78 |
| VII.2.1.1. | Heat dissipation through aqueous environment..... | 80 |
| VII.2.1.2. | Change of sample carrier | 81 |
| VII.2.1.3. | Cryo-stage..... | 82 |
| VII.2.1.4. | Heat dissipation through reduction of laser power/ μm^2 | 86 |
| VII.2.1.4.1. | Change of objective | 86 |
| VII.2.1.4.2. | Laser pointer | 88 |
| VII.2.1.4.2.1 | Toluene reference spectra..... | 88 |
| VII.2.1.4.2.2 | Spore spectra | 89 |
| VII.2.2. | 633 nm Raman laser | 90 |
| VII.2.3. | 785 nm Raman laser | 91 |
| VII.3. | SERS of spores..... | 94 |
| VII.3.1. | SERS substrate and characterization..... | 95 |
| VII.3.2. | Device settings..... | 96 |
| VII.3.3. | First SERS mapping of a spore..... | 98 |

| | | |
|----------|-----------------------------------------------------------------------|-----|
| VII.3.4. | Reproducibility of the SERS signal..... | 99 |
| VII.3.5. | Dead/alive study | 101 |
| VII.4. | Dead/alive study with 785 nm laser | 105 |
| VII.5. | Discussion and conclusion..... | 109 |
| VIII. | Outlook..... | 111 |
| IX. | Appendix | 113 |
| IX.1. | Device settings..... | 113 |
| IX.2. | Phenylalanine metabolism in <i>P. chrysogenum</i> ⁶³ | 124 |
| IX.3. | Bibliography | 125 |
| IX.4. | List of Figures..... | 130 |
| IX.5. | List of Tables..... | 136 |

I. Abstract

In this thesis, appropriate device settings for the investigation of hyphae and spores of *Penicillium chrysogenum* using confocal Raman microspectroscopy were determined. Furthermore, the application of appropriate fluorescent dyes for life/dead staining as reference method was investigated in the context of a combined use of imaging by Raman and fluorescence spectroscopy.

For studying hyphal samples not more than 50 % of the maximum laser power of a 532 nm Raman laser (<52 mW) was applied under the condition that Raman spectroscopy remained a destruction-free method. Application of higher laser power increased the risk of sample destruction due to the thermal impact of the Raman laser. The majority of the measurements were performed with a 100x objective to cover as much detail of the sample as possible. Raman images up to a size of 105x124 μm^2 were recorded where each of the 13020 pixels of the image contained molecule specific information concerning the sample under investigation. Chemometric algorithms such as principal component analysis (PCA) and hierarchical cluster analysis (HCA) were used for data analysis. Based on these investigations differences in the chemical composition of the sample were identified such as an increased intensity of Raman bands characteristic for phenylalanine, proteins (amide I, amide III) and nucleic acids in the cytoplasm.

In this work, three different dyes (DAPI, PI and FDA) were investigated for life/dead staining. However, using fluorescent dyes as reference method got difficult once more than one fluorescent dye was used. Raman spectra of stained fungi could only be recorded as long as the excitation wavelength of the Raman laser is not within the absorption band of the fluorescent dye. In this specific work, bleaching was not a suitable option considering the desired work flow. An ideal procedure would consist of staining the sample, followed by subsequent investigation with Raman spectroscopy and as a third step a fluorescence image should be generated. Although DAPI would not interfere with the Raman spectrum, it turned out to be not very selective. PI used for dead cell staining was not compatible with Raman spectroscopy due to intense fluorescence at 532 nm excitation. FDA was used as life cell stain and showed most promising results in combination with Raman spectroscopy.

Spectroscopic investigation of spores of *P. chrysogenum* was more complex due to autofluorescence and extreme thermolability. Thus, alternative investigation methods such as SERS (surface enhanced Raman scattering) where silver nanoparticles (Leopold-Lendl method) were employed to enhance the Raman signal were applied. Another approach consisted of

replacing the visible Raman laser (532 nm) by a NIR laser source (785 nm). SERS spectra of spores as well as a mapping of a single spore were performed. Furthermore, a dead/alive study was performed using the NIR laser. In this study promising results for the differentiation between living and dead spores based on PCA were obtained.

II. Zusammenfassung

In dieser Arbeit wurden geeignete Messparameter zur Erforschung von Hyphen und Sporen von *Penicillium chrysogenum* mittels konfokaler Raman (Mikro-) Spektroskopie ermittelt. Des Weiteren galt es geeignete Fluoreszenzfarbstoffe zur Unterscheidung lebender und toter Bereiche in den Hyphen hinsichtlich ihrer Anwendbarkeit in Kombination mit Raman Spektroskopie zu untersuchen, um ein bildgebendes Analysenverfahren basierend auf Raman und Fluoreszenzspektroskopie zu entwickeln.

Damit Raman Spektroskopie eine zerstörungsfreie Methode bleibt, wurden die Hyphenproben mit maximal 50 % der Laserleistung des 532 nm Raman Lasers (<52 mW) analysiert, da eine höhere Leistung die biologische Probe aufgrund der thermischen Belastung zerstören würde. Der Großteil der Messungen wurde unter Verwendung eines 100x Objektivs durchgeführt, um möglichst viel an Detailinformation von den Proben zu erhalten. Es wurden Raman Bilder mit einer Größe von bis zu $105 \times 124 \mu\text{m}^2$ aufgenommen, wobei jedes der insgesamt 13020 Pixel, aus denen das Bild aufgebaut ist, molekulspezifische Information enthält. Zur Datenanalyse wurden chemometrische Verfahren wie die Hauptkomponentenanalyse oder die hierarchische Clusteranalyse verwendet. Mithilfe dieser Algorithmen konnten Unterschiede im chemischen Aufbau der Probe wie beispielsweise ein erhöhter Gehalt an Phenylalanin, Protein (Amid I-, Amid III- Bande) und Nukleinsäuren im Cytoplasma basierend auf den spektroskopischen Daten nachgewiesen werden.

Drei lebend/tot- Farbstoffe (DAPI, PI und FDA) wurden im Zuge dieser Arbeit hinsichtlich ihrer Anwendbarkeit in Kombination mit Raman Spektroskopie untersucht, um fluoreszenzspektroskopische Aufnahmen desselben Probenbereichs als Referenz für die Raman Bilder zu ermöglichen. Da jedoch nur jene Farbstoffe verwendbar sind, die keine Absorption im Bereich der Raman Anregungswellenlänge zeigen, wird das Auffinden von geeigneten Farbstoffen bei Verwendung von mehr als einem Farbstoff zunehmend zu einer Herausforderung. Ein idealer Analysenablauf besteht darin, dass zuerst die Probe mit den Fluoreszenzfarbstoffen angefärbt wird, bevor es zur Analyse mittels Raman kommt und anschließend ein Fluoreszenzbild aufgenommen wird. DAPI scheint dabei besonders vielversprechend im Bezug auf die Kombinierbarkeit mit Raman Spektroskopie unter Verwendung eines 532 nm Lasers, zeigte allerdings nur geringe Selektivität beim Färbeprozess. PI wurde zum Anfärben von toten Hyphenbereichen verwendet. Die Anregungswellenlänge des eingesetzten Raman Lasers liegt allerdings genau in der Absorptionsbande des Farbstoffs. Um lebende Bereiche in den Hyphen anzufärben, wurde FDA verwendet, welches einigermaßen

vielversprechende Ergebnisse zur Anwendung in Kombination mit Raman Spektroskopie lieferte.

Die spektroskopische Untersuchung von Sporen von *P. chrysogenum* erwies sich als sehr komplex, da diese Proben nicht nur intensive Autofluoreszenz zeigen, sondern auch extrem thermolabil sind. Um die Limitierung in der einstellbaren Laserleistung zu umgehen, wurden Sporenspektren mithilfe von SERS (Surface enhanced Raman Scattering) gemessen, wobei Nanopartikel aus Silber basierend auf der Leopold-Lendl Methode synthetisiert wurden. Ein weiterer Ansatz bestand darin, den Raman Laser, welcher im sichtbaren Bereich emittiert, durch eine NIR Lichtquelle zu ersetzen. Damit gelang es, sowohl einzelne Ramanspektren als auch Mappings von Sporen mit einem 785 nm Raman Laser aufzunehmen. Zusätzlich wurde eine lebend/tot Studie durchgeführt, welche soweit vielversprechende Ergebnisse in der Unterscheidung zwischen lebenden und toten Sporen mittels Hauptkomponentenanalyse lieferte.

III. Acknowledgement

First and foremost, I want to thank Bernhard Lendl and Christoph Herwig for giving me to opportunity to be part of this exciting project with people from different specializations sharing the same interest and motivation and working for a common goal. Especially, Bernhard Lendl broadened my horizon when I ran against a wall in the process of problem solving and always showed trust in my abilities. I have always appreciated his enthusiasm and wealth of ideas.

A big thank you goes to Cosima Koch who supervised this thesis for her ongoing patience, her support and professional advices, the discussion we had and tips she gave me for writing reports or making presentations.

I also want to thank Hans Lohninger (Epina Software Labs www.epina.at) for his support with ImageLab software used for the analysis of all the spectral data and for accommodating any wishes I had to adapt the software to my current needs. He always had an open door for me and provided me with useful tips concerning chemometric analysis.

Thank you to Daniela Ehgartner for the unbureaucratic cooperation, her support with the fluorescent stains and for providing samples of hyphae and spores of *P. chrysogenum* any time.

Furthermore, I want to thank Hinrich Grothe who provided and helped with the cryo-stage and the oil-sealed vacuum rotary vane pump used for performing spore measurements.

I also want to say thank you to my colleagues at the institute for interesting and helpful discussions. In particular, I have to thank Christoph Gasser and Johannes Ofner for providing me with their expertise about Raman spectroscopy. Thank you Johannes for taking the time to correct this thesis. Thank you Christoph for being a supportive friend and appreciated advisor in every work-related situation. I also want to thank Georg Ramer for his support with Python(x,y) which was used for data plotting.

Thermo Scientific and Martin Kraft (CTR Villach) each provided a spectrometer equipped with an NIR laser which allowed me to perform spore measurements without carbonizing them. Especially Martin De Biasio helped me with the measurements carried out with the InVia Renishaw spectrometer at the CTR in Villach. I want to thank all people involved for the pleasant cooperation.

Finally, I want to thank my family – my parents Johann and Anneliese, my grandmother Romana, my sister Sandra and my brothers Hannes and Martin – for always being there for me and supporting me throughout my student life. I especially want to thank my mother who was

always listening to me, mentally supported me and gave me some 'life-experience'-advices reminding me of taking things in life not too seriously.

Financial support was provided by the Christian Doppler Gesellschaft and the Austrian research funding association (FFG) under the scope of the COMET program within the research network "Process Analytical Chemistry (PAC)" (contract # 825340).

IV. Introduction

A central point in (bio-)process optimization is the need of an improved understanding of the biochemical process in the bioreactor. Knowledge of the morphology, such as the chemical composition of fungal hyphae, gives access to additional information about its current physiological state and thus enables the operators to optimize the product yield. In order to achieve a more efficient product cycle, finding the balance between product yield and the overall duration of the fermentation process is highly important. Not only can the bioreactor be operated at an optimal workload, the downstream processing can also profit from an improved process understanding in terms of undesired by-products that can either be avoided or significantly reduced during the fermentation process. Therefore, the downstream processing can be more efficient and economic as by-products require additional cleaning steps and increased caution is necessary to ensure the quality of the product.

Penicillium chrysogenum is a filamentous fungus producing the β -lactam antibiotic penicillin. In this work, a label-free imaging method based on Raman spectroscopy should be established in order to determine living and dead parts or productive and non-productive areas of the pellets (consisting of hyphae) in the bioreactor, respectively. Fluorescence microscopy should serve as reference method to verify and support the Raman imaging results. Therefore, not only appropriate device settings must be found, but also fluorescent dyes compatible for Raman spectroscopy. This part of the work was supported by Daniela Ehgartner (working group of Prof. Christoph Herwig at the Vienna University of Technology).

Since this project has gratefully been supported by Sandoz GmbH, the research work was strongly influenced by the interests of the company. Thus, the scope of the project shifted somewhat from hyphae to spores of *P. chrysogenum*.

IV.1. Confocal Raman spectroscopy

Raman spectroscopy is a form of vibrational spectroscopy where a sample is illuminated with a monochromatic light source (laser) and the inelastic scattered photons are measured. The inelastic scattered photons have energies different from the incoming light. These differences correspond to vibrational transitions in the sample and thus provide highly characteristic and molecule-specific information. The Raman effect was first discovered by Sir C. V. Raman in 1928. Two years later, he was honored with the Nobel Prize for Physics for his

discovery that the wavelength of inelastic scattered light may be different to the wavelength of the incident light.¹

When incoming radiation of a monochromatic light source hits the sample molecules are excited to a virtual energy state (figure 1 left). The majority of the photons are elastically scattered meaning that after scattering they have the same energy as the incoming light (i.e. Rayleigh scattering). Raman scattering, however, is referred to as inelastic scattering and occurs when a frequency shift happens between incoming and scattered photons. Only 1 in 10^6 - 10^8 incident photons will be scattered in form of Raman photons making Raman scattering a rather weak effect.² If the scattered photon has a lower energy compared to the incoming photon, we are talking about Stokes scattering. This scattering effect is also referred to as red shift due to the shift to a lower frequency range and thus to higher wavelengths (equation 1). An even rarer event is the anti-Stokes scattering (blue shift in the electromagnetic spectrum) where the scattered photon has higher energy (shift to higher frequencies) compared to the incoming photon.

The polarizability α is an important parameter for a molecule to evoke Raman scattering. A change in the polarizability of the molecule during excitation is the key property for a sample to be Raman active (equation 2). The Raman signal is thus directly proportional to the intensity of the incoming monochromatic light source as well as the polarizability α and indirectly proportional to the fourth power of the incoming light (equation 3).

$$E = h\nu = h \frac{c}{\lambda} \tag{equation 1}$$

$$\left(\frac{\partial\alpha}{\partial q}\right)_0 \neq 0 \tag{equation 2}$$

$$I_{Raman} \propto \alpha \left(\frac{1}{\lambda}\right)^4 I_0 \tag{equation 3}$$

If the energy of the incoming light corresponds to the energy difference between ground state and the first electronic state, fluorescence occurs as soon as the excited electrons fall back to the ground state and release the surplus of energy in the form of light. As the fluorescent signal is about six orders of magnitude more intense than the Raman signal³, it needs to be avoided for every Raman measurement. Otherwise, the weak Raman signal would be masked and hidden underneath fluorescence, preventing any access to the molecule-specific information.

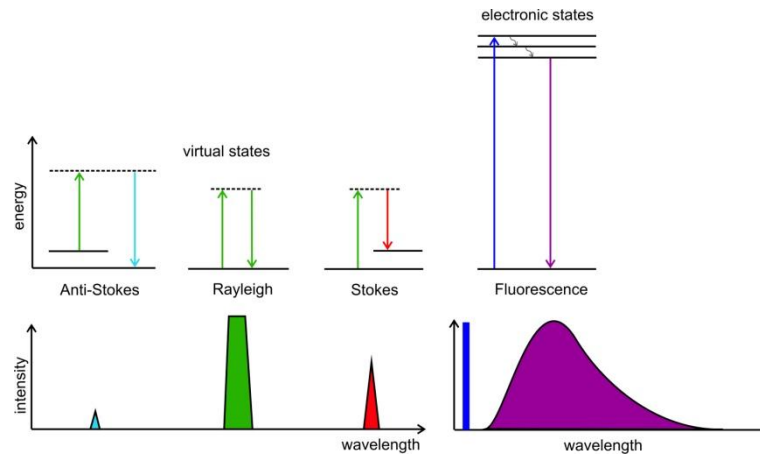


figure 1. Energy and intensity sketch of Rayleigh scattering, Raman (Stokes and anti-Stokes) scattering and fluorescence

Confocal Raman spectroscopy is a powerful tool to gather spectroscopic information from a defined sample area and basically is a confocal microscope combined with a Raman spectrometer. For Raman imaging, the microscope is equipped with an automated x,y-stage enabling step-wise scanning of a defined sample area. Each pixel of the recorded Raman image contains a Raman spectrum. Depending on the size of the confocal aperture, the Raman signal of defined sample layers can be selected depending on where the focus is set to in the z dimension (figure 2). Apart from enabling 3D imaging, a great advantage of the confocal system is the possibility of eliminating interfering fluorescent background and thus improving the quality of the Raman spectrum. Reducing the radius of the confocal pinhole only permits Raman photons from the analyte of interest (focused z-layer) passing through the hole to the detector while photons emitted from other sample layers are rejected.

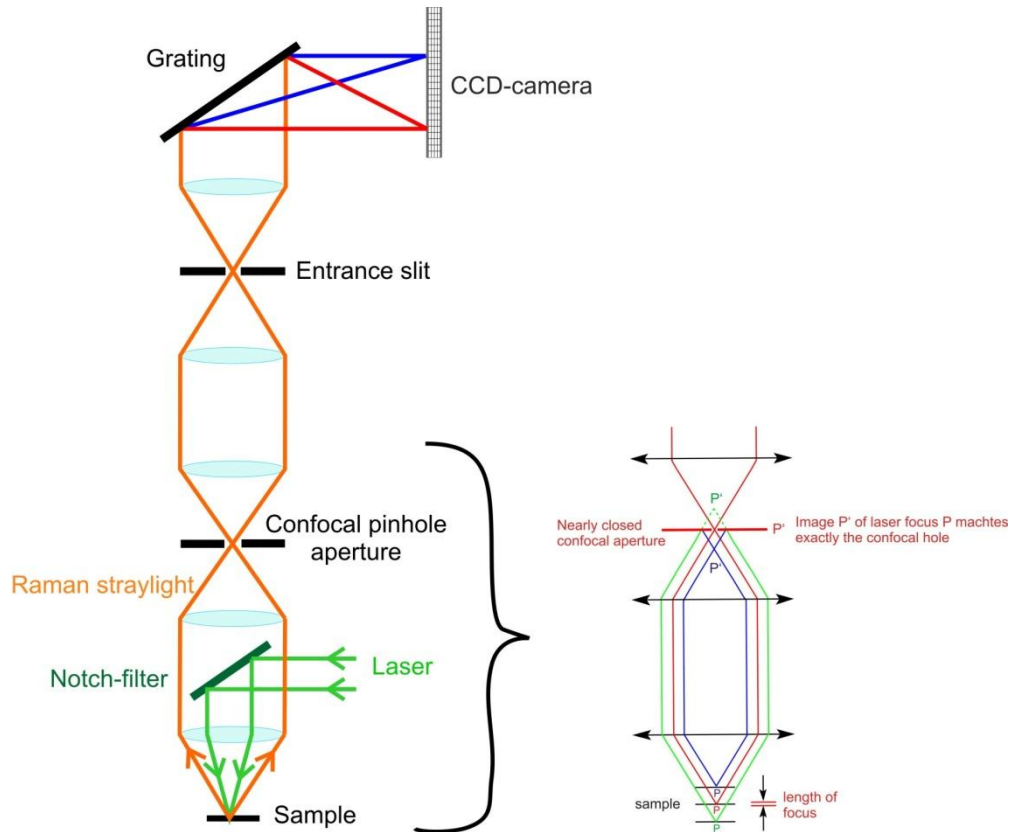


figure 2. Optical path of a confocal Raman spectroscopy set-up (Bernd Bleistein, Jobin Yvon)

A crucial parameter in confocal microscopy is the size of the pinhole as one has to find a compromise between maintaining the confocal image as well as signal intensity. Typically, pinhole sizes between 10 and 100 μm are chosen. According to a practical guide for confocal Raman imaging by WITec⁴, the optimal pinhole size can be calculated according to (equation 4). Using a 532 nm Raman laser in combination with a 100x objective (numerical aperture N.A.=0.9), the optimal pinhole size for $v_p=2.5$ would be 47 μm . However, the loss in intensity of the Raman signal is limiting a possible narrowing of the pinhole which would be required for gaining maximum resolution. With the detector radius v_p being 2.5, the depth resolution is not significantly changed and a collection efficiency of the detector of 75 % is achieved.

$$\frac{M \lambda v_{p_{max}}}{\pi NA} \geq d_0$$

M... magnification

d_0 ... diameter of the pinhole

NA... numerical aperture

v_p ... detector radius ($v_p=(2\pi/\lambda)r_p n \text{sinc}^5$)

λ ... wavelength of monochromatic light source

(equation 4)

IV.1.1. Surface enhanced Raman spectroscopy (SERS)

SERS is a very attractive tool for single molecule detection and a promising method to investigate the Raman spectrum of either very weak Raman scatterers or very thermolabile analytes. Especially biological samples such as spores of *P. chrysogenum* tend to suffer from extreme thermolability. Thus, the power of the Raman laser must be decreased leading to an even weaker Raman signal pushing the sensitivity of the CCD detector to its limit. However, the SERS technique enables signal enhancement by several orders of magnitude. In combination of SERS with resonance Raman scattering (SERRS) signal enhancement by a factor of up to 10^{14} can be achieved and thus can reveal the molecule-specific information which otherwise would be hidden from the spectroscopist's eye⁶.

As a SERS substrate is required for the signal enhancement one of the great advantages of Raman spectroscopy as a label-free method is lost while maintaining the advantage of gaining molecule-specific information. These substrates consist of conductive nanoparticles and are either commercially available or can be made in the laboratory. Very prominent are the SERS substrates prepared according to the Lee and Meisel method⁷ or the Leopold-Lendl method⁸. The nanoparticles should all be of the same size and shape as these properties influence the enhancement factor. Furthermore, the synthesis must be reproducible, making the preparation of the SERS substrate a very delicate process. The exact mechanism leading to this enhancement effect can be explained by two approaches (chemical and the electromagnetic mechanism) which should not be regarded separately as they interplay in creating the SERS signal.

Electromagnetic enhancement

The incident light beam hits a rough metal surface or small metal particles (mostly Au or Ag, sometimes Cu) to which analytes are adsorbed. The plasmons of the metal nanoparticle are excited under resonant conditions and begin to oscillate enhancing the electromagnetic field and therefore the Raman signal (figure 3). However, it needs to be considered that only those vibrations moving in the same direction as the field vector of the electromagnetic field points are enhanced. Furthermore, the signal decreases with increasing distance of the analyte from the surface to the power of twelve making SERS a very surface sensitive method. An even greater signal enhancement can be achieved in the region between two nanoparticles – the so-called hotspots. Consequently, when working with colloidal suspensions of SERS nanoparticles, controlled agglomeration of the particles is intended.

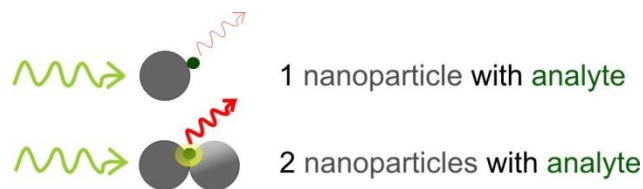


figure 3. SERS principle: additional signal enhancement in the hotspots between two nanoparticles

When an electromagnetic wave of a given frequency interacts with a metal surface, the valence electrons of the metal can be excited under resonant conditions. The resonance frequency of the resulting plasma oscillation ω_{\max} depends on the dielectric functions of the metal itself ($\epsilon_{\text{metal}}(\omega)$) and its surrounding medium ($\epsilon_{\text{m}}(\omega)$) as well as on the size and shape of the nanoparticle. The resonant excitation leads to a charge separation (figure 4) which is why this type of resonance is also called dipolar localized surface plasmon resonance (LSPR). The induced dipole of the nanoparticle μ_{ind} is given by the polarizability of the metal (α_{metal}) and the incident electric field strength ($E_0(\omega_{\text{inc}})$; see (equation 5)). Depending on the angular frequency of the incident electromagnetic wave ω_{inc} , the sign of μ_{ind} changes periodically. Based on this resonant light scattering off the metal nanoparticle an increased local electric field $E_{\text{loc}}(\omega_{\text{inc}})$ is achieved.

$$\mu_{\text{ind}} = \alpha_{\text{metal}} E_0(\omega_{\text{inc}}) \tag{equation 5}^9$$

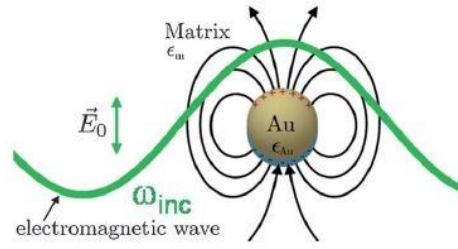


figure 4. Induced dipole of a metal nanoparticle (Au) by excitation of a dipolar localized surface plasmon resonance (LSPR)⁹

Similarly, the induced dipole in a molecule near the metal surface is given by the polarizability of the molecule and the local electric field $E_{loc}(\omega_{inc})$ (equation 6). In classical theory the molecule vibrating with ω_{vib} modulates the incident electric field, resulting in a dipole for each type of scattering: Rayleigh $\mu_{ind}(\omega_{inc})$, Stokes Raman $\mu_{ind}(\omega_{inc}-\omega_{vib})$ and anti-Stokes Raman $\mu_{ind}(\omega_{inc}+\omega_{vib})$.

$$\mu_{ind} = \alpha_{molecule} E_{loc}(\omega_{inc}) \quad \text{(equation 6)⁹$$

Considering the case of Raman scattering, the frequency shifted radiation ($\omega_{inc}-\omega_{vib}$) can also excite the LSPR of the metal nanoparticle resulting in an enhanced emitted radiation of the same frequency.

This means that an optimal SERS intensity based on electromagnetic enhancement does not only depend on the **incident field** being in resonance with the plasmon modes of the metal, but also on the **outgoing field** (figure 5). In other words, the SERS signal is given by the intensity of the incident electromagnetic wave and the intensity of the scattered Raman photons (equation 7).

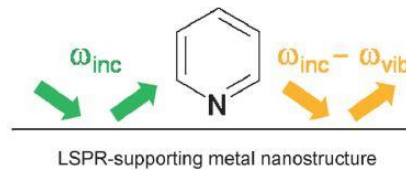


figure 5. Electrochemical enhancement of both fields: incident field ω_{inc} and outgoing field ($\omega_{inc}-\omega_{vib}$); pyridine as example molecule⁹

$$I_{SERS} = I_{inc}(\omega_{inc}) * I(\omega_{inc} - \omega_{vib}) = |E_{inc}(\omega_{inc})|^2 * |E(\omega_{inc} - \omega_{vib})|^2 \quad \text{(equation 7)}$$

IV. Introduction - IV.1. Confocal Raman spectroscopy

For $\omega_{inc} \gg \omega_{vib}$ the intensity of the SERS signal can be described by the widely used approximation of the signal being proportional to the electric field strength to the power of four (equation 8).

$$I_{SERS} \approx |E(\omega_{inc})|^4 \quad \text{(equation 8)}$$

Since the electric field is inversely proportional to r^3 (radial distance; see

(equation 9) and the intensity of the SERS signal is proportional to E^4 , the SERS signal is proportional to r^{-12} . This means that the signal rapidly decreases with increasing distance between molecule and metal nanoparticle. Thus, SERS is a very surface sensitive method.

$$E = \frac{1}{4\pi\epsilon_{metal}} \frac{qs}{r^3}$$

q... charge

s... distance between the two charges of the dipole

r... distance from surface of the nanoparticle to the molecule

ϵ_{metal} ... dielectric constant of nanoparticle

(equation 9)

The reason for silver and gold being the most prominently used metals for SERS is that their resonance falls into the visible region of the electromagnetic spectrum. Moreover, they are both inert and available in a wide range of sizes and shapes. Also, sample preparation and conjunction to ligands is easy manageable with silver and gold nanoparticles.¹⁰

The Drude model describes the valence electrons of metals as a cloud where the electrons move linearly and they only interact through elastic collisions. Based on the lossless Drude model the dielectric function of a metal can be evaluated (equation 10). The dielectric function consists of a real and an imaginary part which is displayed for Ag and Au in figure 6. It can be seen that both metals behave similarly for $\lambda \geq 600$ nm. As bulk metals are not lossless, the imaginary part of $\epsilon(\lambda)$ which is always related to absorption gets important. $\text{Im}[\epsilon(\lambda)] = 0$ means that the metal shows no absorption at this particular wavelength.

$$\epsilon = \epsilon_{\infty} \left(1 - \frac{\omega_p^2}{\omega^2} \right) = \epsilon_{\infty} \left(1 - \frac{\lambda^2}{\lambda_p^2} \right) \text{ with plasma frequency } \omega_p = \frac{2\pi c}{\lambda_p} \quad \text{(equation 10)}$$

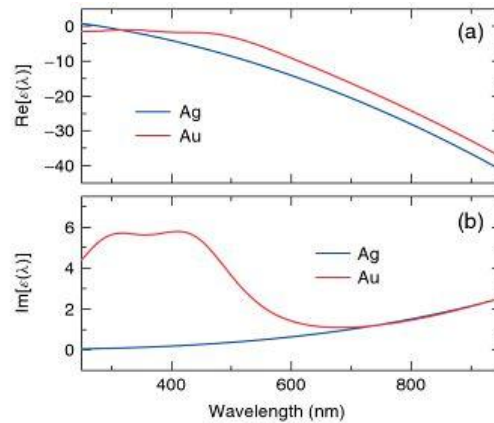


figure 6. Real and imaginary part of $\epsilon(\lambda)$ of Ag and Au¹¹

With increasing size of the nanoparticles the localized surface plasmon resonance is shifted to higher wavelengths (red shift). Also, plasmon resonances are damped and broadened. Moreover, additional resonances that do not appear in small scale particles have to be considered. In addition to the size, the shape of the nanoparticles has an effect on the resulting enhancement factor. Different shape can lead to different points on the surface where the maximum enhancement occurs at different wavelengths. Moreover, the enhancement factor can be particularly high at certain surface areas. It also needs to be considered that resonances depend on the orientation with respect to the direction of the electric field.

Gaps between nanoparticles cause a red shift of the resonance with decreasing distance between the particles (figure 7). Due to the coupled plasmon resonances the enhancement factor increases. For a very narrow distance between particles (hot spots), signal enhancement is high enough for single molecule detection. The local field intensity enhancement factor (LFIEF) as a function of θ is shown in figure 8 and indicates a drastic decrease in enhancement activity for small changes of θ towards higher angles.

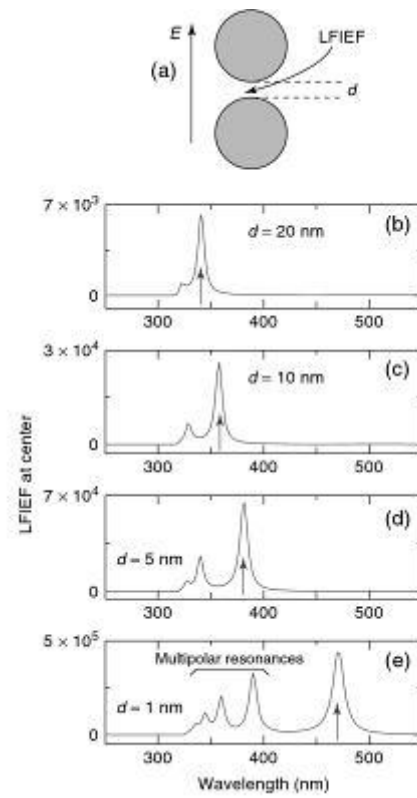


figure 7. Effect of a decreasing gap between two nanoparticles on the plasmon resonance and the enhancement factor¹¹

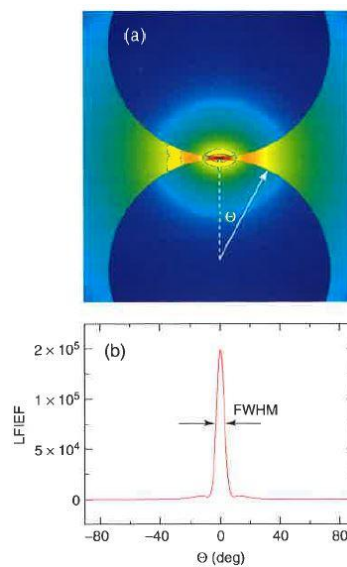


figure 8. Intensity distribution of the enhancement factor (a) and LIEF as a function of θ (b)¹¹

Chemical enhancement

This contribution to the SERS effect is not very well understood so far. However, the key message of various scientific investigations might be summarized as followed: Due to chemisorption and the formation of a surface complex between sample and metal, the electronic structure of the substrate is disturbed leading to charge- transfer resonances as well as enhancement based on molecular excitation resonances. Also changes in the molecular polarizability are possible leading to changes in vibrational modes upon binding to the metal surface.¹²

IV.2. Fluorescent stains

Fluorescent stains have the advantage of giving a very intense signal. Additionally, there is a great variety of stains commercially available for live/dead-analysis. However, not all stains are specific enough for very special requirements. In particular, common stains are almost exclusively developed for bacteria and very often adapted to defined biological compartments of *E. coli*. This means that besides of being expensive, the staining procedure first needs to be adapted to the organism of interest (i.e. *P. chrysogenum*) in order to be applicable for our purpose. As the staining method should not interfere with Raman measurements, the choice of fluorescent dyes is further limited. The most critical issue to be considered is the fact that a stain being fluorescent during Raman measurements will render this useless as the fluorescence will completely mask the weak Raman signal. In order to perform Raman measurements with stained samples, the fluorescent stain might need to be bleached before the measurement or the wavelength of the Raman laser must be chosen such that no fluorescence is produced at this particular wavelength. This latter condition will definitely limit the number of possible stains for successful fluorescence and Raman imaging.

In order to obtain a representative image of the current situation in the bioreactor, the measurement procedure must be as follows: First, the sample is stained immediately after being taken from the bioreactor in order to capture an accurate image of the current situation in the bioreactor. After incubation time, the sample is washed again to remove the stain being present in surplus in the surrounding medium. At this point, the living and dead parts of the sample are stained with two different dyes. Then, the sample is prepared for the Raman measurement to make sure that the analyte is still in the same physiological state during the Raman imaging as in the bioreactor. Afterwards, the fluorescence microscopy can be performed with the same sample. Reversing the last two steps (Raman imaging and fluorescence microscopy) cannot be

recommended as the sample on the sample carrier is exposed to different environmental conditions compared to the ones in the bioreactor and will change its physical and therefore also its chemical composition. The sooner the Raman measurement can be performed, the more representative will be the information that can be extracted from the spectra. Staining the sample first is also a requirement as only by this step the physiological state of the sample in the bioreactor can be captured. Staining the sample after the Raman measurement would probably falsify the analysis as the sample can also be affected by the Raman laser. Additionally, during sample preparation for Raman measurements the sample is washed (and sometimes must be diluted) with deionized water to remove medium components that would interfere with the Raman signal of the analyte. During this washing step, the PBS buffer is removed, destroying the pH-conditions adapted for the sample. So, it is most likely that the fungus is slowly dying on the microscope slide which explains why a fast analysis is required.

An established protocol for tissue investigations is following a dual measurement concept. First, the sample is cut into layers, then one layer is stained with fluorescent dyes while a second one is analyzed with Raman spectroscopy. Due to large sample size it is possible to project the fluorescence results of one layer to the second layer analyzed by Raman imaging. Unfortunately, having a diameter of a few micrometers, this procedure is not suitable for fungal hyphae as the layer cannot be cut thin enough to avoid significant changes between single layers. Thus, an overlay of two layers (one being investigated with the Raman spectrometer, the other one being analyzed with fluorescence microscopy) would not show the same image.

According to Krause et al¹³, Raman microscopy of fluorescence labeled microorganisms is possible if the fluorescent dyes are sufficiently bleached before the measurement or the excitation wavelength of the laser is outside of the absorption band of the dye. Here, bleaching the fluorescent dye is not an option because the fluorescence needs to be measured after Raman imaging has been performed. Staining the sample subsequent to the Raman measurement is not an option either, as an overlay between identical Raman and fluorescence image areas would not be possible. This means, that we have to add an additional feature to the list of requirements for the fluorescent stains. Besides of being highly specific, the Raman laser line must not be within the absorption band of the fluorescent dye.

Krause et al¹³ used a dead/live staining kit containing Syto 9 and PI as fluorochromes for staining bacterial cells. According to their work, Syto 9 can be used for Raman microscopy using a laser excitation wavelength of 532 nm while PI affects the Raman spectrum by masking the Raman signal due to its fluorescence. However, Syto 9 was not suitable for fungal stain

according to Daniela Ehgartner. As described in “The Molecular Probes® Handbook”¹⁴, the affinity of Syto Nucleic Acid Stains is moderate and can be displaced by higher – affinity nucleic acid stains such as SYTOX Green, PI, etc. Nonetheless, a combination of Syto with a red fluorescent high-affinity nucleic acid stain such as PI or TOTO3 is quite common.

Amongst several fluorescent stains that were investigated by Daniela Ehgartner during her PhD thesis regarding their suitability for performing reproducible and representative fluorescence microscopy, she decided on using fluorescein diacetate (FDA), propidium iodide (PI) and 4',6-diamidin-2-phenylindol (DAPI) for further experiments.

IV.2.1. Fluorescein diacetate (FDA)

FDA is used to stain living fungal parts. It penetrates through the cell's membrane and intercalates into the DNA. Due to esterase activity, the acetate groups get split off by hydrolyzation and the green fluorescent stain fluorescein remains (figure 9). However, according to “The Molecular Probes Handbook”¹⁴ FDA rapidly leaks from cells.

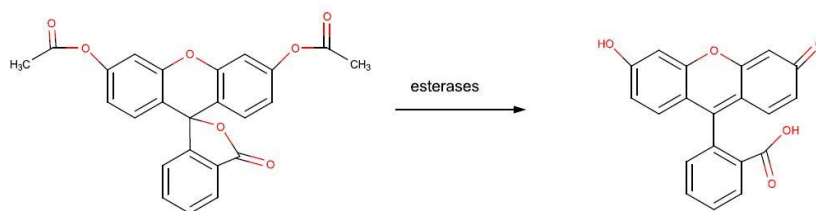


figure 9. Hydrolyzation of FDA to fluorescein in the presence of esterases¹⁵

0.5 mg FDA were dissolved in 1 ml acetone and put onto a CaF₂ sample carrier (figure 10) for reference measurements which were performed using three different Raman laser lines: 532 nm, 633 nm and 780 nm. No Raman signal of the fluorescent dye could be obtained with the NIR-laser (near infrared). While the Raman spectrum recorded with the 532 nm laser is very much masked by fluorescence as can be seen by the high baseline, the Raman spectrum recorded with an excitation wavelength of 633 nm is very well resolved (figure 11). Using the 633 nm laser (marked with a little star * in figure 11), the fluorescent stain does not get excited any more by the laser beam. Consequently, the measurement does not contain any fluorescence which would mask weak Raman signals.

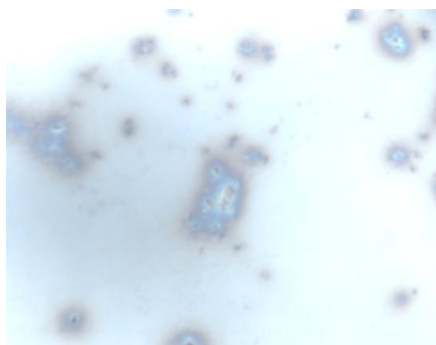


figure 10. FDA dissolved in acetone on CaF_2

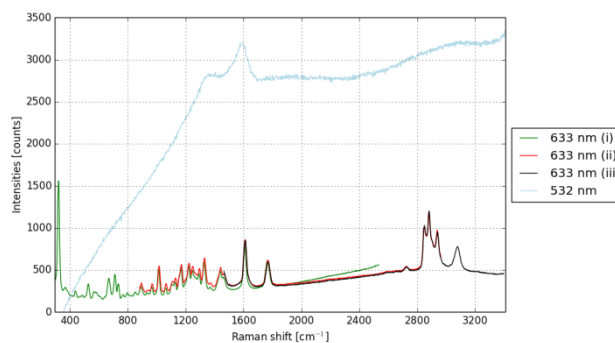


figure 11. Raman spectrum of FDA recorded with the 532 nm laser (blue spectrum) and the 633 nm laser (green, red and black spectrum, each recorded at a different spectrograph position: (i) 1500 cm^{-1} (ii) 2000 cm^{-1} (iii) 2500 cm^{-1})

The excitation/emission spectrum of FDA (figure 12) already suggests that the Raman spectrum recorded with the green laser (532 nm) might be influenced by fluorescence. Even though this laser line is at the very edge of the absorption band of FDA where the absorption is very low compared to the absorption maximum, the resulting fluorescence has a significant impact on the Raman spectrum.

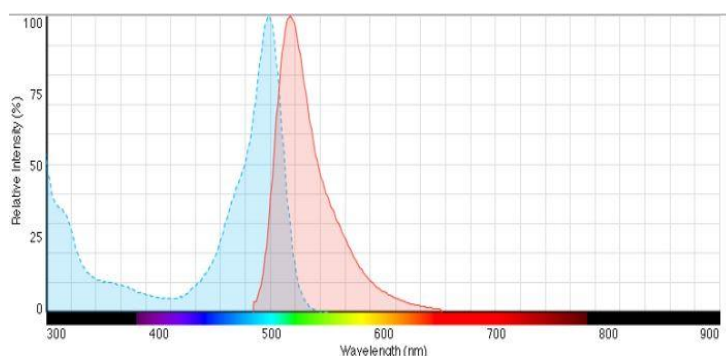


figure 12. Excitation/Emission spectrum of FDA¹⁶

IV.2.2. Propidium iodide (PI)

The fluorescent dye PI (figure 13) can only enter the cell through compromised membranes and thus exclusively stains dead cells resulting in a red fluorescent signal.¹⁴ Measurements with the green Raman laser (532 nm) are not possible as this laser line perfectly lies within the maximum of the absorption band of propidium iodide (PI; figure 14). Also, the 633 nm laser would lead to fluorescence. Therefore, Raman spectra of 2 mM PI (dissolved in PBS buffer on a microscope glass slide; figure 15) were recorded using a NIR-Raman laser (

figure 16; 780 nm; device settings see appendix). However, the Raman spectra still show a very high baseline, i.e. fluorescence, and only a weak Raman signal can be seen in the spectral region between 1200 cm^{-1} and 1500 cm^{-1} Raman shift.

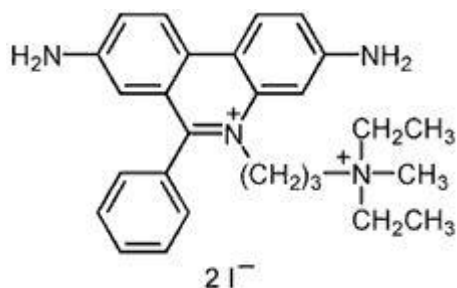


figure 13. Chemical structure of PI¹⁷

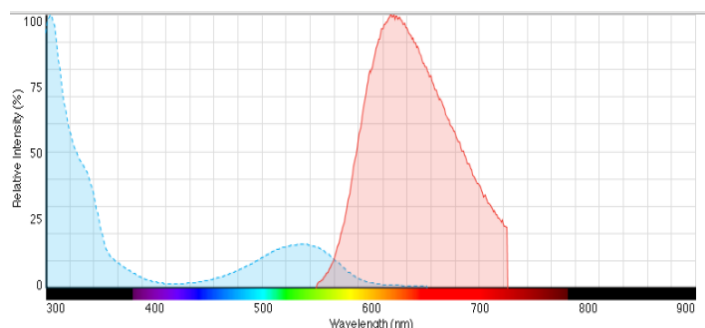


figure 14. Excitation/Emission spectrum of PI¹⁸

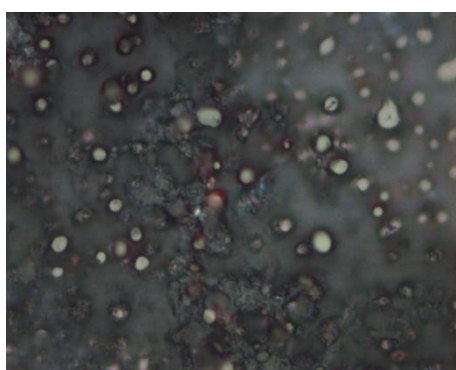


figure 15. PI (2 mM) dissolved in PBS buffer

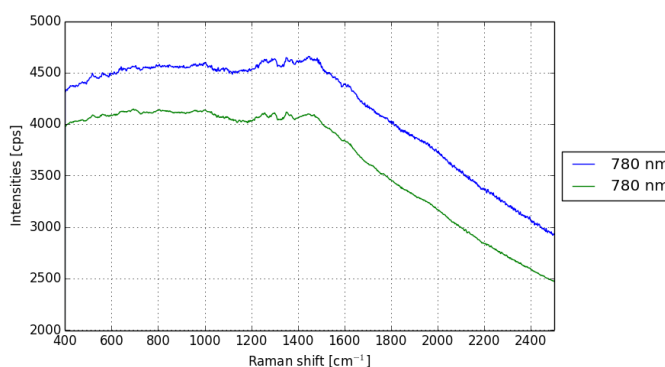


figure 16. Raman spectrum of PI recorded with the 780 nm Raman laser

IV.2.3. 4',6-diamidin-2-phenylindol (DAPI)

4',6-diamidino-2-phenylindole (DAPI) is an AT-selective (adenine-thymine selective) fluorescent dye being semitransparent to live cells and emitting blue light and was used as control for PI. DAPI (figure 18) is used as nuclear counterstain. Due to its high selectivity to double stranded DNA, background staining of the cytoplasm is widely eliminated. However, it is suspected that DAPI sometimes stains all the fungi and not just the dead parts. The maximum of its absorption band is at 358 nm. DAPI should neither be excited by the 532 nm-laser nor by the 633 nm-laser as both wavelengths are outside of the absorption band of the fluorescent dye (figure 17).

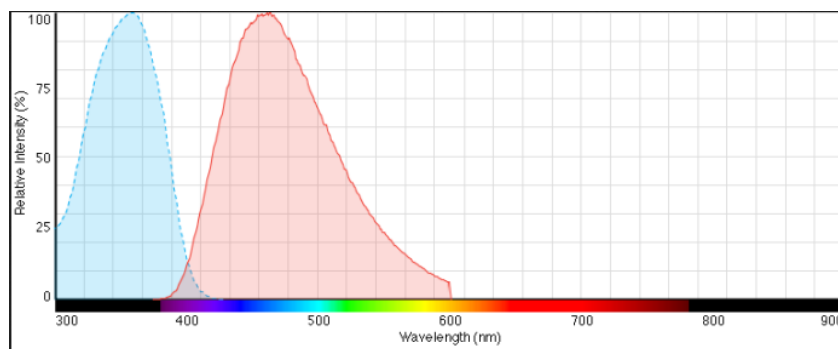


figure 17. Excitation/Emission spectrum of DAPI bound to DNA¹⁹

One droplet of DAPI was put onto a CaF_2 window and dried at room temperature (figure 19) for Raman measurements.¹⁴

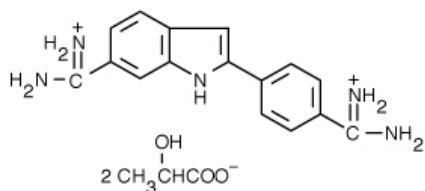


figure 18. Chemical structure of 4',6-diamidino-2-phenylindole (DAPI)²⁰

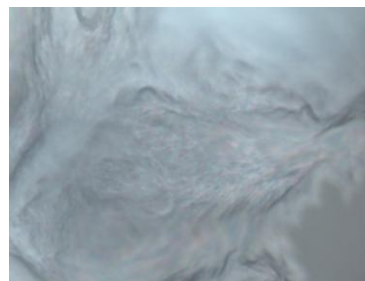


figure 19. DAPI dried on CaF_2

Raman spectra were recorded using two different excitation laser lines: 532 nm as well as 633 nm where three different spectrograph settings (1500 cm^{-1} , 2000 cm^{-1} , 2500 cm^{-1}) were used (figure 20).

The baseline of the spectra recorded with the 633 nm laser (figure 21) is significantly lower than the one of the spectrum recorded using the 532 nm laser line. Nevertheless, Raman signals of both spectra match in great parts. According to the excitation and emission spectrum (figure 17) neither the 532 nm nor the 633 nm Raman laser should excite the fluorescent dye. Apparently, the 532 nm laser still evokes some fluorescence even if it is far away from the spectral region where DAPI absorbs. Still, it needs to be considered that the Ex/Em spectrum in figure 17 represents DAPI bound to dsDNA while in our case DAPI was measured without having been in contact with any biological material.

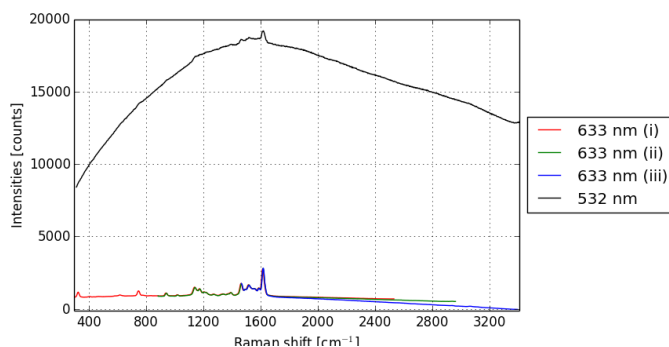


figure 20. Raman spectra of DAPI recorded with the 532 nm laser and the 633 nm- laser (spectrograph position: (i) 1500 cm^{-1} (ii) 2000 cm^{-1} (iii) 2500 cm^{-1})

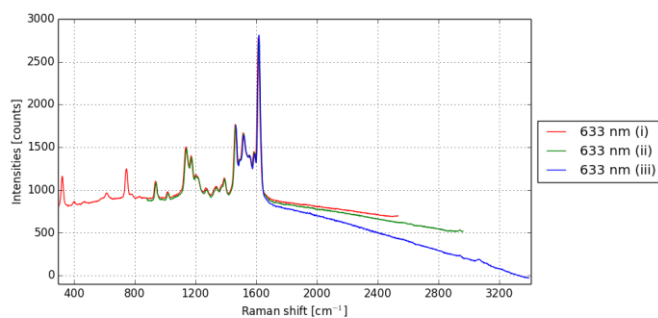


figure 21. Raman spectra of DAPI with the 633 nm laser at three different spectrograph positions: (i) 1500 cm^{-1} (ii) 2000 cm^{-1} (iii) 2500 cm^{-1})

IV.3. *Penicillium chrysogenum*

Mould is ubiquitous, being present in soil, air and water and it is very well adapted to the encountered environmental conditions. *Penicillium chrysogenum* is a filamentous fungus and is accounted amongst mould of the genus Ascomycetes.²¹ It is very popular in biotechnology for its ability to produce the β -lactam antibiotic penicillin. Therefore, pharmaceutical companies are very interested in providing optimal growth and production conditions for this fungus.

P. chrysogenum was discovered by the Scottish microbiologist Alexander Fleming in 1928 as he neglected to clean his lab bench before leaving for the weekend. Thanks to this lucky coincidence, the source of the first antibiotic (penicillin) working against gram-positive bacteria was found. This discovery saved many people's lives already in WWII²² and its use was extended throughout the whole world for the benefit of mankind in the following years. Today, penicillin still is a key drug to fight bacterial infections and is as such of strategic interest in our modern society. Back in 1929, A. Fleming published his discovery where he describes the fungus as '...white fluffy mass which rapidly increase in size and after a few days sporulates, the centre becoming dark green...'²³. In this article, the antibiotic penicillin also got its name assigned.

There is still a lot of microbiological work going on about the original strain used by A. Fleming.²⁴ Several different names such as *P. notatum* or *P. rubens* are mentioned in this context all having very similar properties only differing in tiniest details resulting in listing '*P. chrysogenum*' as *nomen conservandum* by the Committee for Fungi and Lichens.

For a very long time, the species was only known to reproduce asexually. However, also sexual reproduction is possible, a fact which is of great importance for new strain development approaches.²⁵ The spores (conidia) of *P. chrysogenum* are of a few micrometers in diameter, green-colored and turned out to be extremely thermolabile. The hyphae, however, are white and suffer less from thermal degradation. Investigations of the cell wall showed that the morphological differences between spores and hyphae are also reflected in their chemical composition such as differing amounts of carbohydrates and amino acids. Apparently, conidial walls contain more galactose while hyphal walls have a higher amount of glucosamine. Furthermore, some amino acids (glycine, arginine, lysine, threonine) are present in hyphal walls but are absent in spore walls. In general, the amount of amino acids in hyphal walls is smaller than in conidial ones.²⁶

IV.4. Chemometrics

Two non-supervised classification algorithms were applied to the data sets of spores and hyphae of *P. chrysogenum* for detailed analysis: hierarchical cluster analysis (HCA) and principal component analysis (PCA).

IV.4.1. Hierarchical cluster analysis (HCA)²⁷

HCA is a very powerful tool to highlight similarities in the data set. The data points are transformed into a matrix. Each spectrum is described as a vector. First, the distances between each and every data point is calculated applying an appropriate algorithm. Then, the two closest spectra are detected (smallest distance value) and merged to one point, leaving $n-1$ data points which are used in the next step to calculate again the distances between data points. This means that in each step, the complexity of the data set is reduced by replacing the two spectra showing highest similarity with the according average spectrum. Groups of clusters are iteratively formed according to the calculated distance values. The result is then visualized in the form of a dendrogram. Several different methods and algorithms can be applied for calculating the distance of two spectra. In this thesis, data analysis was performed with the Euclidean distance measure²⁸ (equation 11) and Ward's algorithm.

$$d_{jk} = \sqrt{\sum_{i=1}^n (x_{ij} - x_{ki})^2} \quad \text{(equation 11)}$$

IV.4.2. Principal component analysis (PCA)²⁷

PCA is a method to reduce a multidimensional space to a few new dimensions while maintaining the relevant variance in the dataset. It is frequently used to simplify the analysis and to help clarify correlations that could not be seen before. The underlying principle is rather simple. The direction in space showing the greatest variance is chosen as the first axis (the first principle component) of a new coordinate system. Then, the second principal component (second axis of the new coordinate system) is chosen by rotating the original data set perpendicular to the first axis. The second axis of the new coordinate system is again the one covering the greatest variance when rotating around the first axis. This principle can be continued until all dimensions have been used. However, the most relevant information will be concentrated in the first few principle components. By focusing on them, data analysis can be significantly simplified.

The principle of PCA can be nicely explained with a three dimensional data set representing the form of a banana (figure 22 [a]). The first principal component is shown in red, indicating the direction of the greatest variance of the data set. The second principal component is evaluated by looking for the direction showing greatest variance when rotating the data set perpendicular to the first axis (red line in figure 22 [b]). The second principal component is indicated in green (figure 22 [c]). The same procedure is repeated for the third component (figure 22 [d]). Now the data set can be projected into the new coordinate system with the principal components as the new coordinate axis. The new coordinate system may finally be compared with the old cartesian coordinate system (figure 22 [e]). This example can be easily understood with a three-dimensional data set, however, our imagination capabilities are soon limited once the data-set is exceeding those three dimensions. Therefore, PCA is a valuable tool to reduce the number of dimensions and helps focusing on the parameters having the most influence on the data set (i.e. causing greatest variance).

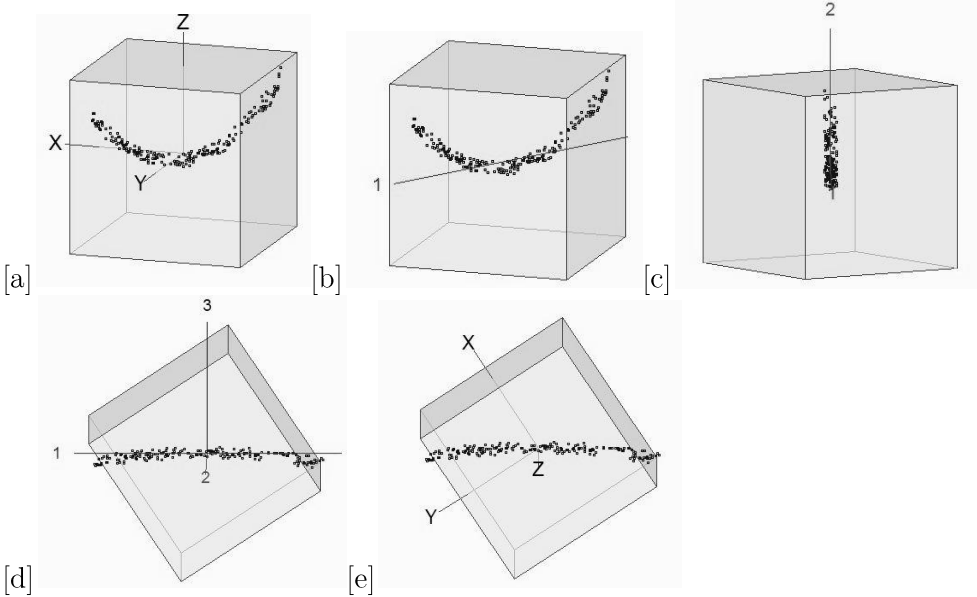


figure 22. Sketch showing the principle of PCA

V. Experimental

V.1. Equipment

Raman experiments were performed using different Raman spectrometers.

V.1.1. Horiba Jobin-Yvon LabRAM 800HR

This spectrometer is equipped with a Synapse Open-Electrode-CCD camera, a motorized xyz-stage, a digital camera and an external frequency-doubled Nd:YAG laser (Oxxius LMX-532, maximum power output <52 mW) for Raman excitation at 532nm. Furthermore, the software version of the LabSpec package was version 6. The spectrometer is further equipped with an internal 633 nm HeNe- laser (maximum power output <20 mW), a 300 lines/mm grating and a 1800 lines/mm grating.

V.1.2. Renishaw inVia Raman Microscope

Measurements were performed with this spectrometer at the Carinthian Tech Research in Villach supported by Martin De Biasio and Martin Kraft. It is equipped with three different lasers (532 nm, 633 nm and 785 nm) and two gratings (1200 lines/mm grating used in combination with the 785 nm laser; 1800 lines/mm grating used in combination with the 532 nm and 633 nm laser).

V.1.3. Thermo Scientific DXR Raman Microscope

This Raman spectrometer was gratefully provided by Thermo Fisher Scientific as a testing device for one week. It was equipped with a 900 lines/mm grating used in combination with the 532 nm laser and a 400 lines/mm grating used with the 780 nm laser.

V.2. Set-up characterization

V.2.1. Laser power

Most of the experiments were carried out with a recently updated system (Horiba Jobin-Yvon LabRAM 800HR) which thus had to be characterized prior to any sample measurements. A very important parameter for destruction-free analysis is the laser power that actually hits the sample. Therefore, power loss through the optical path as well as the objective that is used to focus the laser light onto the sample need to be considered. The power of the 532 nm- laser was

V. Experimental - V.2. Set-up characterization

measured using the laser power detector UP19K-15S-VR (gentec-eo). Measurements were conducted with the 10x objective varying the laser power from 10 % to 100 %. According to the Oxsius test report, the laser should have a CW power output of 51.9mW. Thus, even without considering optical losses, the laser power below 1 % could not be detected due to the power noise level of 2 mW although lower laser powers of 1 %, 0.1 % and 0.01 % are adjustable with the operating software. Consequently, data was only collected for 10 %, 25 %, 50 % and 100 % laser power. 20 single measurements were taken every second and statistically evaluated by the Gentec SOLO 2 Power Monitor. For each laser power set through Labspec 6 software at least 12 measurements were collected. Therefore, each power value in table 1 represents the average of the averaged values of each of the 12 measurements including the according standard deviation $s(x)$.

table 1. Measured average laser power at 10 %, 25 %, 50 % and 100 % laser power set with Labspec 6 software

| Set laserpower [%], (theoretical power value) | Measured laserpower [mW] | $s(x)$ [mW] | Power loss from laser to sample [%] |
|--------------------------------------------------|-----------------------------|-------------|----------------------------------------|
| 10 (5.19 mW) | 3.4 | 0.34 | 35 |
| 25 (12.98 mW) | 6.0 | 0.39 | 54 |
| 50 (25.95 mW) | 11.1 | 0.58 | 57 |
| 100 (51.90 mW) | 20.9 | 1.26 | 60 |

Although there is a great loss in laser power through the optical path of the laser beam from the source to the sample, there is a linear correlation between the set and the measured laser power (figure 23). The set laser power was calculated from the Oxsius test report and the percentage of laser power adjusted through Labspec 6 software. This means that the set laser power is the maximum laser power reachable at the sample spot without any power losses on the way through the optical setup.

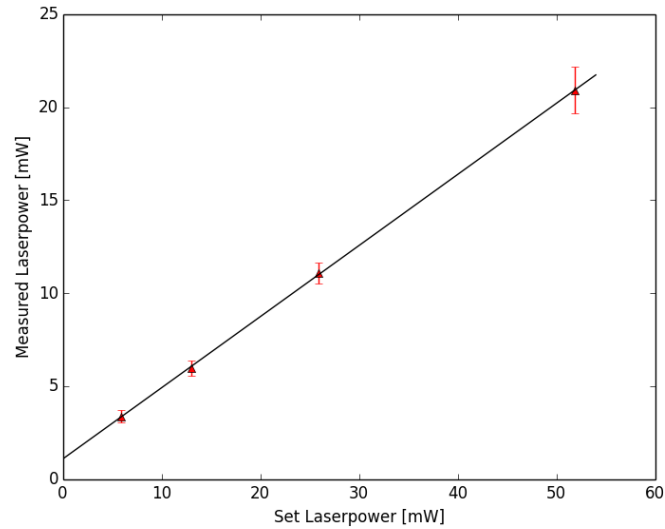


figure 23. Correlation between set and measured laser power (532 nm- laser)

V.2.2. Laser spot size²⁹

The laser power measured with the powermeter gets focused onto the sample through the objective. Depending on the magnification, the laser spot size varies and thus the laser power per area that hits the sample. The size of the laser spot can be approximated with an airy disk. The diameter of the airy disk depends on the numerical aperture (N.A.) of the objective and the wavelength of the Raman laser (equation 12). The laser spot size of the 532 nm Raman laser was calculated for different magnifications (table 2).

$$d = 1.22 \frac{\lambda}{N.A.} \quad (\text{equation 12})$$

table 2. Laser spot size of the 532 nm Raman laser using different magnifications

| Objective | N.A. | d [μm] | Laser spot size [μm^2] |
|-----------|------|---------------------|-------------------------------------|
| 100 | 0.90 | 0.72 | 0.41 |
| 50 | 0.75 | 0.87 | 0.59 |
| 20 | 0.35 | 1.86 | 2.70 |
| 10 | 0.25 | 2.60 | 5.30 |

This means that using the 10x objective with 100 % set laser power the sample is exposed to $3.95 \text{ mW}/\mu\text{m}^2$ laser power when using the 532 nm laser line. Changing the objective to a 100x magnification increases the laser power per area by a factor of 13 ($51.02 \text{ mW}/\mu\text{m}^2$) since the laser spot size significantly decreases. Depending on the degree of magnification, a different number of lenses are installed in the according objective resulting in a different light

V. Experimental - V.2. Set-up characterization

transmission specification. Having a look at the transmittance curves reflecting the percentage of light passing the objective lenses, the transmittance at 532 nm can be determined for each objective. Knowing the laser power at the sample surface with the 10x objective (measured with the powermeter), the laser power can be calculated for the other objectives

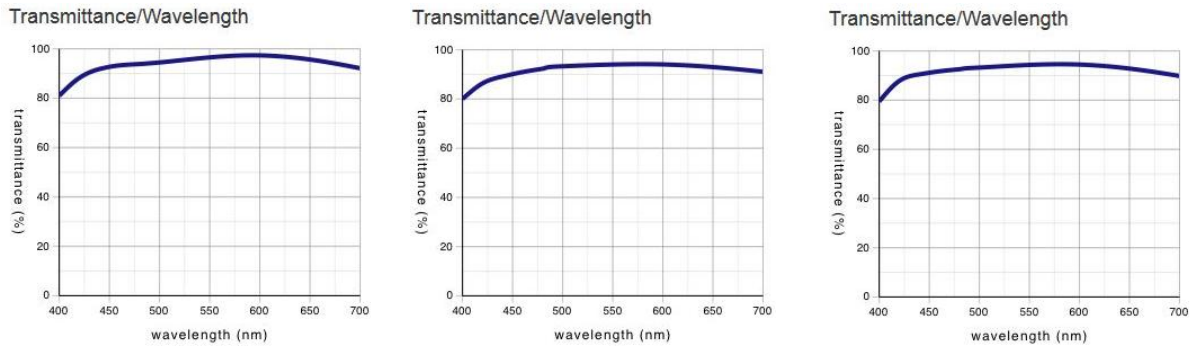


figure 24. Transmittance curves of Olympus objectives (left: 10x; middle: 50x, right: 100x magnification)³⁰

table 3. Transmittance values for the Olympus objectives at 532 nm deduced from figure 24

| Objective | Transmittance at 532 nm [%] | Factor |
|-----------|-----------------------------|--------|
| 10x | 95 | 1.0000 |
| 50 | 93 | 0.9789 |
| 100 | 93 | 0.9789 |

The laser power per area and thus the thermal stress the sample is exposed to can now be calculated for the Olympus objectives with three different magnifications (table 4). Taking into account the weakening of the laser power depending on the objective the correlation between set and actual laser power is almost linear (figure 25).

table 4. Power per area [$\text{mW}/\mu\text{m}^2$] for 10x (measured values), 50x and 100x Olympus objectives with $\lambda=532$ nm

| Set laser power [%] | Olympus objectives | | |
|---------------------|--------------------|-------|-------|
| | 10x | 50x | 100x |
| 10 | 0.64 | 5.63 | 8.11 |
| 25 | 1.13 | 9.94 | 14.31 |
| 50 | 2.09 | 18.41 | 26.51 |
| 100 | 3.95 | 34.76 | 50.06 |

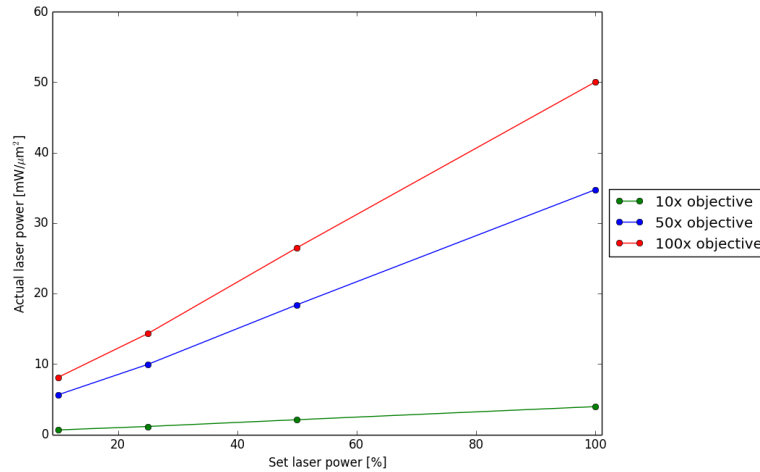


figure 25. Actual laser power on the sample surface using the 10x, 50x and 100x objective (Olympus) with $\lambda=532$ nm

V.2.3. Spatial resolution²⁹

The spatial resolution R depends on the wavelength of the Raman laser and the objective that is used. In practical terms also the precision of the position control of the employed x,y-stage for imaging needs to be considered. However, with regard to the x,y-stage employed for the images recorded in this thesis, no adverse effects with regard to the achieved spatial resolution are expected as the precision of all stages used was better than $0.1 \mu\text{m}$. Additionally to the spatial resolution the accuracy of the stage needs to be considered.

There are several criteria used to calculate the spatial resolution, however, the Rayleigh criterion being defined as half of the laser spot size, is the most frequently one used (equation 13). Therefore, the spatial resolution was calculated for each objective according to the Rayleigh criterion (table 5).

$$R = 0.61 \frac{\lambda}{N.A.} \quad \text{(equation 13)}$$

table 5. Spatial resolution for different objectives with $\lambda=532$ nm

| Objective | N.A. | R [μm] |
|-----------|------|---------------------|
| 10 | 0.25 | 1.30 |
| 20 | 0.35 | 0.93 |
| 50 | 0.75 | 0.43 |
| 100 | 0.90 | 0.36 |

V.3. Sample preparation

Hyphae and spore samples were both prepared following identical sample preparation steps. Spore samples were taken from the shake flasks while hyphae were collected from the bioreactor. One fraction of the original sample was transferred into a new Eppendorf vial after being vortexed to guarantee a homogenous distribution. A small part of the pipette tip was cut off with scissors. Thus larger particles of the sample suspension would not get eliminated by the diameter of the pipette tip inlet. The sample was washed three times with deionized water to eliminate or at least reduce major amounts of by-products or non-consumed nutrients present in the fermentation broth. Each centrifuge step lasted for three minutes at 13300 rpm. During this washing step, the PBS buffer is also removed. Therefore, measurements need to be carried fast as in addition to the lack of oxygen the pH and the ionic strength are different from the fermentation protocol. One droplet of the washed sample was placed onto a microscope slide and dried at room temperature while the liquid sample was stored in the fridge at 5 °C. The original sample was stored in the freezer at -20 °C.

Following the staining protocol developed by Daniela: PI (1:100) and DAPI (1:50) were incubated for approximately 30 minutes at room temperature. A few minutes before performing fluorescence microscopy, Daniela added FDA (1:1000).

V.4. Data analysis

HCA and PCA as well as baseline correction or any other preprocessing of the data sets was performed with ImageLab software version 0.82-0.86³¹. Most of the graphs were plotted using Python(x,y) version 2.7.5.2. Chemical structures were drawn with the online software Marvin (<http://www.chemaxon.com/marvin/sketch/index.php>).

VI. Hyphae of *P. chrysogenum*

VI.1. Raman spectroscopy of fungal hyphae

Raman micro-spectroscopy is a powerful method for analyzing biological samples. With this technique chemical information can be extracted from small sample volumes ($<1 \mu\text{m}^3$) without requiring any type of labeling. Furthermore, Raman spectroscopy is destruction-free. All kinds of biological material in solid and liquid phase can be investigated based on their characteristic vibrational spectrum. A lot of work has been done on investigating bacterial samples with Raman spectroscopy, while little has been published on fungal ones. Significant development could be seen concerning classification of bacterial strains based on Raman spectra.^{32,33,34,35} Rösch et al. (2005) investigated 20 bacterial strains belonging to 9 different species (*B. pumilus*, *B. sphaericus*, *B. subtilis*, *E. coli*, *M. luteus*, *M. lylae*, *S. cohnii*, *S. epidermidis* and *S. warneri*) using a 532 nm Raman laser.³⁶ Krause et al. (2008) demonstrated the use of Raman micro-spectroscopy for identifying different bacterial species which were additionally stained with fluorescent dyes.¹³ Some investigations of fungal samples with Raman spectroscopy are also reported in literature such as the identification of crystalline mannitol in hyphae of *Curvularia protuberata* using a 785 nm Raman laser by M. Isenor et al.³⁷ Furthermore, the cytochrome distribution was investigated by A. Walter et al. in hyphal tips of *Schizophyllum commune* using a 532 nm Raman laser.³⁸ In 2011, Raman spectroscopy was applied to investigate hyphae of ectomycorrhizas found in fossils.³⁹ However, to the best of my knowledge, apart from penicillin investigations⁴⁰, Raman spectra of hyphae of *Penicillium chrysogenum* have not been published yet.

VI.2. Device settings

Due to the size of the fungal hyphae (diameter of a few micrometers) the 100x objective was selected for most of the measurements as long as the laser power did not lead to sample carbonization. A comparison between sample images recorded with the 20x and the 100x objective indicated that investigation of the sample's chemical composition is more efficient with greater magnification (figure 26). Also, spatial resolution is needed to be considered for subsequent Raman mappings. Using the 20x objective, the spatial resolution deteriorates to approximately $1 \mu\text{m}$ compared to $0.4 \mu\text{m}$ with the 100x objective.

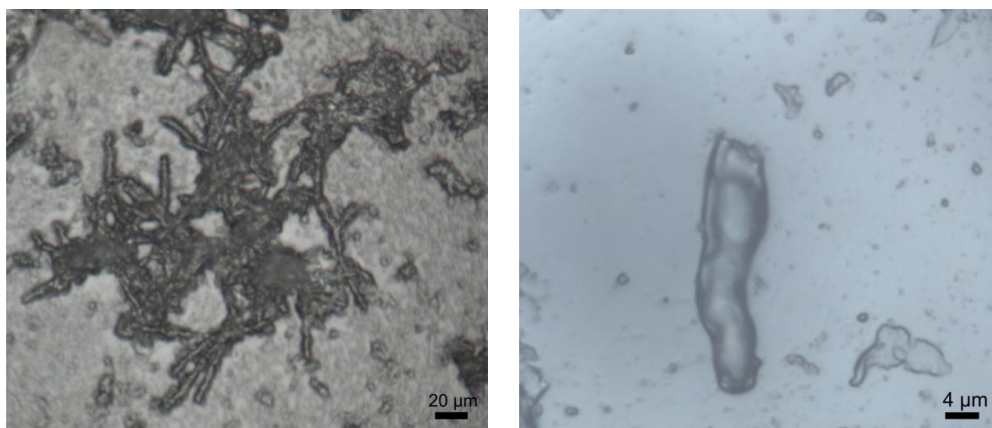


figure 26. Fungal hyphae on microscope slide recorded with 20x magnification (left) and 100x magnification (right)

Before any Raman mapping of the sample of interest could be performed, appropriate device settings such as laser power, integration time, magnification and confocal pinhole size had to be determined for optimal results. The Raman spectrometer available in our laboratory offers two different laser lines: 532 Nd:YAG laser and 633 HeNe laser (see V.1.1). The Raman shift needs to be calibrated for each laser using a small piece of Si-wafer fixed onto a microscope slide. Silicon is one of the most commonly used calibration materials as it has a sharp Raman band at 520 cm^{-1} (triply degenerate F_{2g} bend vibration^{41,42}) and shows neither a fluorescent nor a photobleaching effect.⁴³ For comparing the two available excitation wavelengths, the same sample spot was investigated with the green and the red laser. In order to guarantee an identical measurement position, both samples (Si and fungal hyphae) were mounted onto the x,y,z-stage. The position of the Si-wafer as well as the position of the sample were noted. The first laser (e.g. 532 nm laser) was calibrated, then a measurement of the sample was performed. Afterwards, the second laser was calibrated before recording a spectrum using the second excitation wavelength at the exact same measurement spot of the sample as with the first laser.

Measurements were conducted with different spectrograph settings. Raman spectra recorded in this thesis cover a spectral range from 400 cm^{-1} to 3400 cm^{-1} Raman shift. Depending on the excitation wavelength, this range corresponds to a different area covered in the electromagnetic spectrum (532 nm laser: $\Delta\lambda=106\text{ nm}$, 633 nm laser: $\Delta\lambda=157\text{ nm}$, 785 nm laser: $\Delta\lambda=260\text{ nm}$). With greater wavelength range but constant size of the CCD array, the position of the spectrograph needs to be changed in order to cover the same spectral region in the Raman spectrum as with lower excitation wavelength.

Spectra were recorded using the 100x objective. The Raman signal was diffracted at a 300 lines/mm grating onto the OE-CCD-detector. The Rayleigh lines for both laser

wavelengths were eliminated using appropriate holographic SuperNotch® filters (Kaiser Optical Systems, Inc.). The device settings for both lasers are listed up in table 6.

table 6. Device settings for both lasers

| Laser- λ [nm] | Laserpower [%] | Entrance slit [μm] | Confocal hole diameter [μm] | Acquisition time [s] | Number of accumulations |
|-----------------------|----------------|---------------------------------|------------------------------------------|----------------------|-------------------------|
| 532 | 10 | 150 | 300 | 2 | 20 |
| 633 | 25 | 300 | 500 | 2 | 20 |

The obtained spectra are compared in figure 27 which outlines the advantage of using a 532 nm laser for microorganisms such as *P. chrysogenum* very well. The baseline rises strongly with 633 nm as excitation wavelength and hardly any band is visible. This is due to the fact that the Raman spectrum is affected by autofluorescence of the sample. In contrast, the spectrum obtained with the 532 nm laser reveals a number of bands in the spectral region from 700 cm^{-1} to 1700 cm^{-1} . Additionally, the CH stretch vibration around 2930 cm^{-1} is very intense which is also indicated in the spectrum of the 633 nm laser (red line). The original idea of additionally using the 633 nm laser to collect Raman spectra of hyphae of *P. chrysogenum* was to gain flexibility with the fluorescent dyes which otherwise would get excited by the 532 nm laser. However, this experiment clearly shows that a 633 nm excitation is not suitable for the samples of *P. chrysogenum*.

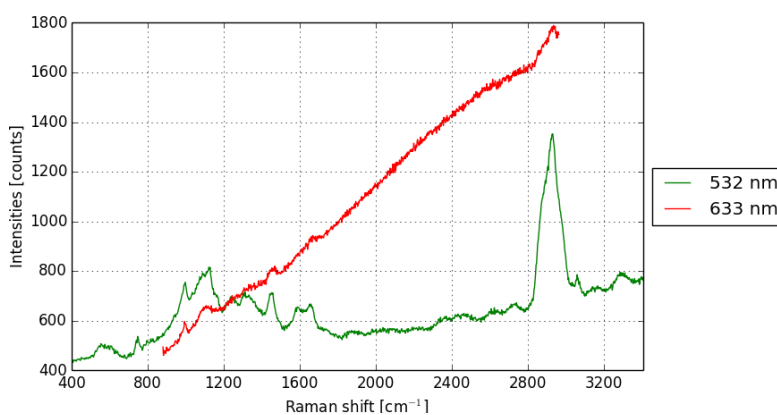


figure 27. Raman spectra of *P. chrysogenum* recorded with 532 nm and 633 nm excitation wavelength

Once the optimal laser wavelength had been determined, an appropriate laser power needed to be found. As the Raman signal is directly proportional to the intensity of the incident light beam, more Raman photons can be collected with increasing laser power. The resulting increase of chemical information in the Raman spectrum is demonstrated in figure 28. The laser power per area increases with greater magnification and thus the intensity of the Raman signal

VI. Hyphae of *P. chrysogenum* - VI.2. Device settings

increases as well. At low magnifications (10x) a strong contribution of the glass slide to the recorded Raman spectra is visible which, however, significantly decreases at higher magnifications. Using the 50x and 100x objective, bands in the region between 1250cm^{-1} - 1750cm^{-1} indicating the presence of nucleic acids, lipids and proteins² get visible in the Raman spectrum. However, the analyzing method should remain destruction-free. Thus, the laser power in combination with the used objective must be adapted to the thermal load resistance of the sample under investigation.

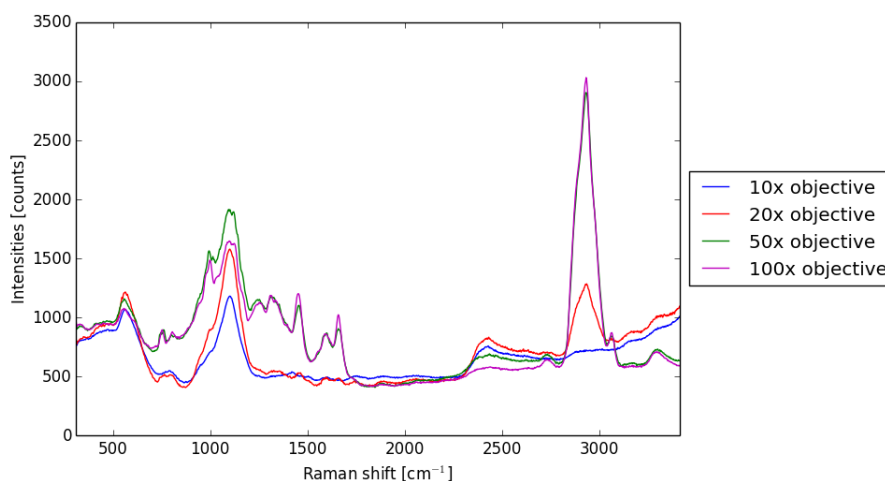


figure 28. Single spectra of hyphae of *P. chrysogenum* generated with 50 % laser power using different objectives (device settings see appendix)

Applying 50 % laser power in combination with 100x magnification is permissible for Raman measurements of hyphae of *P. chrysogenum*. The next laser power adjustable through the filter wheel of the Horiba spectrometer is 100 %. A picture of the sample with the measurement spot marked in red is shown in figure 29 before as well as after the measurement with this laser power. In this case, the sample clearly was exposed to an overload of thermal stress indicated by degradation of the fungal cell wall. Therefore, we can conclude, that 100 % laser power in combination with the 100x objective led to carbonization of the sample and was subsequently avoided.

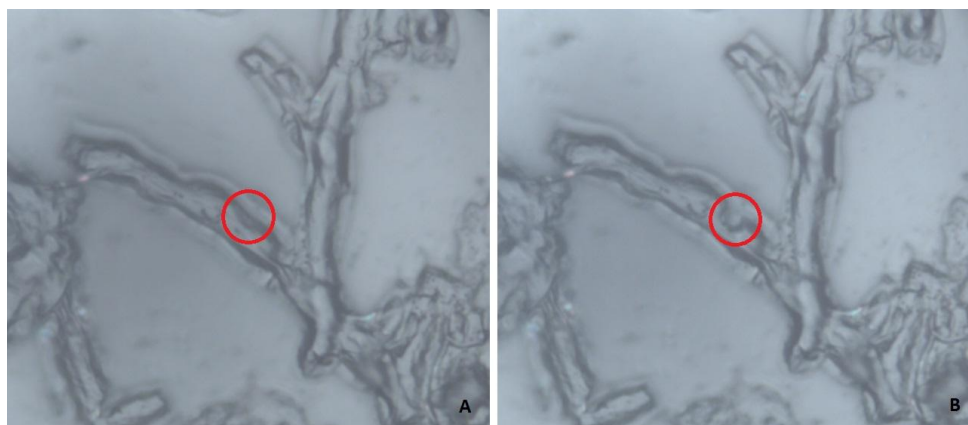


figure 29. Picture of the sample before (A) and after (B) the measurement with 100 % laser power (device settings see appendix)

A Raman spectrum recorded with the maximum laser power adjustable for hyphae of *P. chrysogenum* is shown in figure 30. The very intense CH stretch vibration at 2930 cm^{-1} is visible along with other characteristic bands mainly appearing in the spectral region between 900 cm^{-1} and 1700 cm^{-1} (see table 7 for band assignment).

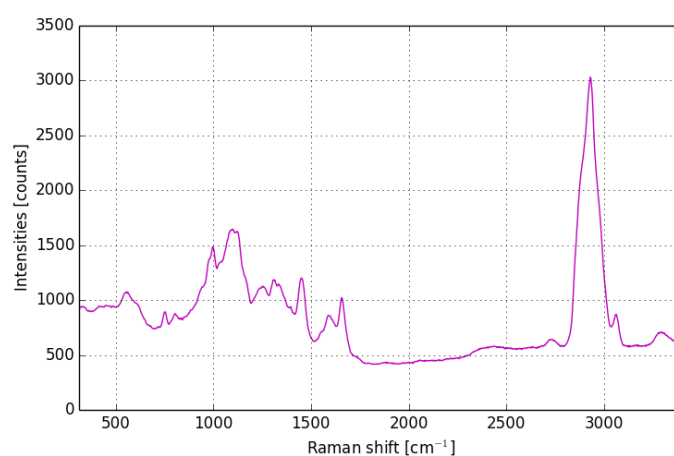


figure 30. Raman spectrum of a hypha of *P. chrysogenum* (device settings see appendix)

table 7. Band assignment: Hyphae of *P. chrysogenum*

| Band shift [cm ⁻¹], this work | Band shift [cm ⁻¹] Huang et al ² | Assignment |
|-------------------------------------------|---------------------------------------------------------|-------------------------------------------------|
| 552 | 550 range | Glass background |
| 753 | 752 | ν (T ring) |
| 803- 805 | 810-820 | Nucleic acids (C-O-P-O-C in RNA) |
| 999 | 981 ⁴⁴ | (NH ₄) ₂ SO ₄ |
| 1084- 1088 | 1085 | ν (C-O) |
| 1123 | ~1130 | =C-C= (unsaturated fatty acids in lipids) |
| 1255 | 1254 | Adenine, Amide III |
| 1311 | ~1320 | Amide III, δ (CH) |
| 1336 | 1336-1339 | Adenine, guanine, tyrosine, tryptophan |
| 1455- 1459 | 1440- 1460 | δ (CH ₂) |
| 1592 | 1582, 1593 | Protein |
| 1657 | 1650- 1680 | Amide I |
| 2929- 2937 | 2935 | ν (CH) |
| 3061 | 3059 | ν (C=C-H) aromatic |

VI.3. First Raman mappings

After device settings for single Raman spectra have been defined, first Raman mappings could be performed. A Raman image/map consists of a defined number of pixels within a horizontal rectangle of the sample. The size of a pixel is set by the step-size between single measurement spots in the operating software. This step-size can be adapted in x- and y- dimension for a 2D mapping. On each of those pixels, a Raman spectrum is recorded creating a hyperspectral data cube. This cube consists of the x- and y- axis defining the position of the pixel and approximately 1000 layers each representing the intensity values at a specific wavenumber of the Raman spectrum (figure 31).

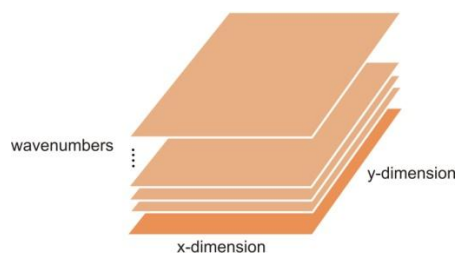


figure 31. Sketch of a hyperspectral data cube

The Raman laser is a CW-laser (continuous wave). For Raman mappings, this means that the sample is not only thermally stressed during a certain integration time needed to record a Raman spectrum at a single measurement spot, but is also affected by the heat of the laser beam when measurements are performed in close proximity to this measurement spot. So, the thermal stress is also linked to the step-size of a Raman map. Thus, a compromise needs to be found between good S/N ratio (signal to noise ratio) of the Raman spectrum, i. e. greater integration times, and Raman spectroscopy remaining a destruction-free analyzing method. Also, photobleaching effect resulting from the impact of the CW-laser can be observed during Raman mapping for biological samples.

VI.3.1. Small scale mapping

A mapping of the washed fungal sample taken from the bioreactor und placed on a microscope glass slide was performed over night. Spectra were recorded with a step size of $0.6 \mu\text{m}$ between single measurement spots. Thus all in all, 2583 (63×41) spectra were obtained, each representing one pixel of the resulting image ($37.8 \times 24.6 \mu\text{m}^2$). Considering an integration time of $10 \times 2 \text{ s}$ for each spectrum, the overall measurement time was 14.35 hours. The laser power was set to 50 % and the 100x objective was used.

Within the 2583 spectra, eight were affected by the high laser power which led to carbonization of the sample. This can be traced by bands corresponding to amorphous carbon visible around 1350 cm^{-1} (D-peak) and 1580 cm^{-1} (G-peak). Other bands resulting from lipids, amino acids or sugars vanish underneath these intense graphite bands. Therefore, those spectra (figure 32) were replaced by calculated ones obtained by averaging the neighboring spectra. The comparison of spectra containing graphite bands to the one of a fungal hypha in figure 32 shows the necessity of this correction. The corrected spectra were excluded from data analysis to prevent falsification of the results. Except for this correction, the spectra were not additionally preprocessed.

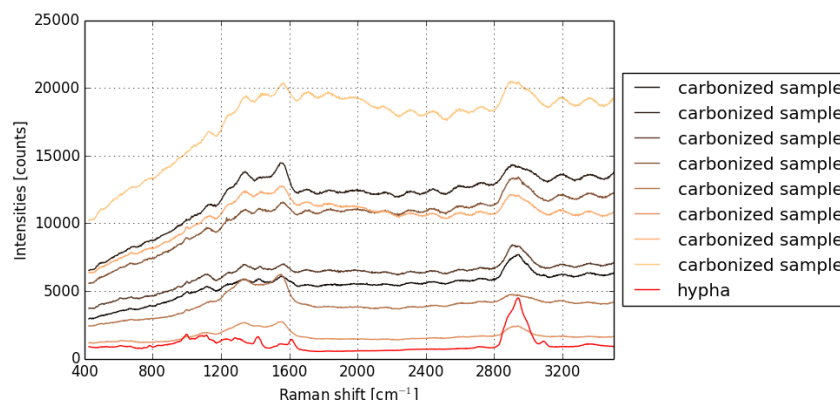


figure 32. Spectra of fungal parts burned by the laser beam which were excluded as bad pixels and replaced by averaged neighboring spectra, and spectrum of a fungal hypha for comparison (Spectra 0-7 represent carbonized sample parts)

The spectrum recorded in the middle of the hypha is shown in figure 33. The CH stretch vibration around 2931 cm^{-1} is very intense. Furthermore, the amide I band is visible at 1655 cm^{-1} . The band at 1450 cm^{-1} most likely is evoked by lipids (CH_2 deformation vibrations) and is also listed up as protein marker according to the band assignment of Huang et al.². Additionally, the band at 999 cm^{-1} is the result of ammonium sulfate which apparently had not been completely washed out by the preceding washing step (washed 3x with DI) and precipitated at the edge of the hypha. Ammonium sulfate was part of the growth medium in the bioreactor. The measurement spots of the Raman spectra are marked in figure 34 (left) and are cross color-matched to the according spectrum.

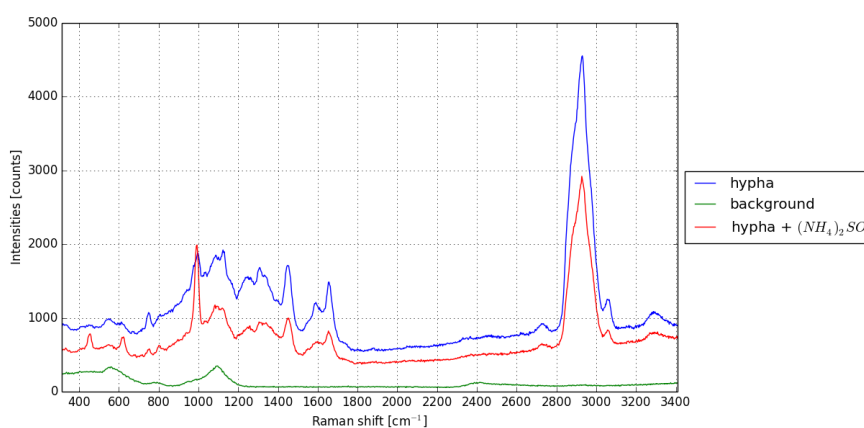


figure 33. Raman spectrum recorded in the middle of a hypha of *Penicillium chrysogenum* (blue), next to the hypha (green) and at the edge of the hypha (red); measurement position see figure 34 (left)

An intensity map comparing the CH stretch vibration at 2930 cm^{-1} between all the spectra was performed with ImageLab software and overlaid with the recorded picture of the sample. The intensity map perfectly matches the sample image.

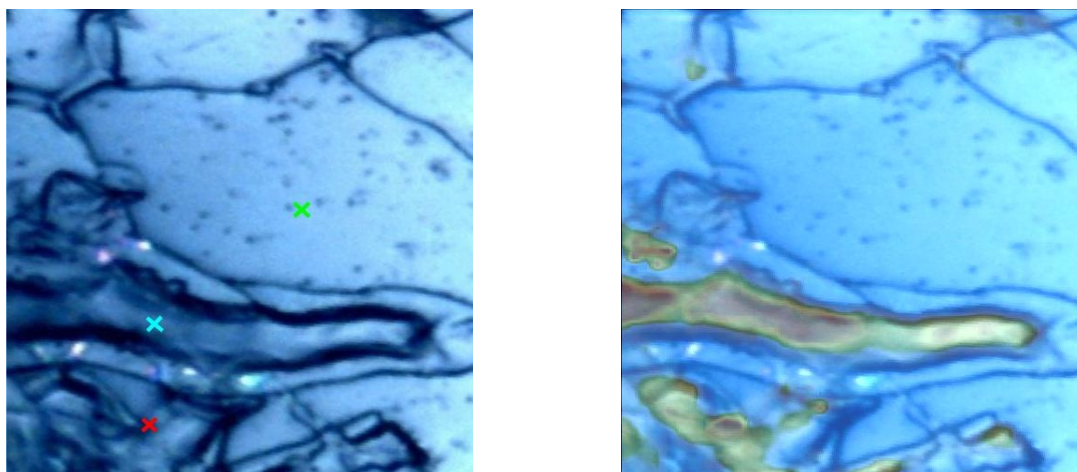


figure 34. Picture of the sample (left) and overlay with the intensity map based on the intensity of the CH stretch vibration (right)

The area of the highest intensity of CH stretch vibrations is clearly visible in the middle of the fungal hypha. Furthermore, some small parts in the lower image area contain CH stretch vibrations as well. The fungal hypha in the upper image area (figure 34) seems hollow and does not contain protein material which is verified by the absence of CH stretch vibrations in this particular part of the sample. However, the protein concentration might not be zero but is at least under the limit of detection of this spectroscopic method.

The intensities of the amide I band at 1656 cm^{-1} which mostly results from the C=O stretch vibration were also investigated. As can be seen in the Raman spectrum of *P. chrysogenum*, the intensity of the CH stretch vibration is three times more intense than the amide I band (figure 33). By setting the maximum intensity value of each Raman shift to 100, the intensity maps of single Raman bands gets more comparable as the predominant intensity difference is eliminated allowing to focus on actual changes in the Raman image. The resulting intensity map (figure 35) outlines the parts of the sample with higher amounts of proteins and polypeptides which also correlate with the regions where CH stretch vibrations were detected. CH stretch vibrations may not only result from lipids but also from carbohydrates, amino acid side chains, etc which explains the greater area covered compared to the intensity map of the amide I band.

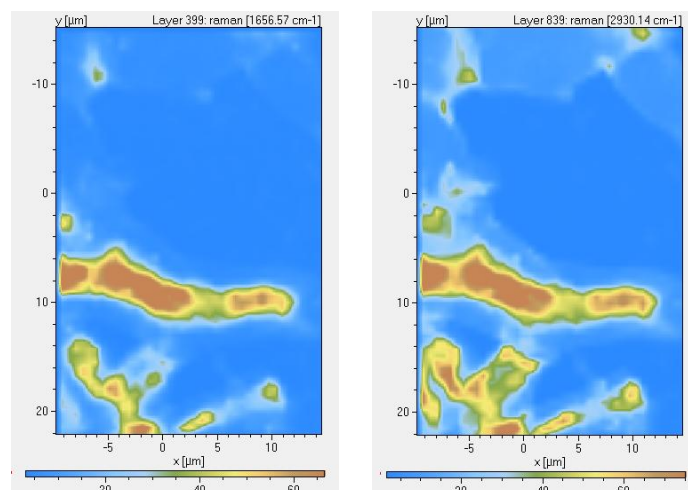


figure 35. Intensity map of the amide I band at 1656 cm^{-1} (left) and the band at 2933 cm^{-1} evoked by CH stretch vibrations (right); maximum intensity value of each wavelength as set to 100

Hierarchical cluster analysis (HCA) was applied to the data set (spectral descriptor list see appendix) to evaluate chemical similarities in the composition of the fungal hypha based on the information extracted from the Raman spectra. The Euclidean distance measure was selected. Ward's algorithm was applied to the standardized data set for calculating the dendrogram.

The cluster analysis performed for three clusters mirrors the same differences as were expected from the single spectra in figure 33 taken at different positions of the fungal sample. An average spectrum including its standard deviation of each cluster is shown in figure 36 (right). The main distinction based on the spectral information is indicated within the first two branches of the dendrogram (figure 37) where the background signal is separated from the sample signal. The overlay of sample and cluster image shows good agreement (figure 36 left). The cluster with highest protein content (orange) perfectly covers the area inside the membrane of the hypha (cytoplasm). The second cluster (violet) refers to regions with lower protein content such as the area between cell wall and plasma membrane (periplasm). Also, there are some parts of the hypha where the cell wall was destroyed, leaving an empty shell with low protein content. The third cluster (pink) represents the background (microscope glass slide) which differs greatly from the sample spectrum, most notably by the absence of the CH stretch vibrations at 2930 cm^{-1} .

Cluster two differs from cluster one by the absence of the amide I band (1657 cm^{-1}) which is a very important protein marker band. Also, the form of the Raman band evoked by CH stretch vibrations differs between the two clusters. Additionally, cluster one contains aromatic stretch vibrations (3060 cm^{-1}) which are absent in cluster two and three.

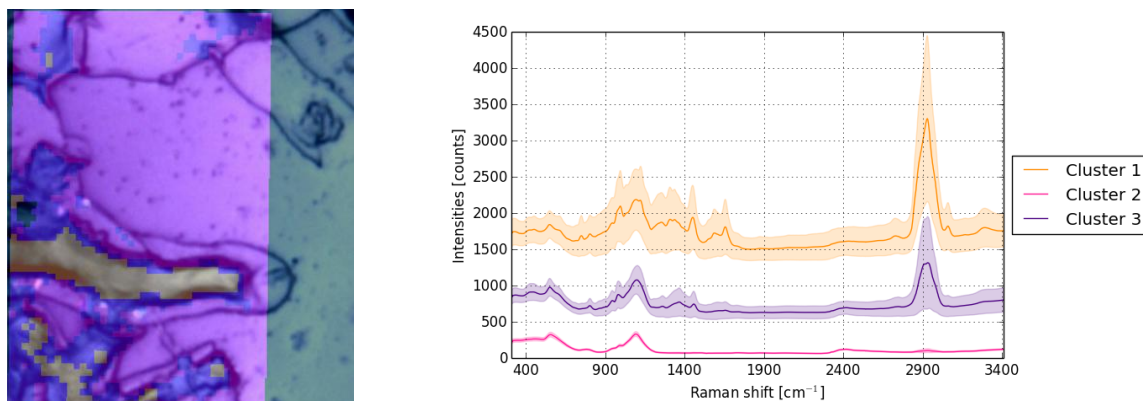


figure 36. Overlay of cluster image and sample image (left); average spectra of each cluster (right)

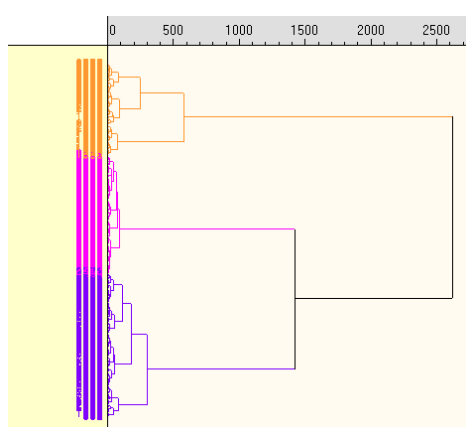


figure 37. Dendrogram of HCA with three clusters

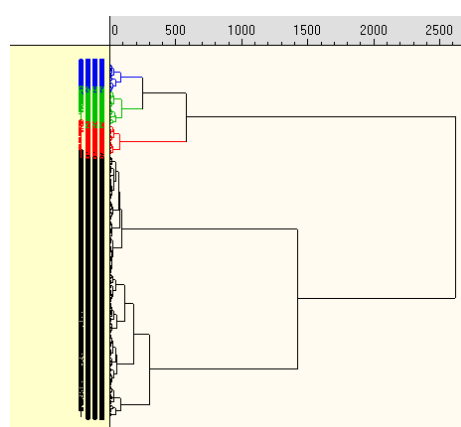


figure 38. Dendrogram of HCA showing further subdivisions of one component

The first cluster (high protein content) can be further divided into finer subdivisions inside the fungal membrane (figure 38). The blue cluster represents the chemical composition in close proximity to the fungal membrane. The red cluster shows highest protein content in the middle of the hypha while the green cluster marks the intersection area (figure 39 left). The same information is mirrored by the average spectra of the three subdivisions (figure 39 right). This time, all the average spectra contain aromatic stretch vibrations at 2960 cm⁻¹ which makes perfectly sense since these spectra represent subdivisions of the first cluster from the previous cluster image (figure 36). Also, it can be seen that the intensity of amide I band decreases from the first to the third cluster indicating lower protein content near the fungal membrane.

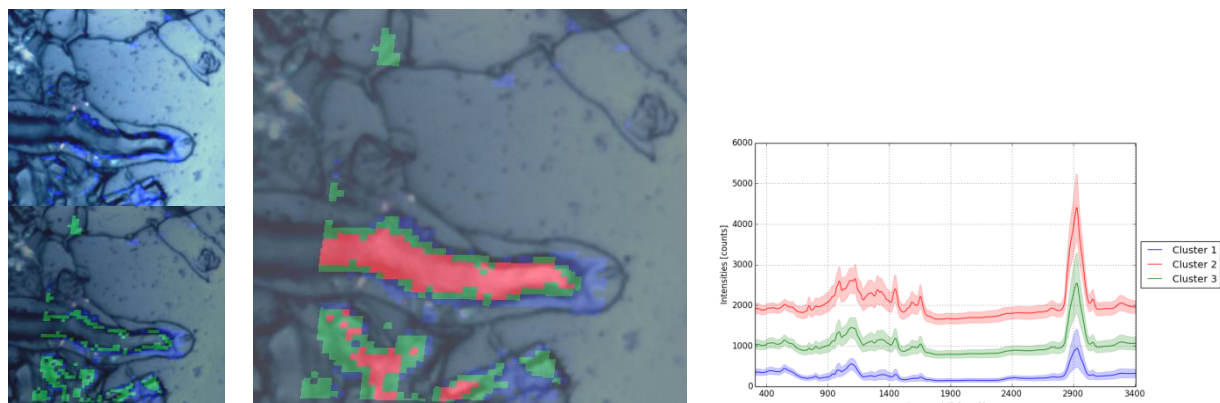


figure 39. Overlay of cluster image (subdivision of cluster with highest protein content) and sample image (left); average spectra of the three subdivision of the hypha-cluster (right)

It seems that the CH stretch vibration has great influence on the formation of the clusters as the greatest differences in the average spectra can be seen in this spectral region. However, the fact that this band shows highest intensity should not influence the result as all data points are standardized (subtraction of average spectrum and division by standard deviation) before HCA is performed.

Due to the CH stretch vibration, it is easy to determine the presence of biological material and thus to differentiate between sample and background for which this specific vibration is missing. In order to further investigate differences between dissimilar sample areas the fingerprint region from 400 cm⁻¹ to 1900 cm⁻¹ was analyzed by hierarchical cluster analysis (HCA).

Comparison between the three subdivisions describing the composition within the fungal hypha with calculations based on two different sets of spectral descriptors (with and without the CH stretch vibrations) further indicates minor but statistically relevant differences. The hypha show lower protein content at the tip compared to the first HCA where the protein content increases uniformly from the plasma membrane to the middle of the hypha. Those slight differences are also indicated in the dendrogram.

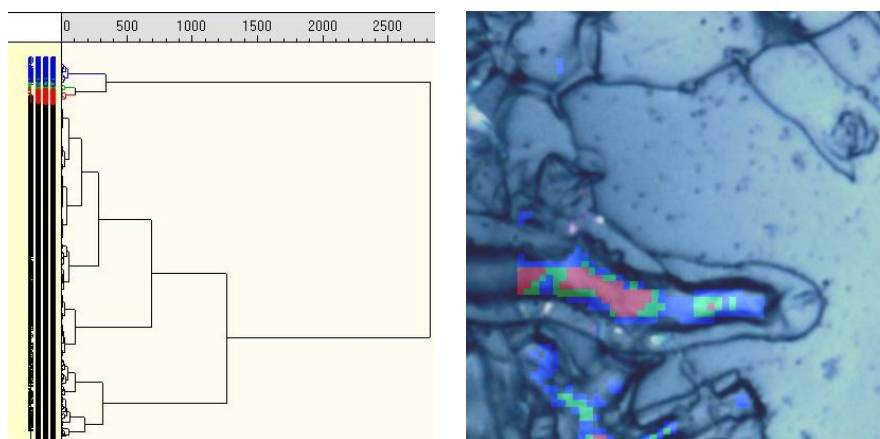


figure 40. Dendrogram and overlay of cluster image and sample image of the second HCA covering the spectral region from 400 cm^{-1} to 1900 cm^{-1}

Also, the average spectra look similar for both cluster analyses. Having a closer look at the fingerprint region, some changes between the average spectra get visible. Therefore, the intensity ratio of three double bands (A, B and C marked in grey in figure 41) was investigated here to test whether focusing the analysis on selected variables could provide further insight. In this investigation, variable selection was guided by choosing strongest bands in the available Raman spectra. In doing so, for each double band (e.g. A) the band positioned at lower wavenumbers (e.g. band at 1085 cm^{-1} in area A) was divided by the band located at higher wavenumbers (e.g. band at 1123 cm^{-1} in area A).

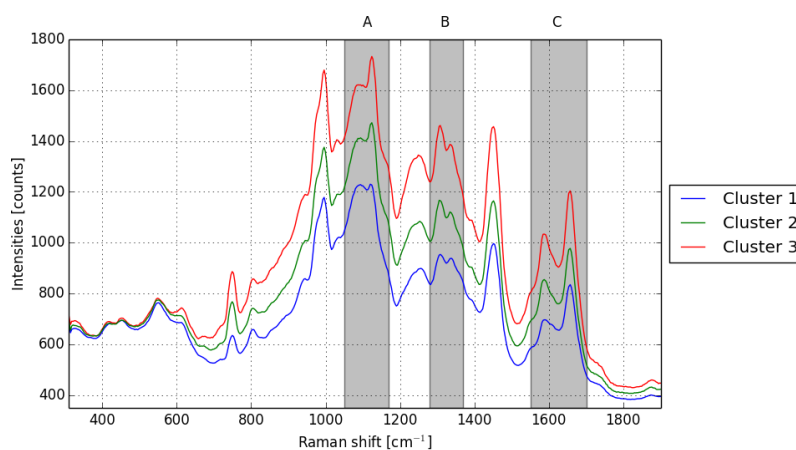


figure 41. Average spectra of each cluster from the second HCA (cluster image see figure 40); double bands with changing intensity ratio are marked in grey

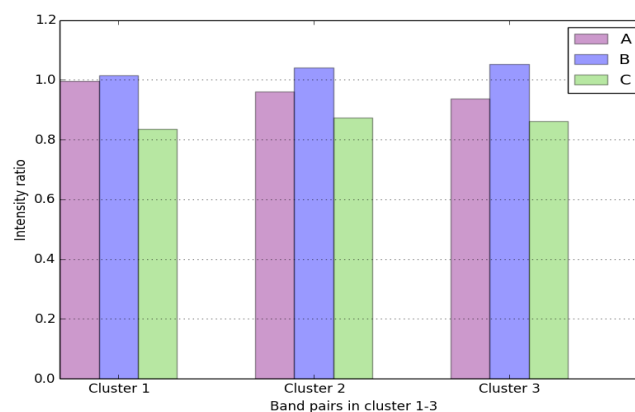


figure 42. Intensity ratios of three double bands of the average spectra from the first to the third cluster

Considering double band A, the intensity of the C-O stretching vibration located at 1088 cm^{-1} increases towards the middle part of the hypha while the amount of unsaturated fatty acids ($=\text{C}-\text{C}=\text{ at } 1125\text{ cm}^{-1}$) remains almost unchanged. Also, the ratio between double band B changes significantly within the hypha. From cluster one to cluster three, the amide III band located at 1308 cm^{-1} increases compared to the Raman band at 1336 cm^{-1} which is mainly evoked by vibrations of the bases adenine and guanine, but also influenced by vibrations of the aromatic amino acids tyrosine and tryptophan. A third double band (C) was investigated. In this case, the intensity ratio changes most between first and second cluster while it remains almost constant for the average spectrum of the third cluster. Therefore, it can be assumed that the concentration of the amide I band (1656 cm^{-1}) increases constantly towards the middle part of the hypha while the amount of nucleic acids is lower at the edge of the hypha. With these investigations it can be demonstrated that different chemical groups can be detected within the fungal hypha based on the spectral information extracted from the Raman image.

Principal component analysis (PCA) was applied to the data set without applying any preprocessing steps except for the exclusion of bad pixels as mentioned previously. Standardization (subtraction of average spectrum and division by standard deviation) of the spectra was done prior to PCA which was performed with the same list of spectral descriptors as was used for HCA (including CH stretch vibration). Principal component 1 (93.09 %) and 2 (3.46 %) explain 96.55 % of the variance of the data set.

According to the bi-plot (figure 43) the first principal component does not differentiate between the spectral descriptors. The second component, however, is more influenced by spectral descriptors 4, 7, 2 and 11 with descriptor 2 having the greatest impact (see table 8 for spectral descriptor list). Compared to the amide III band and Raman bands evoked by unsaturated

fatty acids in lipids as well as CH stretch vibrations, unsaturated lipids have the least influence on PC2 which makes no sense as unsaturated lipids and unsaturated fatty acids in lipids would be expected to have loadings pointing approximately into the same direction. This inconsistency and the fact that loadings in the bi-plot do not differentiate between single groups within the spectral data make interpretation of the PCA appear questionable. Further data processing removing the glass background from PCA analysis by including it in the bad pixels mask might be required for obtaining reasonable results.

Therefore, in a second approach the data set was mean centered (standardized data was used for first PCA) for PCA analysis. The difference between the first PCA and second one differing in data preprocessing is displayed in figure 44. Also, the score plot of the PCA calculated from mean centered data excluding background spectra is shown (figure 44 right) and seems to be more structured indicating a clearer differentiation between spectral features.

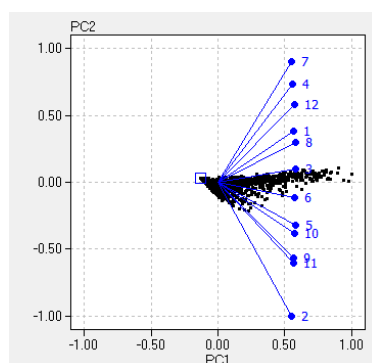


figure 43. Bi-plot of first PCA

table 8. List of spectral descriptors according to their impact on PC2; band assignment according to Huang et al.²

| Spectral descriptors with high impact on PC2 | | Spectral descriptors with low impact on PC2 | |
|----------------------------------------------|----------------------------------------------------------------|---------------------------------------------|----------------------------------------------------------------|
| 7 | Adenine, amide III | 1 | $\nu_{\text{aromatic}}(\text{C}=\text{C}-\text{H})$ |
| 4 | Protein | 8 | Adenine, amide III |
| 12 | $\nu(\text{T})$ | 3 | Unsaturated lipids |
| 2 | $\nu(\text{CH})$ | 10 | Phosphate, CC skeletal, $\nu(\text{COC})$ from glycosidic link |
| 11 | $(\text{NH}_4)_2\text{SO}_4$ | 5 | $\delta(\text{CH}_2)$ |
| 9 | $=\text{C}-\text{C}=\text{}$ unsaturated fatty acids in lipids | 6 | Adenine, guanine, tyrosine, tryptophan |

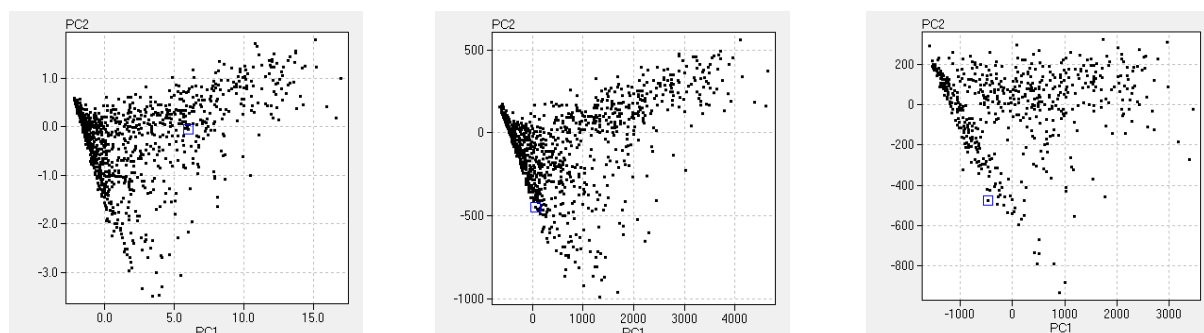


figure 44. Score plot of the first PCA: standardized data (1st plot) and mean centered data (2nd plot); Score plot of the second PCA (3rd plot)

This time, the bi-plot indicates rather distinct differences considering the loadings of spectral descriptors (figure 45). Identical spectral descriptors as were used for the first PCA (see table 8) were also investigated within the second PCA. The amide III band has again greatest impact on principal component 2 and is separated from the rest of the loadings. Also spectral descriptors 2, 11 and 6 seem to point at similar directions while the remaining descriptors form a cloud of loadings indicating moderate impact on PC2. Again, PC1 cannot differentiate between single descriptors. However, this time vibrations evoked by unsaturated fatty acids and lipids as well as the ones from unsaturated lipids are in close proximity to each other in the bi-plot.

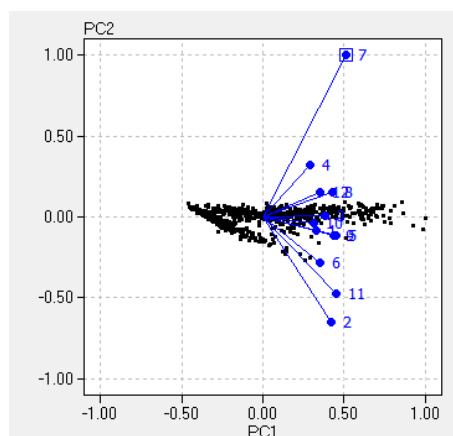


figure 45. Bi-plot of second PCA

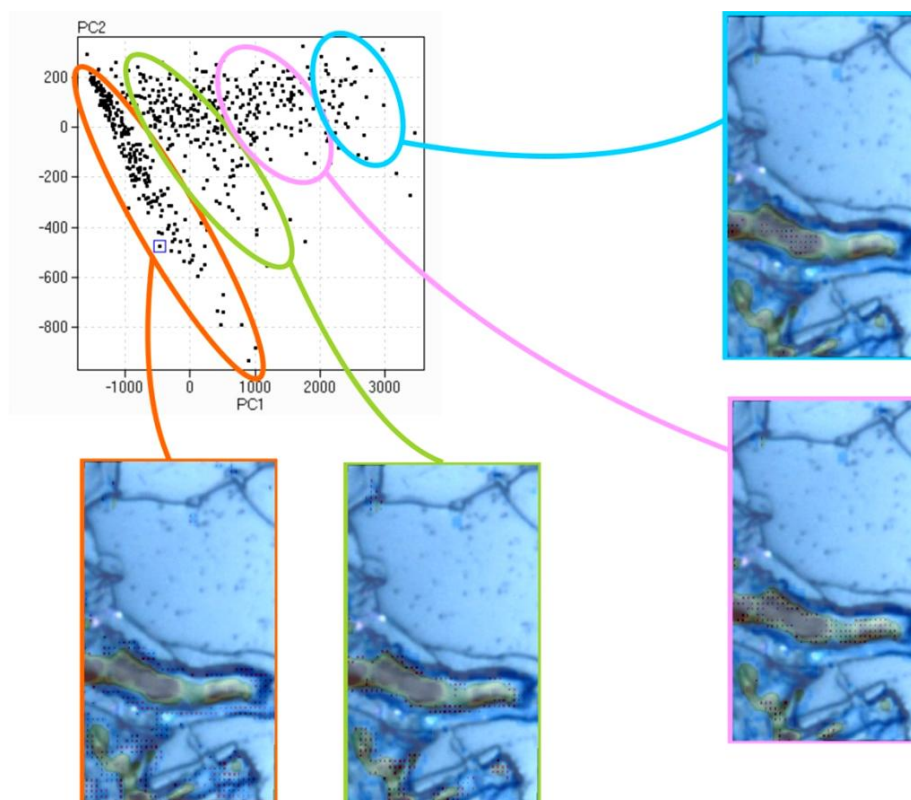


figure 46. Score plot PC1 vs PC2

In the score plot of PC1 vs. PC2 areas can be identified representing different parts of the Raman image. Raman bands representing different chemical groups in the hyphae exhibit high scores for PC1. The PCA supports the information gained from the HCA. Different chemical groups can be identified in the Raman image such as the amide III band which shows great influence on PC2. However, no clear differentiation between single chemical structures mixed within the hypha can be extracted by PCA. Still, eliminating the glass background from PCA analysis improves the score plot allowing to distinguish regions with low (periplasm) and high (cytoplasm) protein content.

In this specific investigation, the importance of spectra preprocessing could be demonstrated as a clearer insight into the sample composition was gained with the mean centered data set than with the standardized one. Excluding background spectra from data analysis further improved the score plot. There is a lot of information packed in the Raman spectra, however, no clear unambiguous picture could be obtained yet.

VI.3.2. Large scale mapping

A 300 μm x 300 μm image was taken showing hyphae of *Penicillium chrysogenum*. An area of 105x124 μm^2 was selected for Raman imaging with 100x magnification (figure 47). To decrease the overall measurement time, a compromise between S/N ratio and integration time needed to be found which resulted in decreasing the integration to 3x2 s (compared to the 10x2 s for the small scale mapping in VI.3.1). Also, the step size between two single measurement spots (1 μm compared to 0.6 μm for the small scale mapping) was modified to reduce measurement time. All in all, 21.7 hours were required for this mapping (device settings see appendix).

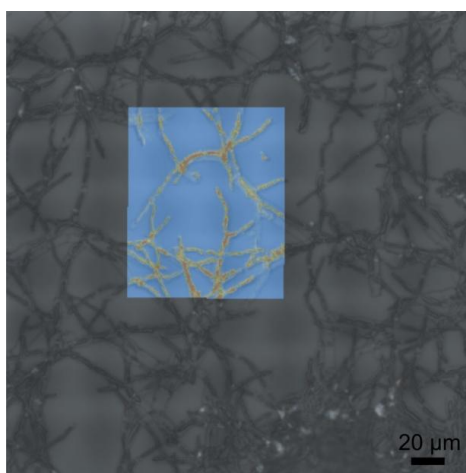


figure 47. 300x300 μm^2 sample image with the mapping area (105x124 μm^2 ; intensity map of CH str. vibration)

The comparison of the Raman spectrum resulting from the hypha and the glass background of the sample carrier (figure 48) outlines the bands that exclusively result from the sample. This means that the spectral region from 1200 cm^{-1} to 1800 cm^{-1} reveals important information concerning the hypha. Furthermore, the CH stretch vibration around 2933 cm^{-1} is a very intense band indicating the presence of biological material. After a baseline correction based on a spline function with 10 pivots (stiffness: 0.020; pivots see appendix) the intensity map of characteristic bands such as the CH stretch vibration (2933 cm^{-1}), amide I band (1663 cm^{-1}), the CH_2 deformation vibration (1451 cm^{-1}) or the Raman band dominated by purine bases (adenine, guanine; 1338 cm^{-1}) were investigated.²

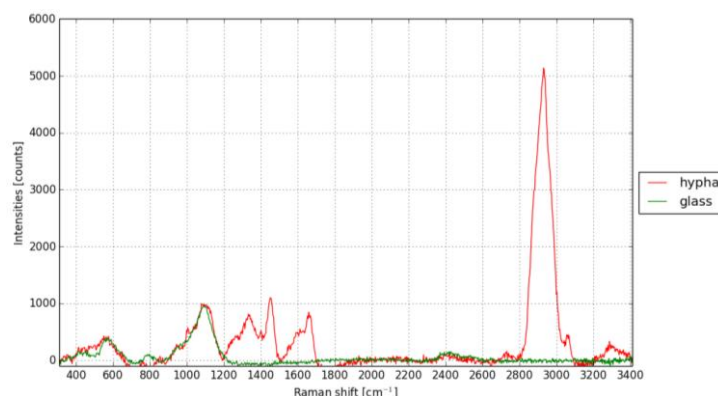


figure 48. Comparison of the Raman spectra evoked by hyphae (red) and glass background (green)

The **intensity map** clearly distinguishes between hyphae and background which can be seen in the overlay with the sample picture. While lipids, purine bases as well as the amide I band are almost in the same intensity range, the CH stretch vibrations are 6 times more intense compared to the other Raman bands investigated (figure 49). The CH stretch vibration which can result from glycoproteins in the membrane, DNA in the nucleus, various amino acids, unsaturated fatty acids and many more is ubiquitously present in the cytoplasm.

To overcome these extreme intensity differences observed between single Raman bands, the maximum intensity value at each wavenumber was set to 100. This scaling of the data set facilitates the comparison of intensity maps showing the distribution of different Raman bands within the imaging area. Using this approach, intensity maps of the spectral region dominated by purine bases, lipids, amide I and CH stretch vibrations were investigated (figure 50- figure 53).

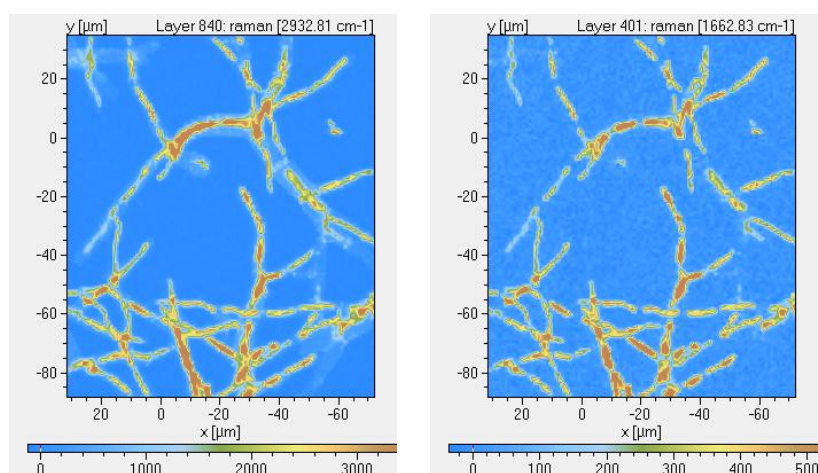


figure 49. Intensity map of the CH stretch vibration (left) and the amid I band (right)

According to the intensity maps, the hyphae contain a higher amount of CH₂ deformation vibrations compared to the amide I band (figure 51, figure 52). CH₂ vibrations often indicate the presence of lipids such as fatty acids (especially long saturated structures), phospholipids, sphingolipids and many others. Furthermore, purine bases (adenine, guanine) and aromatic amino acids (tyrosine and tryptophan) are distributed over a large area in the hyphae. However, based on these intensity maps, no clear insight into the chemical composition of the hyphae can be gained. None of the four groups investigated could be assigned to specific sample areas.

Proteins inside the plasma membrane (cytoplasm) are indicated in all four images (figure 50- figure 53). Hyphae with lower intensity of CH stretch vibrations might already have a damaged membrane leading to leakage of the biological material inside the membrane. Furthermore, it is noticeable that the CH stretch vibrations get less intense in the thinner ends of the branched hyphae which means that inside of the hypha, more protein is present than in its tips. This perfectly correlates with the structure of the hypha which gets thinner towards the tip and thus cannot contain as many proteins as the older, thicker part of the hypha.

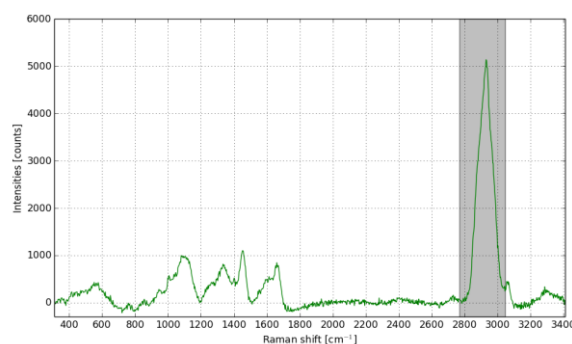
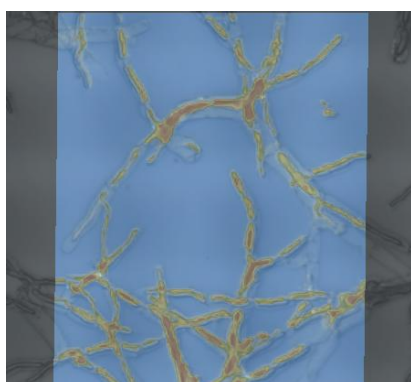


figure 50. Overlay of intensity map and sample image (left) of the CH str. vibration (right)

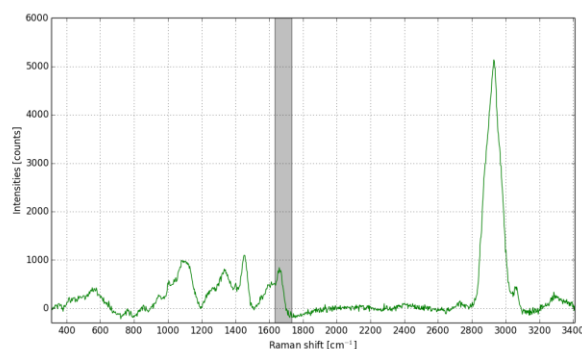
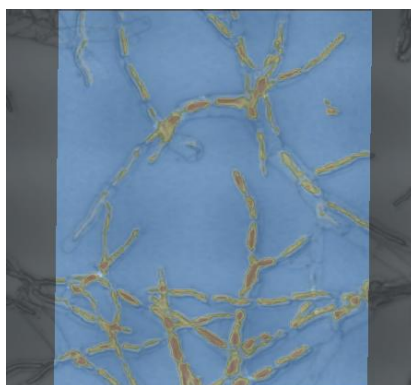


figure 51. Overlay of intensity map and sample image (left) of the Amide I band (right)

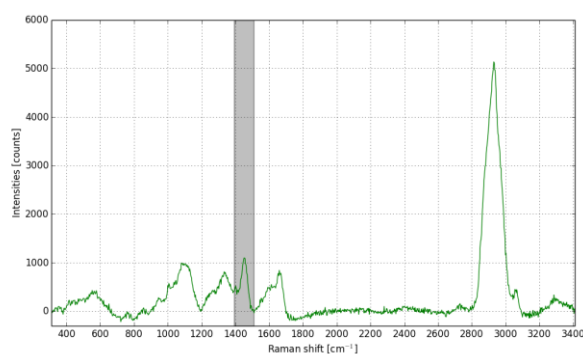
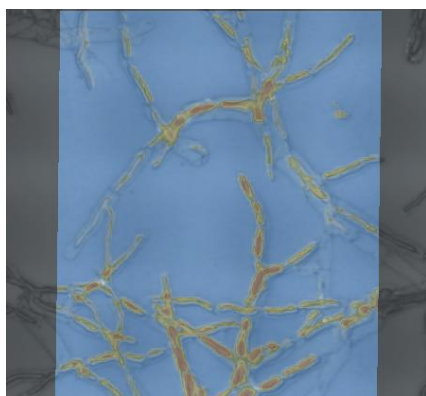


figure 52. Overlay of intensity map and sample image (left) of lipids (right)

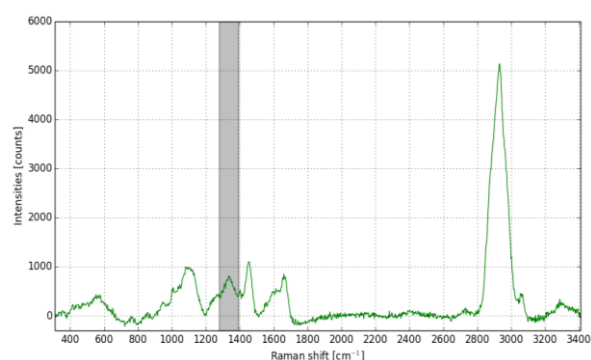
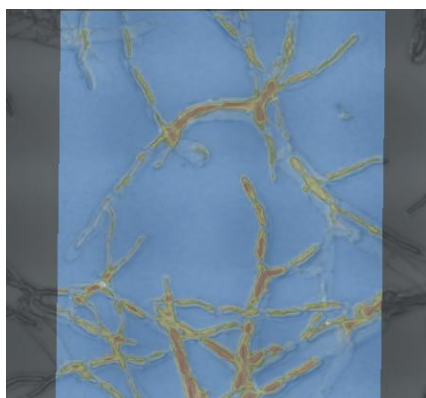


figure 53. Overlay of intensity map and sample image (left) of the band mainly evoked by purine bases (right)

To get a better insight into the distribution of different chemical groups in the hyphae, **HCA** was performed with the baseline corrected data using the Euclidean distance measure and Ward's algorithm (spectral descriptors see appendix). The overlay of sample image and cluster image with three clusters shows a perfect match (figure 54 left). High protein content is indicated by the blue colored cluster in the middle of the hyphae outlined by the according average spectrum (figure 54 right) containing an intense band evoked by CH stretch vibrations and additional Raman bands in the protein fingerprint region ($800\text{ cm}^{-1} - 1800\text{ cm}^{-1}$). The average spectrum of the green cluster mirrors the Raman spectrum of glass. Thus, the green area represents the microscope glass slide. Furthermore, the spectrum of the red cluster looks very similar to the background cluster, but already contains a few protein bands. This component is mainly present in the periplasm between cell wall and plasma membrane.

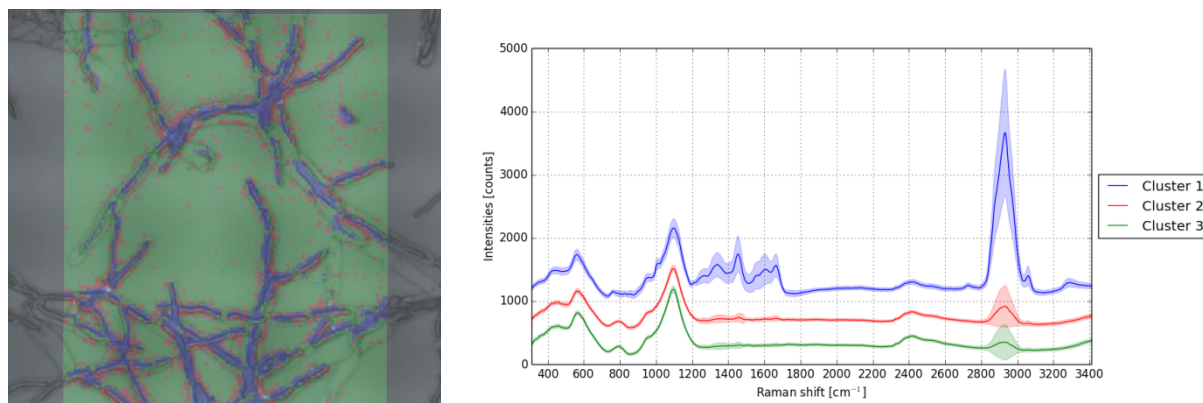


figure 54. Overlay of cluster image and sample image (left) with the according average spectra and the standard deviation (right)

The dendrogram shows a clear differentiation between hyphae and background (microscope glass slide) indicated by the division in two main branches (figure 55). The blue cluster which contains the information about hyphae was further divided into subdivisions for better insight into the chemical composition of the sample (figure 56).

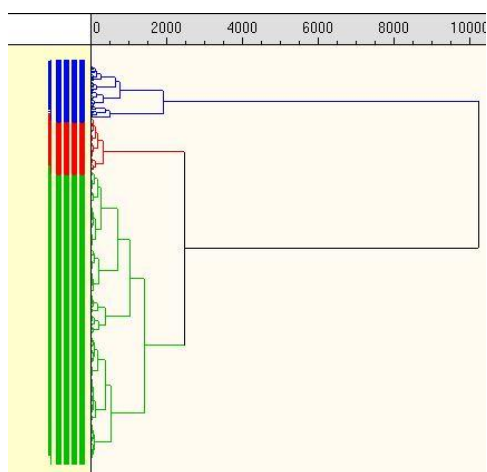


figure 55. Dendrogram of HCA with 3 clusters

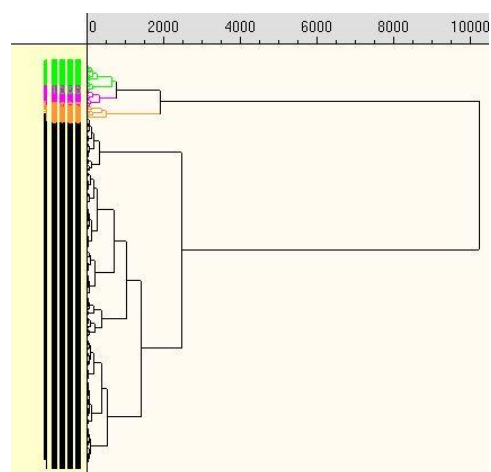


figure 56. Dendrogram of HCA showing subdivisions of the sample branch

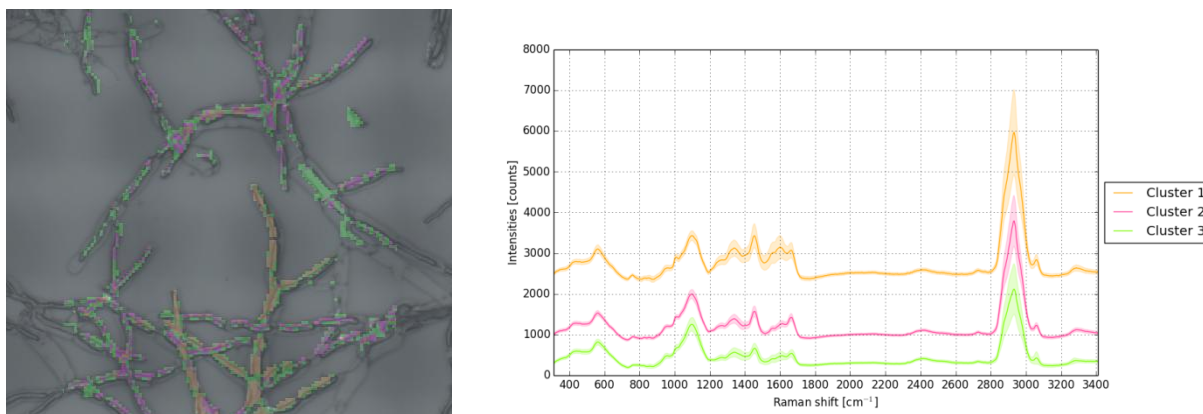


figure 57. Overlay of cluster image and sample image (left) with the according average spectra and the standard deviation (right)

First analysis by color distinction regarding the overlay of cluster image and sample image indicates a different composition of one fungal branch (orange colored in figure 57 left). Intensity ratios of several Raman bands were calculated in order to investigate this difference outlined by the cluster image (figure 58). Band pair A corresponds to the intensity ratio between phenylalanine (1600 cm⁻¹) and amide I band (1664 cm⁻¹). B marks the intensity ratio between CH stretch vibration (2933 cm⁻¹) and the C=C-H aromatic stretch vibration (3060 cm⁻¹).² Each ratio was calculated by division of the Raman band at lower wavenumbers by the Raman band at higher wavenumbers.

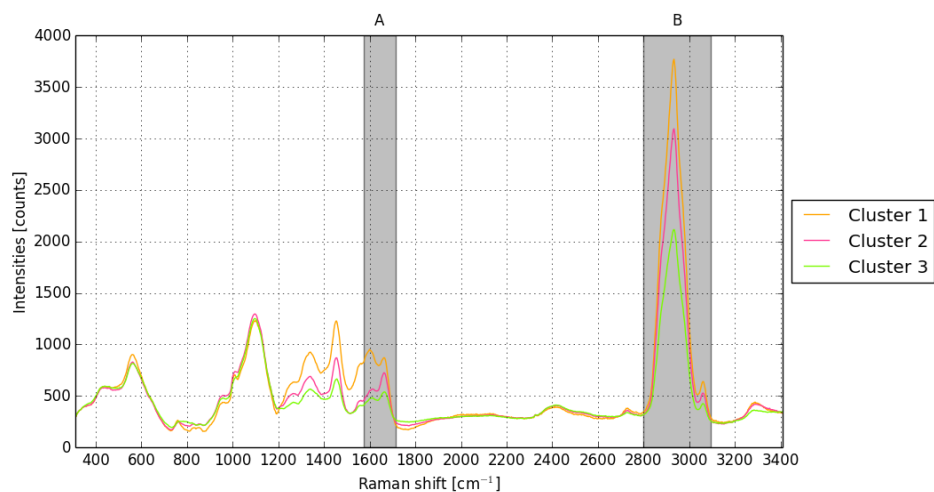


figure 58. Average spectra of HCA: intensity ratios are calculated of bands pairs A and B marked in grey

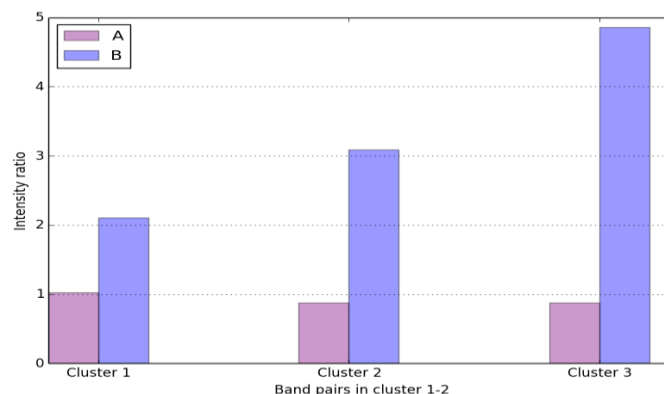


figure 59. Intensity ratios of three double bands of the average spectra from the first to the third cluster

From the pink to the orange colored cluster, the intensity ratio phenylalanine : amide I band (band pair A) increases (figure 59). This indicates that the phenylalanine content increases relative to the amide I band which is also supported by the Raman band around 1000 cm^{-1} which is the spectral region where phenylalanine also shows a very characteristic vibration. However, it needs to be considered that the bands in the investigated spectral region overlap to a great extent. Moreover, there is a third band at 1556 cm^{-1} with unknown contribution to the bands in close proximity. From the pink to the green cluster, the intensity ratio of band pair A is almost the same. The difference between these two clusters can mainly be attributed to the intensity ratio of band pair B. It is significantly smaller for the orange than for the pink cluster and thus indicates an increase of aromatic stretch vibrations from the pink to the green and orange cluster. Also, the CH_2 deformation vibration (1454 cm^{-1}) as well as the band dominated by purine bases (1336 cm^{-1}) show an increase in intensity from the green to the orange cluster. Thus, it can be concluded that the orange cluster basically exhibits greater protein content, but mostly differs due to its higher phenylalanine concentration compared to other parts of the sample. This also correlates with the increase in aromatic stretch vibrations as phenylalanine is an aromatic amino acid.

PCA was applied to the baseline corrected standardized data set using the same spectral descriptors as were used for HCA. Component 1 (68.24 %), 2 (13.69 %) and 3 (7.87 %) together explain 89.79 % of the variance of the spectral data although the scree plot suggests that only two principal components are appropriate for this investigation (figure 60). Therefore, only the first two principal components were analyzed which explain 81.92 % of the variance.

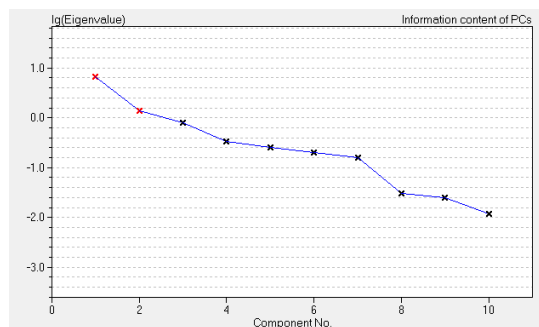


figure 60. Scree plot

Spectral descriptors 1 and 3 have moderate impact on principal component 1 (figure 61). The remaining descriptors have greater influence on PC1 but only little influence on PC2. Spectral descriptor 1 (band at 566 cm^{-1}) and 3 (band at 1094 cm^{-1}) represent Raman bands resulting from the glass background and have great impact on PC2. The other descriptors correspond to Raman bands evoked by the fungal sample. Whether a Raman signal is evoked by the glass background or by the sample seems to be differentiable by principal component 2 and is additionally indicated by the loadings of each spectral descriptor.

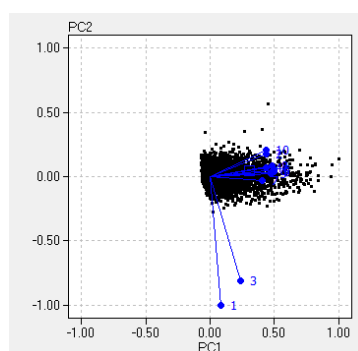


figure 61. Bi-plot

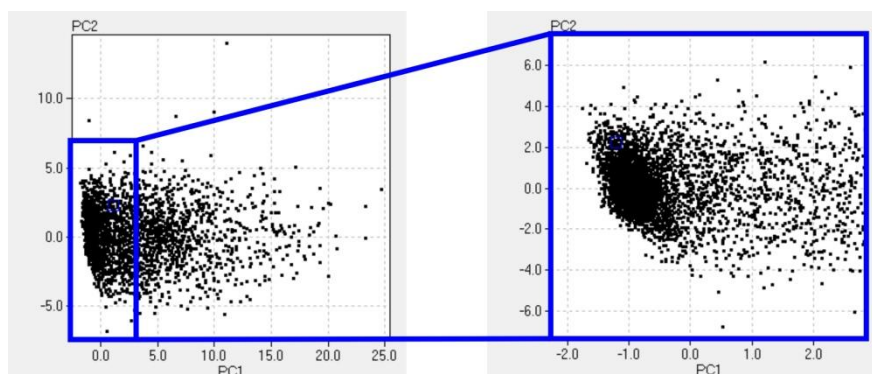


figure 62. Scores of PC1 vs PC2

VI. Hyphae of *P. chrysogenum* - VI.3. First Raman mappings

The scores of the first two principal components are plotted in figure 62. The zoom visualizes a great accumulation of points representing the background of the Raman image which can be further differentiated into pure sample carrier and background containing small amounts of protein mostly located in the periplasm (figure 63). Then, there is the part of the score plot showing increasing score values for PC1. This part represents the hyphae in the Raman image and can further be divided into parts with high protein content and those with lower content towards the tips and edge of the hyphae (figure 64).

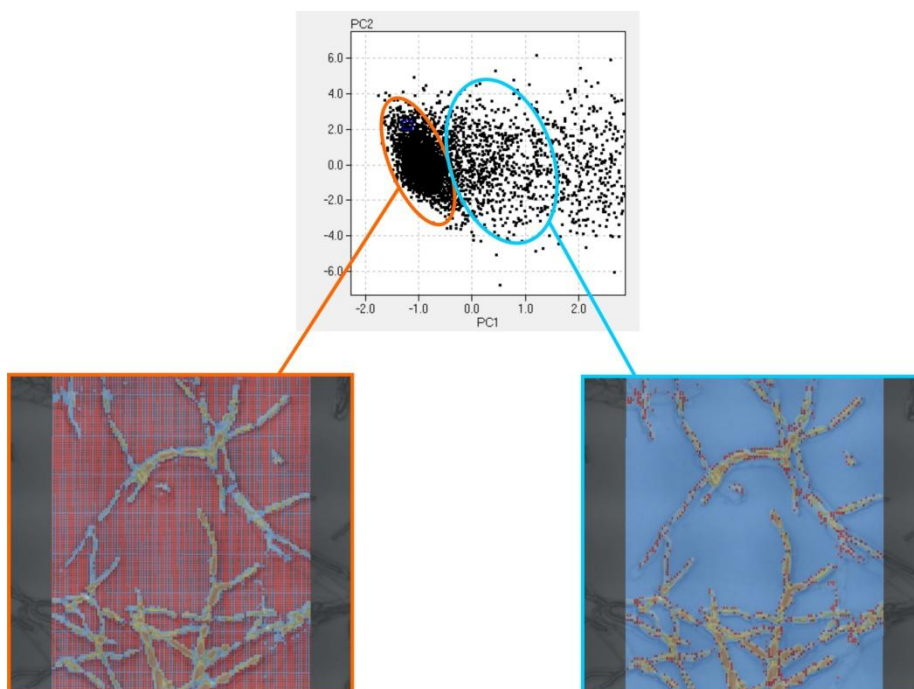


figure 63. Score plot of PCA representing the glass background

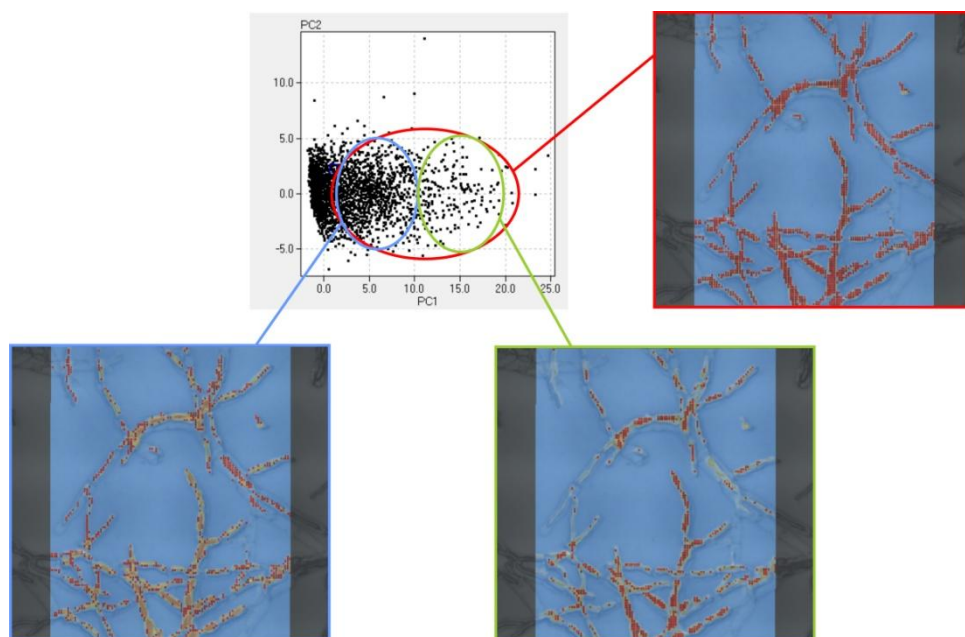


figure 64. Score plot of PCA representing the sample

A better PCA approach was found by excluding the Raman spectra of the background (glass) from data analysis (orange circled points in figure 63). Additionally, the data set was not standardized but mean centered. Standardization compensates the impact of very intense Raman bands such as the CH stretch vibration compared to smaller, but equally important vibrations. To prevent that the result of analysis is too much affected by this intensity difference, the Raman band evoked by CH stretch vibrations was excluded from the spectral descriptor list. Furthermore, spectral descriptors 1 and 3 representing glass bands were also excluded from the list of spectral descriptors.

In the bi-plot of the second PCA (figure 65), the loadings of spectral descriptor 2 evoked by $\nu_{\text{sym}}(\text{O-P-O})$ and spectral descriptor 4 (Amide III) point into similar direction which means that these two vibrations have something in common. Also, spectral descriptor 5 (purine bases and aromatic amino acids) and 10 ($\nu(\text{C=C-H})$ aromatic) show similar orientation. Spectral descriptor 6 representing vibrations mainly evoked by lipids strongly influences PC1 while it has no effect on PC2. The spectra of those scores which are distributed around spectral descriptor 6 differ from the spectra recorded at other parts of the hyphae in their lipid content.

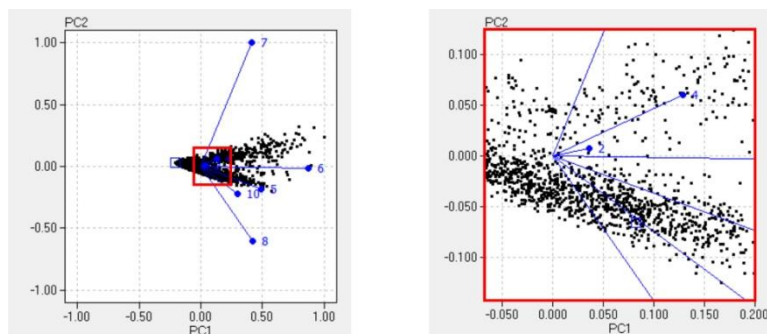


figure 65. Bi-plot of second PCA (mean centered data; spectral descriptor 1,3 and 9 excluded)

Based on the score plot in figure 66 (PC1 vs. PC2) two main areas in the Raman image can be differentiated. The part of the hyphae which was associated with the orange cluster in the previous HCA (figure 57) can also be distinguished from the rest of the data by PCA. The corresponding data points in the score plot are circled in blue.

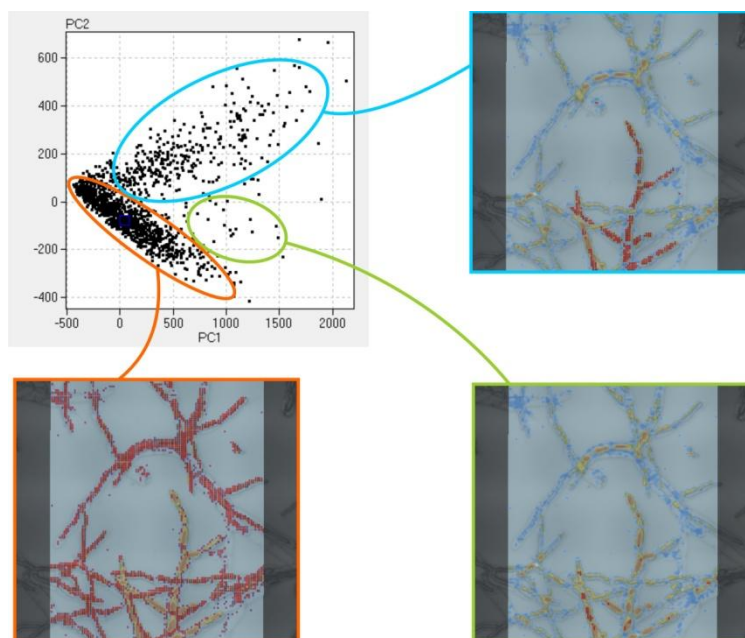


figure 66. Score plot of the second PCA (mean centered data; spectra descriptor 1,3 and 9 excluded)

The PCA mirrors the results obtained by HCA although both methods are based on different principles. In this case, the better insight into the hyperspectral data cube was provided by PCA based on mean centered data compared to the standardized one. However, HCA gives more detailed information about the chemical composition of the hyphae due to the average spectra calculated for each cluster.

VI.4. Raman spectra of stained fungal hyphae

VI.4.1. Fluorescein diacetate (FDA)

Raman measurements were performed using hyphae which were stained with FDA by Daniela. The samples were not washed after staining, as they were immediately investigated by fluorescence microscopy. Therefore, first Raman spectra were recorded of the **stained sample** without any preceding washing steps. The 532 nm Raman laser was used for all measurements as this was the laser most suitable for the sample. It might, however, not be the best choice in combination with FDA. The excitation laser line lies within the absorption band of the fluorescent dye (see IV.2.1) and thus the resulting Raman spectrum will very likely be affected by fluorescence.

In the first spectra that were recorded of the hyphal sample stained with FDA, the Raman bands were masked by an intense fluorescent signal which was to be expected considering the excitation/emission spectrum of the fluorescent dye (figure 67 left). However, the baseline decreased from the first to the third spectrum recorded with 10 % laser power. This indicates that FDA got bleached by the Raman laser. Nonetheless, the bleaching was not sufficient enough to reveal Raman bands. Subsequent increasing of the laser power resulted in an increased baseline. The image of hyphae stained with FDA reveals that the fluorescent stain affects the morphology of the fungus (figure 67 right). The cell wall seems to be damaged resulting in hyphae with low protein content due to cell leakage. Either, the hyphae were already damaged when the sample was taken, or FDA negatively affects the cells' integrity.

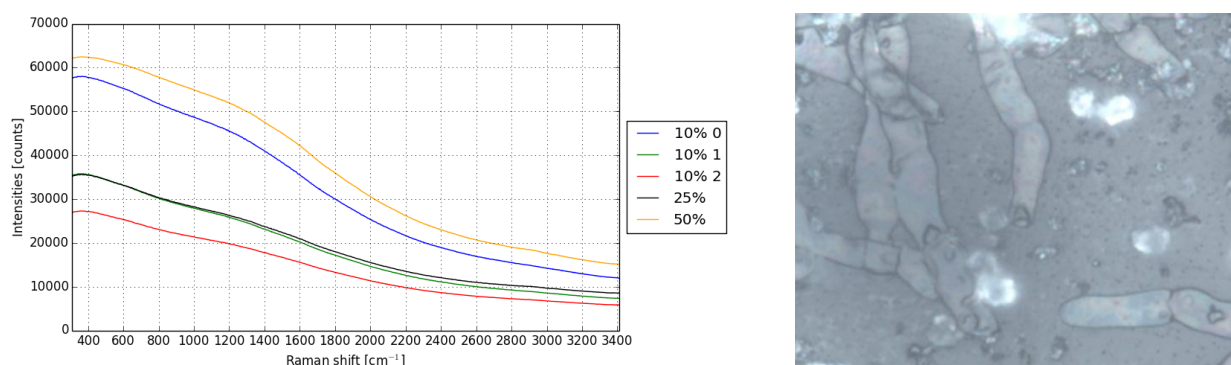


figure 67. Raman spectra (left) and sample image (right) of hyphae stained with FDA (device settings see appendix)

Raman spectra were also collected on a different measurement spot with 10 % laser power. This time, the bleaching effect was sufficient to detect some Raman signal. For the purpose of band assignment the spectrum is compared to spectra of FDA (recorded with 633 nm laser)

and the unstained fungus (recorded with 532 nm laser). This comparison shows that the small Raman band at 1466 cm^{-1} is evoked by the fluorescent dye as it is not present in the spectrum of the unstained hypha, but perfectly matches the band position of one band in the spectrum of FDA (figure 68).

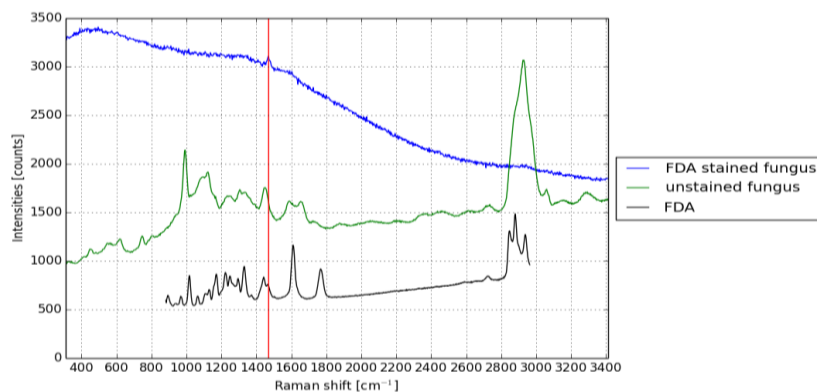


figure 68. Comparison of the Raman spectra of FDA stained hyphae, unstained hyphae and FDA (device settings see appendix)

In a second approach, the FDA stained sample was washed (3x with DI) to remove the surplus of fluorescent dye in the surrounding medium. This should also help to increase the quality of the Raman spectrum. The successful optimization of the Raman spectrum by adding a washing step between staining procedure and measurement can be seen in figure 69. As a next step, it needs to be verified if this improvement is the result of a decreased FDA concentration in the surrounding medium or if the fluorescent stain is completely removed by the washing step due to cell leakage. Furthermore, the investigated part of the hyphae might already have been dead at the time of staining. Thus, fluorescein diacetate would not have been hydrolyzed by esterases to fluorescein and therefore no fluorophore would be present.

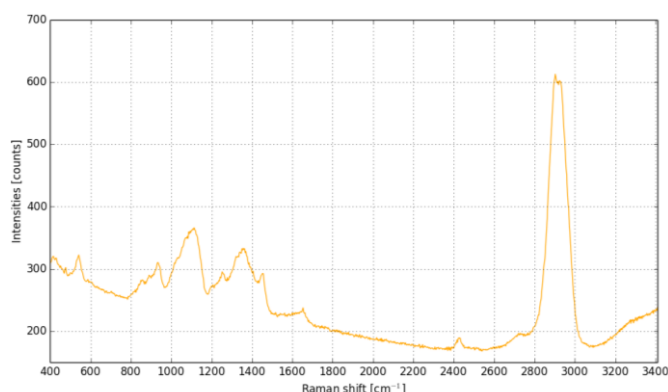


figure 69. Raman spectrum of washed FDA stained hyphae (device settings see appendix)

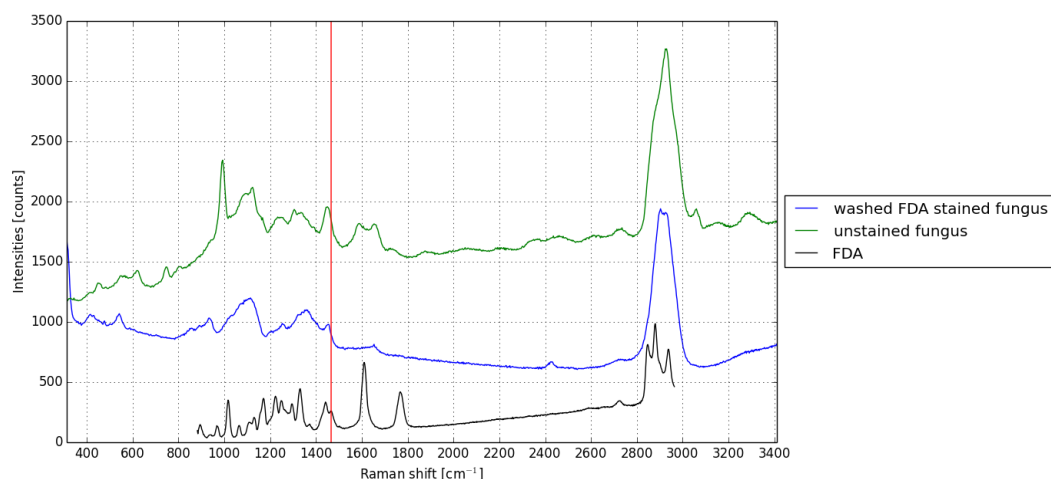


figure 70. Comparison of the Raman spectra of FDA stained and washed hyphae, unstained hyphae and FDA (device settings see appendix)

The band located at 1466 cm^{-1} is probably mainly due to CO and CC stretch vibrations⁴⁵ and is only present in the Raman spectrum of FDA. Comparison of the spectra recorded of the stained and washed sample, the unstained sample and FDA indicates that this precise band is also absent in the spectrum of the stained and washed fungus (figure 70). Thus, it is very likely that the fluorescent dye was completely removed in the course of the washing procedure. Reducing the number of washing steps probably increases the quality of the Raman spectrum without removing fluorescein completely from inside of the hypha. Additionally, it needs to be considered that the hyphae on the sample carrier were damaged prior to the washing step as can be seen in the sample image (figure 67 right). Therefore, the loss of fluorescein during the washing procedure is very likely due to leakage of ruptured cells walls.

VI.4.2. Propidium iodide (PI)

Hyphae stained with PI were washed prior to the investigation with Raman spectroscopy. From previous experiments, it is known that Raman spectra of PI using the green excitation wavelength (532 nm) are very much affected by fluorescence (see IV.2.2). As a result, Raman spectra of PI stained hyphae were recorded using the 780 nm Raman laser in combination with the DXR Raman Microscope provided by Thermo Fisher Scientific. However, only Raman signal of the glass sample carrier could be collected as confirmed by acquiring a spectrum of the microscope slide (figure 71). Characteristic bands resulting from either the hypha or PI could not be detected in the recorded Raman spectrum.

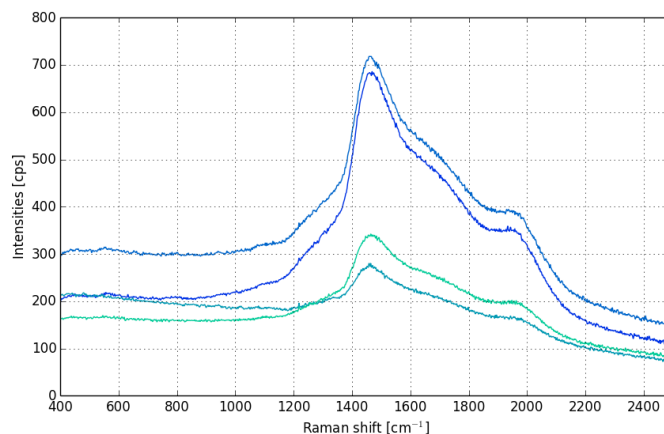


figure 71. Raman spectra of PI stained and washed hyphae (device settings see appendix)

VI.4.3. Fluorescein diacetate (FDA), propidium iodide (PI) and 4',6 diamidin-2-phenylindol (DAPI)

The final protocol for life/dead staining of *P. chrysogenum* was established with FDA and PI. Other dyes were tested e.g. DAPI which was used as reference for PI. DAPI is a popular counterstain and shows great contrast in combination with green fluorescent dyes. Thus, it is perfectly suitable as counterstain for FDA to investigate the sensitivity of PI in fungal samples.

PI (Ex/Em=490/635 nm) has its excitation maximum very close to the excitation wavelength that is most suitable for the hyphae (532 nm). As a result, all spectra recorded with 100 % laser power led to saturation of the CCD detector. Since the laser power per μm^2 increases with the magnification and thus also results in an increased fluorescence, the 50x objective was used for further measurements.

Measurements were performed on the same sample spot varying the laser power between 1 % and 100 %. The bleaching effect of the fluorescent stains can be observed by the decreasing baseline and Raman bands getting visible. The spectra were recorded in the same chronological order as they are listed up in the legend on the right side of figure 72.

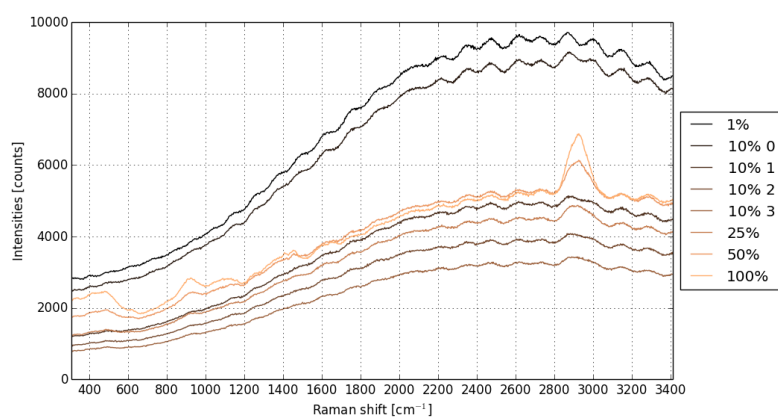


figure 72. Raman spectra of hyphae stained with FDA, PI and DAPI (device settings see appendix)

As those Raman spectra had been recorded a few days before the employed edge filter was replaced by a new notch filter, the interference pattern characteristic for the filter is apparent in the spectra. Nonetheless, the CH stretch vibration at 2930 cm^{-1} becomes visible with increasing bleaching effect. The other bands in the spectral region from 600 cm^{-1} to 1700 cm^{-1} , however, cannot be clearly distinguished from the background noise.

After a washing step, the sample was again investigated with Raman spectroscopy. This time, the 100x objective was used. As it was already observed for the FDA stained hyphae the Raman spectrum of the washed sample is less affected by fluorescence (figure 73 left). The image of the stained and washed hypha indicates damage of the sample by the fluorescent stains as the plasma membrane cannot be identified any more (figure 73 right). The cell wall seems to be intact, however, the hypha looks wrinkled and compromised. Therefore, it is possible that FDA was washed out of the sample again. Nevertheless, PI and DAPI intercalate into the DNA and thus should still be present in the nucleus of the hypha. However, it is unlikely that the chosen measurement spot matches the position of the nucleus. Thus, the recorded Raman spectrum which is again affected by the filter characteristics, probably results from a compromised hypha where the fluorescent stain was removed during the washing step.

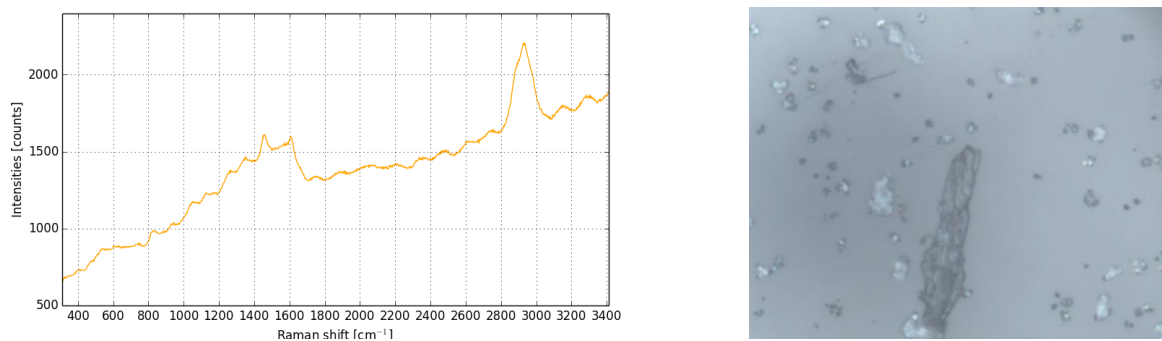


figure 73. Raman spectrum (left) and sample image (right) of a stained (FDA, PI and DAPI) and washed hypha (device settings see appendix)

All in all, attention needs to be focused on the washing step to avoid complete removal of the fluorescent stains. However, the necessity of a washing step is outlined in the recorded spectra of unwashed samples which are mostly masked by fluorescence. Also, the hyphae seem to be compromised by the fluorescent stains which needs to be considered for further interpretation of the recorded Raman spectra.

VI.5. Conclusion

A lot of research is done in the field of Raman spectroscopy of bacterial samples compared to the spectroscopic investigation of fungal samples. Even less information could be found about Raman spectra of *P. chrysogenum* in current literature.

Device settings need to be adapted to the sample considering laser power, magnification, integration time and confocal pinhole size. For covering every detail of the sample, the 100x objective was chosen for the majority of measurements. The maximum laser power adjustable was 50 %. Setting a laser power of 100 % results in carbonization of the hypha which is indicated by intense graphite bands and an increased baseline. Due to the use of a CW laser, the sample was not only exposed to thermal stress during the measurement on a single measurement spot, but during the entire imaging time. Therefore, a compromise needed to be found between, image size, integration time (S/N ratio) and step size for optimal results corresponding to the requirements of the operator.

Small and large scale mappings were performed with different device settings. Both were analyzed through PCA and HCA algorithms. The focus was set onto the investigation of different chemical groups representing single parts of the sample. An increase of phenylalanine concentration in the cytoplasm could be observed for several hyphal branches in the large scale

mapping. Observations in the small scale mapping indicate that the amount of nucleic acids and the intensity of the amide III band are higher in the cytoplasm. Still, an interpretation is difficult as the hyphae are dried at room temperature on the microscope glass slide. This drying process results in shrinking of the biological material due to denaturation. However, primary aims were the establishment of appropriate device settings, the recording of Raman spectra of hyphae and the investigation of those spectra concerning promising marker bands for future dead/alive studies. So far, only dead (denaturated) hyphae were investigated. For the study of living sample, the sample preparation needs to be improved to obtain more representative Raman spectra.

Raman spectra of fungi stained with fluorescent dyes can be recorded as long as the excitation laser wavelength does not lie within the absorption band of the fluorescent stain. A certain overlap between excitation wavelength and absorption band cannot be avoided once several fluorescent stains are used. Improvement of the quality of the Raman spectrum can be achieved by bleaching the fluorescent dye (if the sample can stand the thermal stress) which excludes the possibility of performing fluorescent microscopy after Raman measurements or by a washing step prior to the measurement to remove the surplus of dye in the surrounding medium. This washing step needs to be optimized to avoid complete washing out of the fluorescent stain. Furthermore, the sample's integrity is affected by the fluorescent stains which needs to be considered in the interpretation of corresponding Raman spectra.

VII. Spores of *P. chrysogenum*

VII.1. Raman spectroscopy of fungal spores

The investigation of fungal spores is getting more and more attention since fungi are ubiquitously present and may affect our health in various ways. In 2012, Ghosal et al.⁴⁶ presented the investigation of spores from several species of microfungi using Raman microspectroscopy (RMS). The aim was to develop a RMS-based library for fast identification of indoor and outdoor fungi. In their research, they also mentioned laser- induced degradation of some basidiomycete spores leading to graphitization of organic material. Various species of the genus *Lactarius* were investigated by De Gussem et al.⁴⁷. Based on Raman spectra of spores and reference spectra of polysaccharides, lipids, and other biomolecules which are likely to be present in fungal samples, they analyzed the chemical composition of spores. Although they were facing some difficulties due to many overlapping bands, they could confirm that *Lactarius* spores contain high amount of lipids. Furthermore, they had reason to believe that the spore walls contain chitin. Vibrational spectroscopy was also applied for investigating spores of wild growing mushrooms. In their study, Mohacek-Grosev et al.⁴⁸ analyzed fungal samples of more than 20 different genera of Asco- and Basidiomycetes regarding their chemical composition. Most of the samples were analyzed using infrared spectroscopy while four samples of spore powder were investigated with Raman spectroscopy. An improved measurement set-up for fast Raman imaging with point-scan resolution based on the application of galvo-mirrors was presented by Kong et al.⁴⁹ in 2011. With this multifoci-scan scheme for dynamic confocal Raman microscopy, they were able to show the spatial distribution of Ca-dipicolinic acid during germination of *Bacillus megaterium* spores.

This short overview of literature shows that there is vivid interest in classification and investigation of chemical composition of fungal samples (and also of bacteria) as they play an important role in biotechnology, the medical sector and the food- industry. Furthermore, they are essential organisms of our ecosystem and masters in adaption to extreme environmental conditions. Detailed knowledge of the early stages of the fungal life cycle implicates the investigation of spores which can help improving yields in current biotechnological processes, achieving an even more time efficient production cycle or reducing time and therefore money for downstream processing.

VII.2. Device settings

Three different laser excitation wavelengths were investigated to define proper device settings for collecting Raman spectra of spores.

VII.2.1. 532 nm Raman laser

First measurements were performed using the 532 nm Raman laser with similar parameter settings as were set for the hyphae. However, lower laser power was adjusted to avoid graphitization of basidiomycete spores due to laser-induced damage as reported by Ghosal et al.⁴⁶. Nevertheless, the Raman spectrum of spores was mostly affected by fluorescence and intense graphite bands resulting from carbonization of the organic material (figure 74) once a laser power ≥ 0.1 % was adjusted. At lower laser powers, however, a Raman signal is not collectable. Although the Raman spectrum contains graphite bands applying 1 % laser power, the CH stretch vibration indicating intact biological material is still visible. None of those bands are present in the spectra recorded with lower laser power. Thus, it can be concluded that 0.01 % laser power is too low for detecting a Raman signal as the CCD detector is not sensitive enough for this small amount of scattered Raman photons. The thermolability of spores compared to hyphae indicates a significant difference in the chemical composition and physical properties between the two samples. Rizza et al.²⁶ investigated chemical differences between hyphae and spores of *Penicillium chrysogenum* in 1969 using electrophoresis. According to their research, hyphal walls contain less galactose but more glucosamine. Generally speaking, cell walls of spores contain less amino acids than hyphal ones. In particular, amino acids such as glycine, agrinine, lysine and threonine were proven to be only present in hyphal walls. Maybe, there is a link between different sugar contents and thermolability. The disaccharide trehalose for example is well known for its property of preventing cells from dehydration due to its clam shell conformation which allows perfect interaction with the headgroups of the phospholipid bilayer.⁵⁰

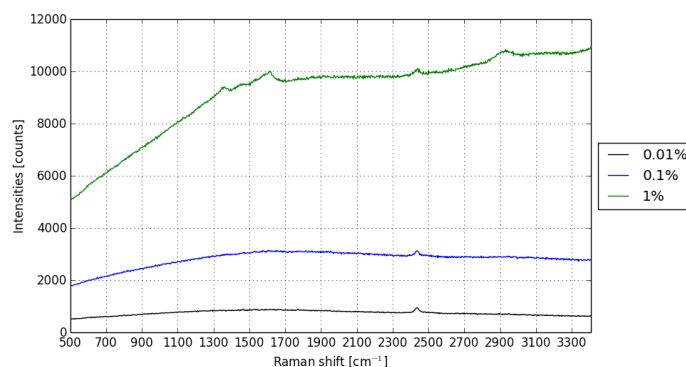


figure 74. Raman spectra of spores of *P. chrysogenum* (device settings see appendix)

The Raman band at 2435 cm^{-1} is present in all three spectra shown in figure 74. However, the signal is not evoked by the sample but instead results from the light in the laboratory where measurements were performed. This was confirmed by Raman spectra collected with the shutter (permitting the laser light passing through the optical path) being closed with lights in the room switched on and off. One of the most intense bands in the Raman spectrum with lights on (blue spectrum in figure 75) is positioned around 2435 cm^{-1} which corresponds to the band visible in the spore spectra (figure 74). If the Raman signal of the sample is not very intense, those bands will be visible in the sample spectrum. Therefore, further spore measurements were conducted with the lights in the room switched off.

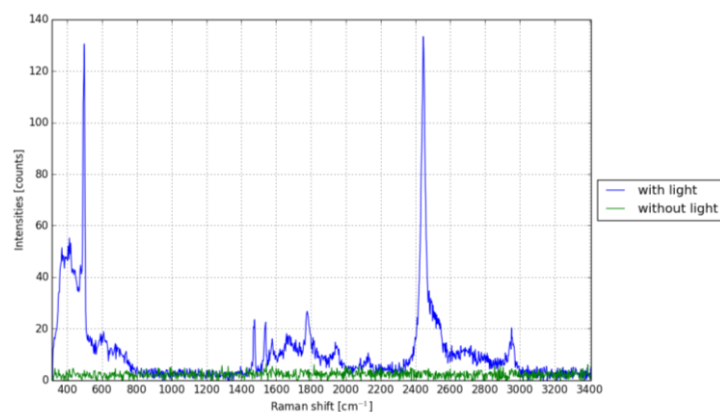


figure 75. Raman spectra recorded without a sample with the room lights switched on and off (devices settings see appendix)

The fact that spores are carbonized at higher laser powers can also be seen in the images taken by the camera before and after a series of measurements at one single measurement spot. The spore literally vanishes after being hit by the laser beam (figure 76).

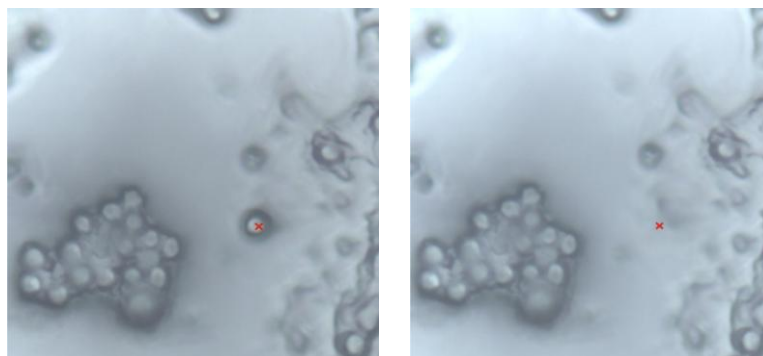


figure 76. Measurement position (red cross) before (left) and after (right) the Raman laser (532 nm) hits the sample

In conclusion, no Raman signal of spore samples could be detected underneath 1 % laser power while graphitization of the organic material occurred once this laser power had been set. Therefore, different strategies for heat dissipation were investigated.

VII.2.1.1. *Heat dissipation through aqueous environment*

One attempt to avoid carbonization of organic material consisted of putting the sample into an aqueous environment. Therefore, a spore sample dried on a microscope slide was carefully put into a petri dish filled with dionized water (figure 77). Even in contact with water the spores remained on the sample carrier. Measurements were carried out with the 100x water immersion objective.

Heat dissipation, however, could not be achieved. Instead, the graphitization effect can already be observed by applying 0.1 % laser power (figure 78). Differences in the spore sample provided by Daniela may result in different chemical properties and therefore different sensitivity for thermal stress which explains dissimilar response to the same laser power. Again, no Raman signal at all could be detected below 0.1 % laser power.



figure 77. Spore sample on microscope slide in aqueous environment in the petri dish

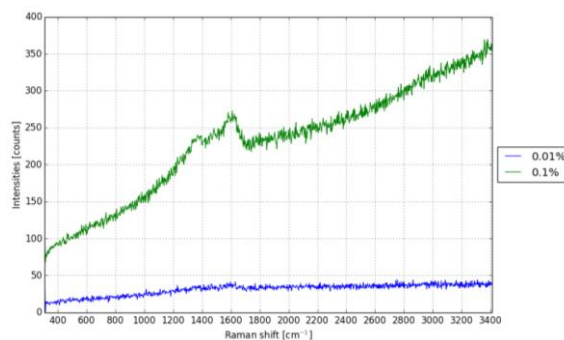


figure 78. Raman spectrum of spore sample in aqueous environment (device settings see appendix)

VII.2.1.2. *Change of sample carrier*

Using commercially available aluminum foil as sample carrier instead of a glass slide was the second attempt to achieve heat dissipation. Additionally, the aim was to increase the Raman signal due to multiple reflections of the photons on the aluminum foil such that a laser power of 0.01 % would be sufficient enough to obtain a Raman signal.

This time, three different measurement positions were investigated with the 100x objective (figure 79). An increasing integration time results in an increased time for the collection of Raman photons but also increases the risk of laser-induced damage of the sample. Therefore, different integration times were set at a constant laser power of 0.1 %. The Raman spectra are color-matched with the according measurement position in figure 79.

The Raman spectra in figure 80 illustrate differences in the thermolability between spores of the same sample. While carbonization is indicated in the blue spectrum, no Raman signal (and thus probably no graphitization) could be recorded for another spore even with higher integration time (red spectrum). Further measurements (green spectra) were performed with the same settings except for integration time (see figure 80). The resulting spectra indicate a significant baseline increase that can be observed for the green spectra compared to the red one. Carbonization of the sample increases the background signal which becomes even more intense with higher integration times. This increase in signal results in saturation of the CCD detector. The Raman spectra in figure 80 outline that spores are not only thermolabile, they also show autofluorescence which additionally masks the Raman signal and thus affects the quality of the Raman spectrum.

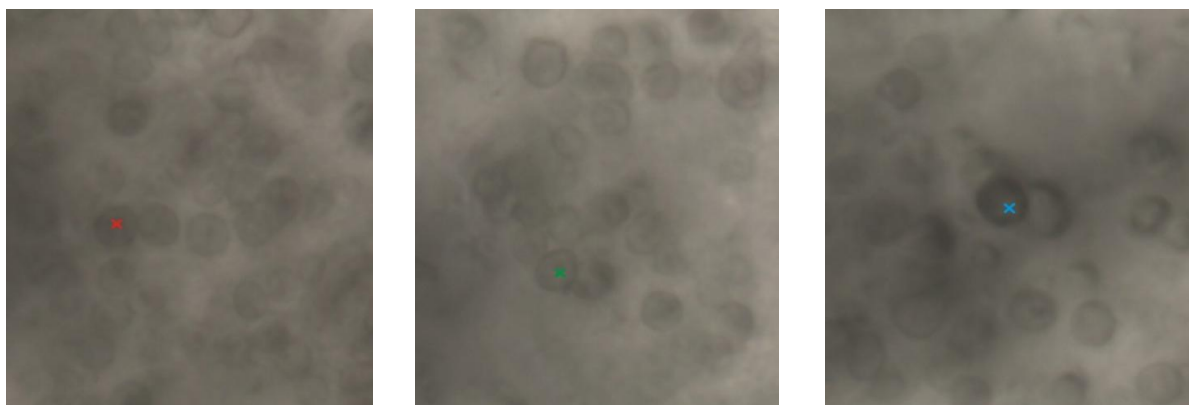


figure 79. Three different measurement spots for collecting Raman spectra of spores on aluminum foil

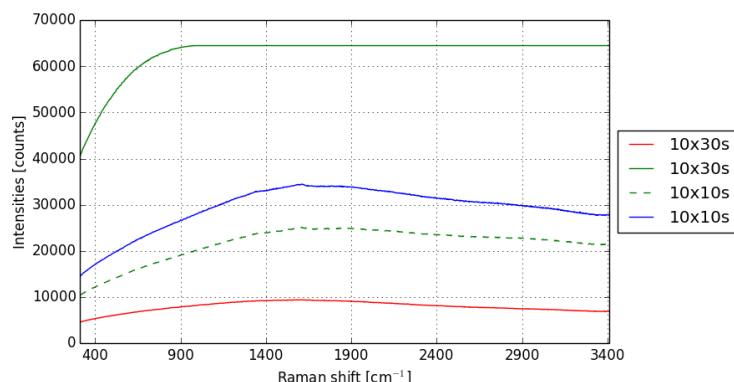


figure 80. Raman spectra of spores on aluminum foil recorded at three different measurement spots; the set integration times are indicated in the legend on the right (see figure 79; device settings see appendix)

As has already been observed previously with the attempt of heat dissipation based on the establishment of an aqueous environment, the only bands visible in the recorded Raman spectra result from carbonization of organic material and are additionally affected by autofluorescence of the spores and graphite.

VII.2.1.3. *Cryo-stage*

A cryo-stage (figure 81) consisting of a Dewar vessel connected to an evacuated sample chamber was fixed onto the x,y,z-stage of the Horiba LabRAM 800HR spectrometer. A vacuum of approximately 5×10^{-2} mbar was achieved with the oil-sealed vacuum rotary vane pump. The Dewar vessel was continuously cooled with liquid N_2 . The whole set-up consisting of the Raman spectrometer, the cryo-stage and the vacuum pump is shown in figure 82. Stage and vacuum pump were kindly provided by Prof. Grothe of the Institute of Materials Chemistry.

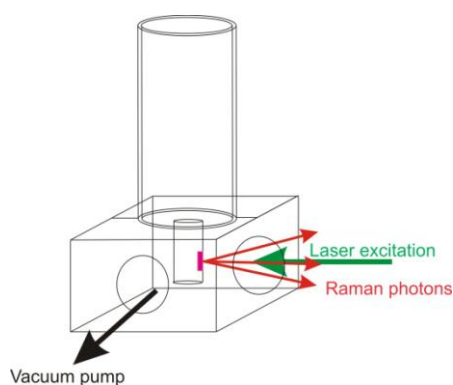


figure 81. Schematic representation of the cryo-stage

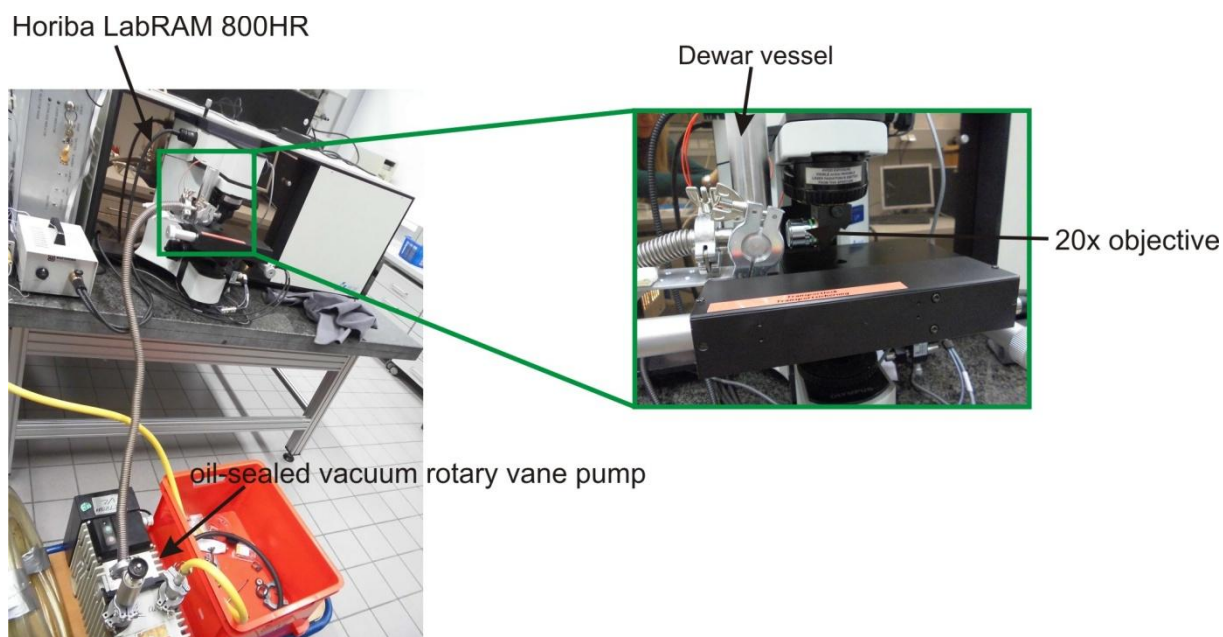


figure 82. Photograph of the set-up consisting of the Raman spectrometer (Horiba LabRAM 800HR), the cryo-stage fixed onto the XYZ-stage and the vacuum pump

A droplet of washed spores was put onto the gold surface of the cryo-stage and dried at room temperature over night. After calibration of the 532 nm- laser with silicon the cryo-stage was mounted onto the x,y,z-stage of the LabRAM instrument. The vacuum pump was put into operation. It is very important not to turn off the vacuum pump as long as it is connected to the vacuum chamber in order to avoid getting oil into the sample chamber. Once a vacuum of approximately 5×10^{-2} mbar has been obtained, the Dewar vessel was filled with liquid N_2 . A closer look on the cryo-stage with the cooled Dewar vessel connected to the vacuum pump is given in figure 83. The laser beam was focused on the sample through a quartz window of the evacuated sample compartment. Due to the distance between quartz window and sample carrier, objectives with a working distance of at least 5 mm had to be used. Therefore, measurements were exclusively performed with the 20x objective (working distance $WD=20.50$ mm) as the working distances of the standard 100x ($WD=0.21$ mm), 100x long working distance ($WD=3.40$ mm) and standard 50x objective ($WD=0.38$ mm) are too small.

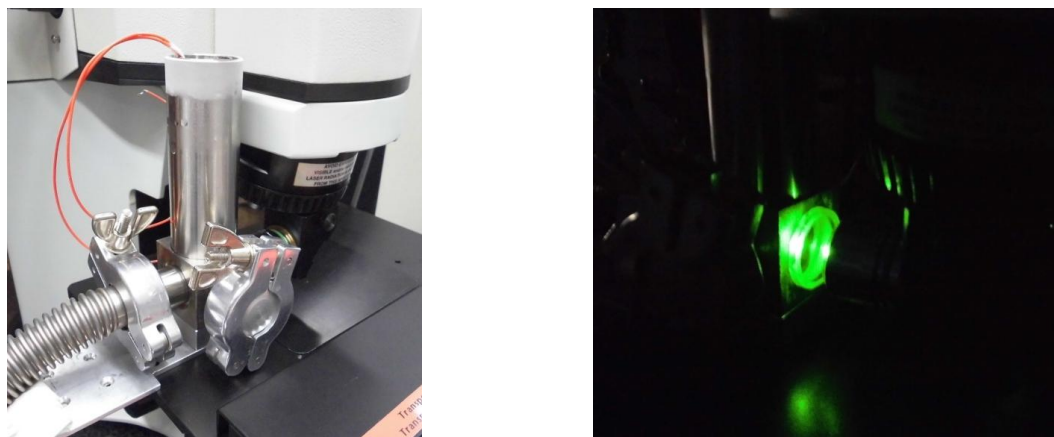


figure 83. Cryo-stage with the cooled Dewar vessel (left); the laser beam is focused with a 20x objective through a quartz window onto the sample on the gold surface (right)

First measurements were carried out with the **532 nm- laser** using 0.1 % and 1 % laser power. Measurements were performed in the same chronological order as they are listed up in the legend of figure 84. Using this set-up, it seems that graphitization of the sample could be avoided as no Raman bands of amorphous carbon are visible in the recorded Raman spectra. However, using 532 nm as excitation wavelength leads to an intense fluorescence signal evoked by the spores which renders this laser unsuitable for this kind of measurements. In order to overcome this fluorescence, a laser in the near infrared (e.g. 785 nm Raman laser) would probably be of advantage as wavelengths in this spectral region are less probable of exciting fluorescent transitions. Therefore, the Raman signal would be more intense than the fluorescence of the sample.

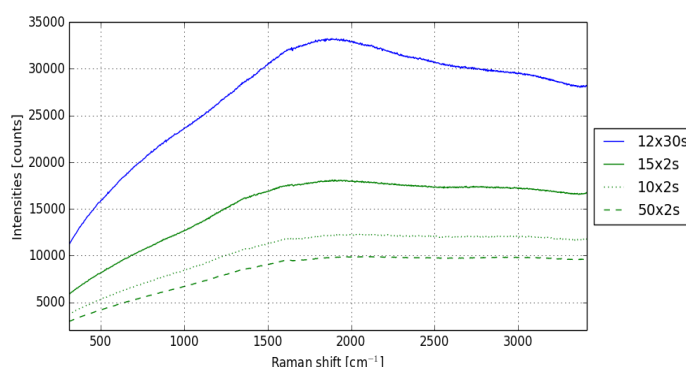


figure 84. Raman spectra of spores on the cryo-stage with the set integration time in the legend on the right: blue spectrum = 0.1 % laser power, green spectra = 1 % laser power (device settings see appendix)

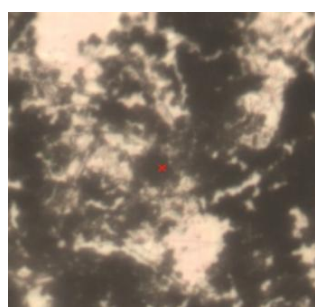
However, a bleaching effect is observable (figure 84). Spectra recorded with 1 % laser power (green spectra) show a lower baseline than the spectra recorded with a 10^{-1} times weaker laser

power (blue spectrum). Taking into consideration that the blue spectrum was recorded prior to the green spectra, the bleaching effect of the Raman laser is nicely demonstrated. However, no Raman band is observable except for some very weak signal masked by the intense fluorescence around 1365 cm^{-1} and 1614 cm^{-1} which most certainly is evoked by graphite (green spectra). It can thus be hypothesized that the spore sample was carbonized with 1 % laser power using the 20x objective and cooling with liquid nitrogen.

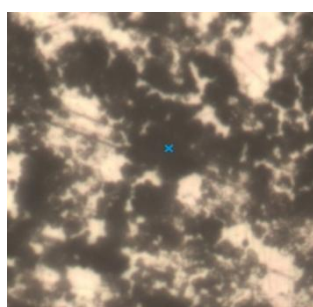
The same sample was also investigated with the **633 nm- laser**. Raman spectra of fungal spores were collected at three different measurement positions (figure 85) with the parameter settings listed up in table 9. Each spectrum in figure 86 is color-matched to the according measurement spot. However, neither varying the laser power (0.01 % and 0.1 %) nor changes in the integration time (see table 9) did lead to a significant improvement of the resulting Raman spectrum. Again, heat dissipation is not efficient enough to prevent the spore sample from carbonization. As the region where the intense heat effect takes place is very small ($1.9\text{ }\mu\text{m}^2$), the cooling system cannot react quickly enough to efficiently prevent damage of the sample through thermal stress. Nevertheless, there is a decrease in baseline observable compared to the spectra recorded with the 532 nm laser indicating that chromophores of the sample are less excited by the 633 nm laser.

table 9. Parameter settings for the spectra in figure 86

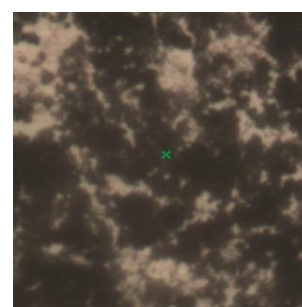
| Spectrum | Laserpower [%] | Confocal hole [μm] | Entrance slit [μm] | Acquisition time [s] | Number of accumulations |
|------------|----------------|---------------------------------|---------------------------------|----------------------|-------------------------|
| red | 0.01 | 500 | 1000 | 60 | 12 |
| Red dotted | 0.01 | 500 | 1000 | 60 | 30 |
| Blue | 0.1 | 500 | 1000 | 20 | 30 |
| Green | 0.01 | 500 | 1000 | 90 | 30 |



Measurement position I



Measurement position II



Measurement position III

figure 85. Three different measurement spots (I-III) of the Raman spectra in figure 86

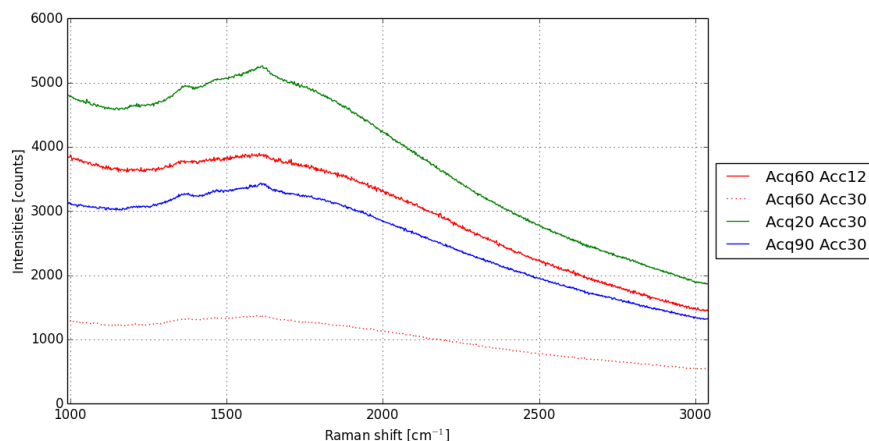


figure 86. Raman spectra of spores the cryo-stage with the set integration time in the legend on the right (device settings see table 9)

To conclude, there is intense fluorescence in the spectra recorded with 532 nm excitation. Therefore, neither Raman bands of the sample nor bands of amorphous carbon are visible in the spectra. However, using the 633 nm laser in combination with the cryo-stage reduces fluorescence in the Raman spectra. Nonetheless, heat dissipation is not effective enough to prevent damage of the sample.

VII.2.1.4. Heat dissipation through reduction of laser power/ μm^2

Another way of reducing thermal stress for the spores during measurements is to decrease the laser power per μm^2 that hits the sample. There are several ways to accomplish this goal. First of all, reduction of the laser power would be an option. However, this did not lead to any improvement (see previous paragraphs). The diameter of the laser spot size and thus the power per μm^2 depends on the objective and the wavelength of the Raman laser (see V.2.2). Therefore, the second possibility is to use an objective with smaller magnification (and thus a smaller numerical aperture). The third solution is to use different laser wavelengths which will be discussed in more detail in sections VII.2.2 and VII.2.3.

VII.2.1.4.1. Change of objective

As with greater magnification the laser power is focused on a smaller area, one possibility to prevent carbonization of the sample is to increase the area covered by the laser beam. This means that the same amount of energy is distributed over a greater area and thus the laser power per μm^2 decreases. Therefore, measurements were conducted using the **20x objective**

instead of the 50x or 100x objective. Using the 50x objective instead of the 100x objective leads to a reduction of the laser power per μm^2 of about 30%. Replacing the 50x objective with the 20x objective further decreases the laser power per μm^2 to approximately 15% compared to the 100x objective (see V.2.2).

As the laser power per area decreases, longer integration times were set to increase the chance of collecting enough Raman photons at the CCD detector. Three different measurement spots were investigated (figure 87). The little cross indicating the measurement spot matches the color of the according Raman spectrum (figure 88). As could already be seen in previous measurements, little spectral information can be gained with a laser power of 0.01 %. Due to the longer integration times that were used in this experiment, amorphous carbon bands are already visible in the Raman spectrum of spores recorded with 0.01 % laser power.

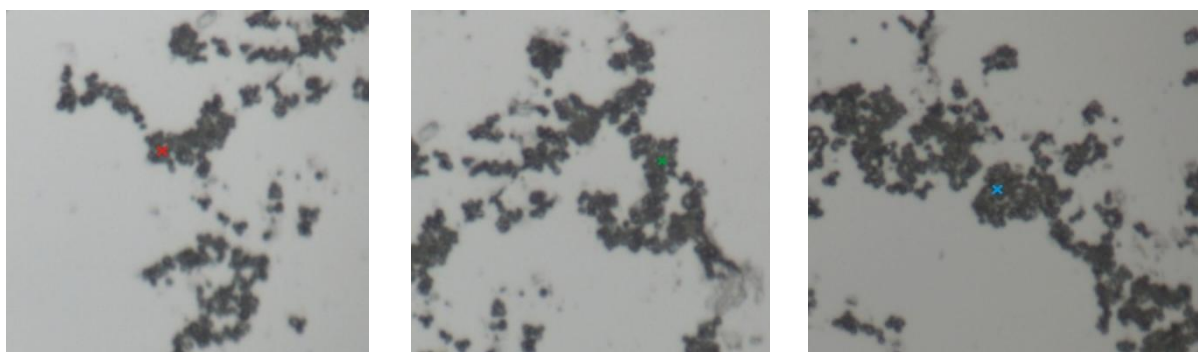


figure 87. Three different measurement spots were investigated to record Raman spectra of spores with smaller magnification (20x)

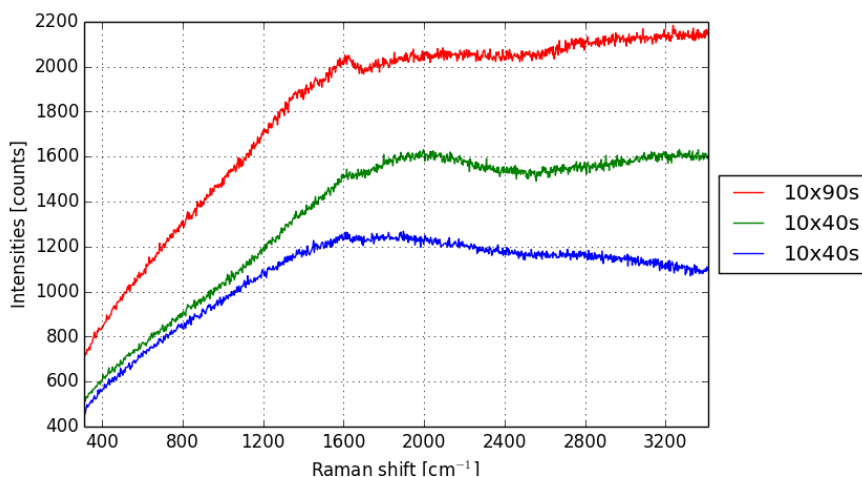


figure 88. Raman spectra of spores recorded with 20x objective; the integration time is listed up in the legend on the right (device settings see appendix)

VII. Spores of *P. chrysogenum* - VII.2. Device settings

Thus, we can conclude, that with the lowest laser power adjustable (0.01 %) no Raman bands of the intact sample are recorded (blue spectrum in figure 88). With increasing integration time, the spores are also longer exposed to the heat of the Raman laser. Therefore, the only Raman bands visible in the spectrum are carbon bands resulting from graphitization of the sample.

VII.2.1.4.2. *Laser pointer*

A green laser pointer ($\lambda=532\text{ nm} \pm 10\text{ nm}$; class III laser) with a maximum output of <20 mW was used to generate Raman spectra. The laser pointer was adjusted to the sample surface with a tripod. However, it had to be manually switched on and off. Raman photons were then collected through the 20x objective and the notch filter with the CCD camera.

VII.2.1.4.2.1 Toluene reference spectra

Before spore measurements were conducted, toluene measurements were performed using the 532 nm Raman laser and the green laser pointer (see figure 89) in order to investigate any possible band shifts in the obtained Raman spectrum depending on the light source.

A cuvette (Hellma; 10 mm light path) was filled with toluene (Fluka $\geq 99.5\%$) and tightly sealed. The optimal measurement position was found by varying the z-focus of the 20x objective until the signal of the toluene spectrum was at its maximum.

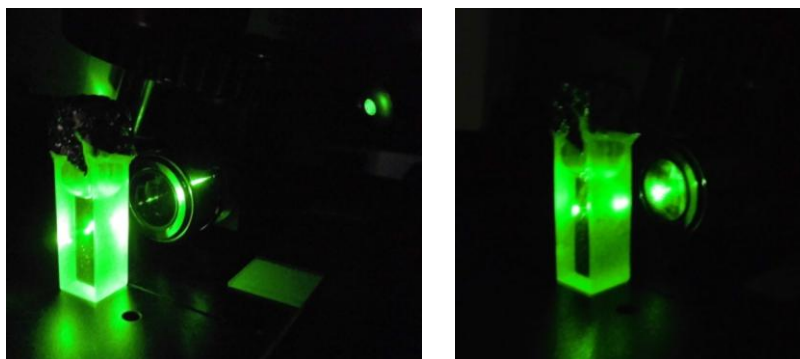


figure 89. Measurement with laser pointer (left) and Raman laser (right)

Even though the Raman signal of the spectra recorded with the laser pointer is significantly weaker than the one with the Raman laser, the band position as well as the relative band intensities remain identical between both spectra (figure 90). This means that Raman spectra recorded with the green laser pointer are in good agreement with the ones recorded with a

standard Raman laser and additionally allow reduction of the thermal stress the sample is exposed to during a specific measurement time.

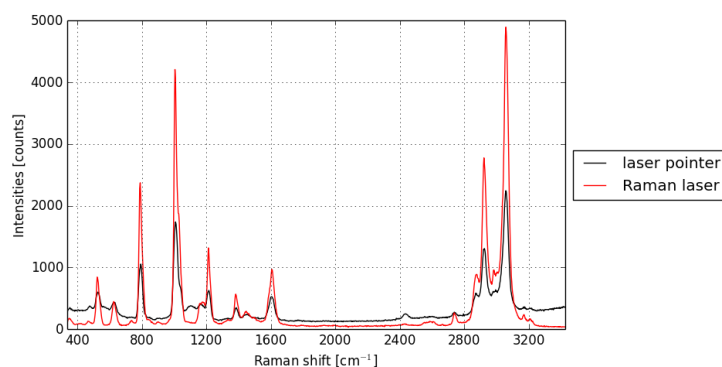


figure 90. Raman spectra of toluene with the green Raman laser and the laser pointer as light source (device settings see appendix)

VII.2.1.4.2.2 Spore spectra

Raman spectra of spores on a microscope glass slide were recorded using the green laser pointer. First, the focus was set on the desired sample area. Then, the laser pointer was set accordingly for maximum signal by visual adjustment via the camera image. Raman photons were collected through the 20x objective.

Spores and hyphae show different distribution of biomolecules which was investigated by Rizza et al.²⁶ but they still share several bands in their Raman spectra such as the CH stretch vibration, amide I band or lipids. Therefore, a comparison of hyphal spectra recorded with the 532 nm laser with spore spectra recorded with the green laser pointer can be done in order to evaluate the significance of the recorded spore spectra. The grey shaded area in figure 91 indicates the spectral regions where Raman bands would be expected.

Raman spectra of spores recorded with the green laser pointer contain four bands (figure 91). However, none of them seems to fit the bands from the Raman spectrum of a hypha of *P. chrysogenum* except for the glass band at 1100 cm⁻¹ evoked by the sample carrier. The remaining bands could be explained assuming that the bands in the spore spectrum shift to the left with increasing wavenumber. However, as it was previously outlined by toluene measurements (chapter VII.2.1.4.2.1) there is no band shift observable between Raman spectra recorded with the Raman laser and the laser pointer. Thus, a band assignment in comparison with the Raman bands evoked by hyphae is not possible. Maybe, the laser pointer was not focused on the right z-plane. Furthermore, the focus could have been changed when the laser

VII. Spores of *P. chrysogenum* - VII.2. Device settings

pointer was manually switched on and off. Nonetheless, the spore sample most probably did not get carbonized as there are more than two bands visible in the spectrum. If amorphous carbon was present, other Raman bands would have been masked underneath intense graphite bands. However, the CH stretch vibration which dominates the Raman spectrum of a hypha is absent in the spore spectrum recorded with the laser pointer.

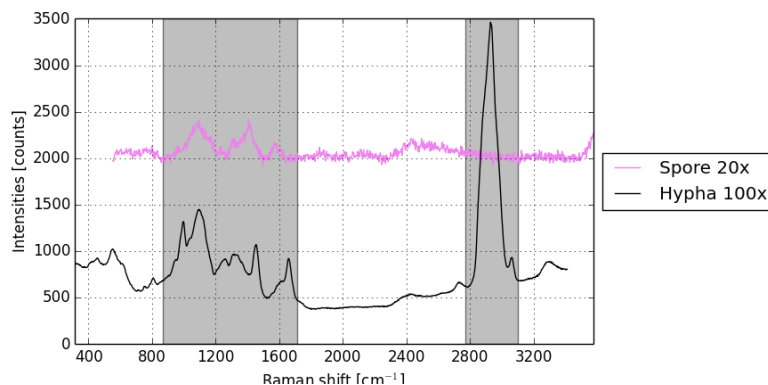


figure 91. Raman spectra of spores (532 nm laser pointer) compared to a Raman spectrum of a hypha (532 nm- laser)

In conclusion, Raman bands are visible in the spectrum recorded with the green laser pointer. The observed bands are probably not evoked by carbonized organic material. However, further improvement of the set-up is needed to avoid the laser pointer being manually operated and thus enhance the reproducibility and quality of the Raman spectra.

VII.2.2. 633 nm Raman laser

Besides of lowering the laser power and using different objectives to decrease the laser power per area, a different laser wavelength can be used. Similar spore measurements with varying laser power were performed with the 633 nm excitation wavelength. However, the same observation as with the 532 nm laser was made: Organic material is carbonized (figure 92). Nonetheless, the CH stretch vibration at 2933 cm⁻¹ is visible in the spectra recorded with a laser power >10 % which indicates the presence of intact sample parts. Compared to the Raman bands evoked by amorphous carbon, the CH stretch vibration is less intense which outlines the effect of carbonization in terms of an increased baseline in the Raman spectrum. A closer look at the spectra recorded with lower laser power is given in figure 93 indicating that carbonization already happens at 0.1 % laser power. Also, no Raman signal could be collected with the lowest laser power adjustable (0.01 %).

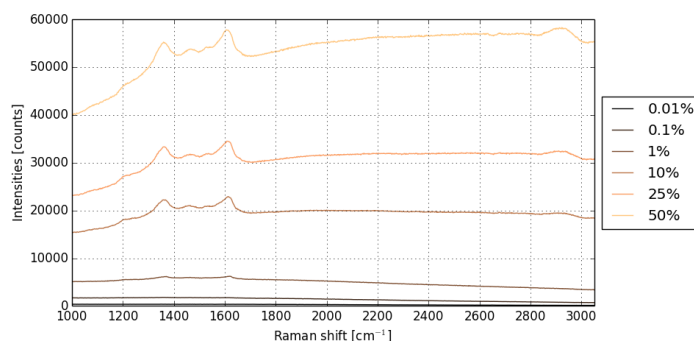


figure 92. Raman spectra of spores recorded with the 633 nm Raman laser (device settings see appendix)

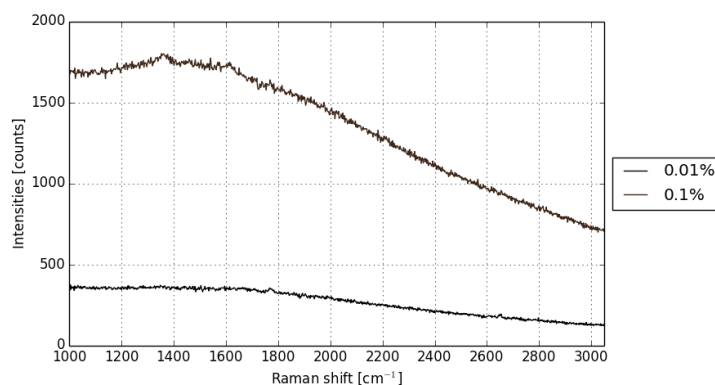


figure 93. Zoom of figure 92 showing spore spectra recorded with 0.01 % and 0.1 % laser power

To conclude, the observations made for spectra recorded with the 532 nm laser were mirrored in the Raman spectra obtained with the 633 nm laser. Thus, no improvement was noticeable with this laser line.

VII.2.3. 785 nm Raman laser

The third laser investigated emits in the near infrared region which has lower energy due to the higher wavelength and thus reduces fluorescence in the Raman spectra as chromophores are not excited any more.³⁴ Based on excitation with higher wavelengths, the limits of quantum efficiency of the CCD detector are reached at higher Raman shifts. Therefore, the CH stretch vibration (2933 cm^{-1}) which was the only band visible so far in the Raman spectra of spores besides of carbon bands cannot be recorded any more.

The Raman shift and thus the positions of the bands in the Raman spectrum do not depend on the excitation wavelength. Nonetheless, measurements of the sample carrier (microscope glass slide) indicate different band positions in the Raman spectra recorded with the 532 nm laser or the 785 nm laser, respectively (figure 94). Using the 532 nm Raman laser, the glass band is

positioned at 1087 cm^{-1} Raman shift while a very intense band at 1380 cm^{-1} is visible in the Raman spectrum recorded with the 785 nm laser. This observation can be explained by the 785 nm laser causing fluorescence of the sample carrier. Considering the fluorescence spectrum of a glass slide with 532 nm and 785 nm as excitation wavelengths (figure 95), there is an intense fluorescent signal recorded at 693 nm and 880 nm . The Raman band at 1380 cm^{-1} Raman shift recorded with the 785 nm laser (equation 14) corresponds exactly to the fluorescent signal at 880 nm , respectively. Thus, the Raman spectrum recorded with the NIR-laser is affected by fluorescence of the glass slide. On the contrary, the Raman spectrum with 532 nm excitation wavelength covers the range from 544 nm (400 cm^{-1} Raman shift) to 649 nm (3400 cm^{-1} Raman shift). Therefore, the Raman spectrum recorded with the 532 nm laser is not affected by the broad band in the fluorescence spectrum of the glass slide. However, the band at 1100 cm^{-1} (565.07 nm) and 550 cm^{-1} Raman shift (548.04 nm) may also result from fluorescence of the glass slide as they perfectly match the two peaks at 548 nm and 565 nm in the fluorescence spectrum with 532 nm excitation. Nonetheless, fluorescence is not very intense and the Raman signal of the sample placed on the microscope glass slide is only slightly affected but not hidden underneath the fluorescent signal (see VI.2).

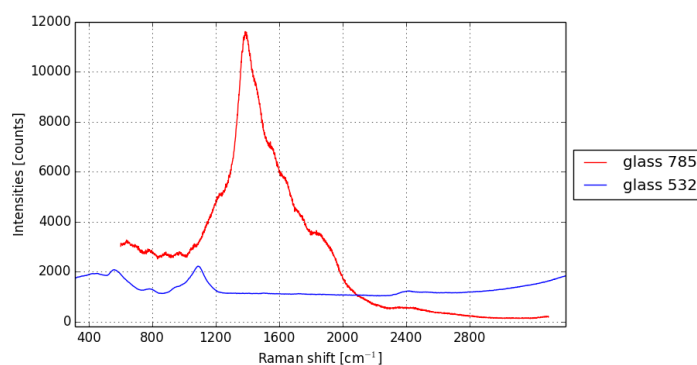


figure 94. Raman spectra of glass recorded with the 532 nm Raman laser and the 785 nm Raman laser (device settings see appendix)

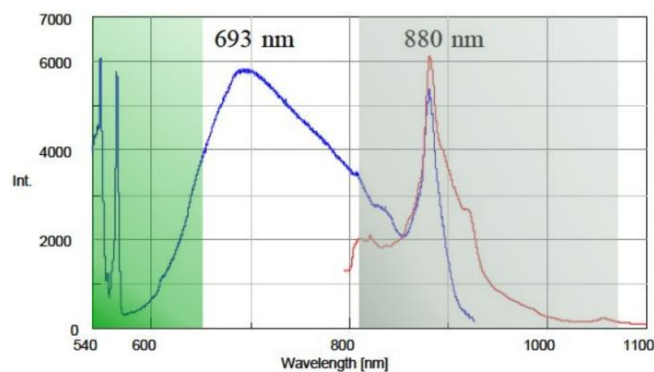


figure 95. Fluorescence spectrum of a glass slide using 532 nm (blue) and 785 nm (red) as excitation wavelength¹; green and grey shaded areas indicate the spectral region covered by the recorded Raman shift evoked by 532 nm and 785 nm laser excitation, respectively

$$\frac{1}{\lambda_{Ex}} - Raman\ shift = \frac{1}{785} 10^7 cm^{-1} - 1380 cm^{-1} = 11358.85 cm^{-1} = 880.47 nm \quad (\text{equation 14})$$

As there is no NIR-Raman laser available at the institute, measurements were performed using the Renishaw inVia Raman Microscope equipped with a 785 nm Raman laser kindly provided by the Carinthian Tech Research (CTR Villach). Furthermore, the 780 nm laser in combination with the Thermo Scientific DXR Raman Microscope was used for spore measurements. Despite of differences in the intensity mainly resulting from varying device settings (see appendix), both spore spectra look similar to each other (figure 96).

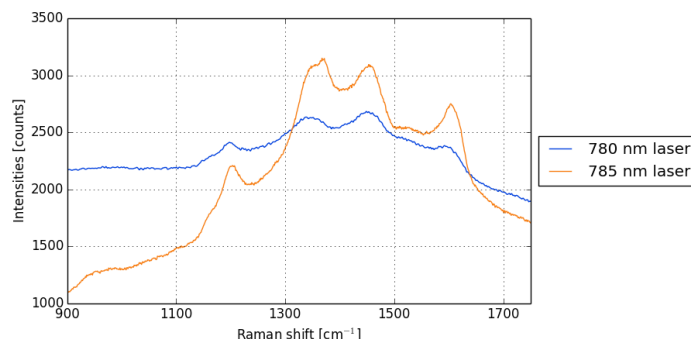


figure 96. Spores spectra recorded with an NIR-Raman laser (Thermo Scientific: 780 nm laser; Renishaw: 785 nm laser; device settings see appendix)

According to band assignments of Huang et al.² the Raman band at 1370 cm^{-1} is mainly evoked by the purine bases adenine and guanine and. Considering that the glass slide also evokes intense fluorescence in this spectral region, it is difficult to clearly assign this band to a specific group of analytes. Most likely, it is a combination of both. However, comparison of the amount

¹ Modified diagram: Jasco Application Note (030-AN-003) ©JASCO Corporation

VII. Spores of *P. chrysogenum* - VII.3. SERS of spores

of glass background to the comparatively small concentrations of bases and tyrosine leads to the conclusion that the glass slide makes a major contribution to the intensity of this band and is therefore assigned to the sample carrier. The recorded Raman spectra also outline the presence of phenylalanine (1198 cm^{-1} and 1602 cm^{-1}) and the amino acid tryptophan (1338 cm^{-1}). Furthermore, CH_2 deformation vibrations (1454 cm^{-1}) are visible in the Raman spectra (table 10).

table 10. Band assignment of spore spectra according to Huang et al.²

| Band position [cm^{-1}] | Band assignment |
|------------------------------------|---------------------------------------------|
| 1198 | Tyrosine, phenylalanine, protein, amide III |
| 1338 | Adenine, guanine, tyrosine, tryptophan |
| 1370 | Glass slide |
| 1454 | $\delta(\text{CH}_2)$ |
| 1602 | Phenylalanine |

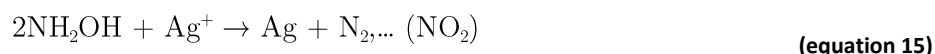
To conclude, Raman spectra of spores of *P. chrysogenum* were successfully recorded using a NIR-Raman laser. Not only could the fluorescent background be reduced, also carbonization of the sample was prevented. However, due to the high excitation wavelength, quantum efficiency of the CCD detector is not high enough to record the CH stretch vibration at 2933 cm^{-1} (≈ 1020 nm) which is the most intense band in the Raman spectra of hyphae. Additionally, the bands in the Raman spectrum of the glass slide could be assigned to fluorescence of the sample carrier. However, the fluorescence has more influence on the Raman spectrum of glass with 785 nm excitation than with 532 nm excitation.

VII.3. SERS of spores

So far, recording a Raman spectrum with the 532 nm Raman laser applying a laser power >0.01 % resulted in carbonization of the sample while no Raman signal could be recorded with 0.01 % laser power. Therefore, enhancement of the signal would be favorable in order to enable Raman measurements with 532 nm excitation wavelength. Signal enhancement of up to a factor of 10^8 and more can be achieved with Surface enhanced Raman Scattering (SERS). However, an appropriate SERS substrate is needed for generating the SERS effect rendering Raman spectroscopy a non label-free method.

VII.3.1. SERS substrate and characterization

Silver nanoparticles were prepared according to the Leopold-Lendl method⁸ which has the advantage of being a quick and easy principle for nanoparticle synthesis. Moreover, except for the silver nanoparticles, all the products are in the gas phase. Therefore, the SERS spectrum is not affected by by-products of the SERS substrate (equation 15). 4.5 ml of 0.1 M NaOH were mixed with 5 ml of $6 \cdot 10^{-2}$ M $\text{NH}_2\text{OH} \cdot \text{HCl}$ and then rapidly added to 90 ml of $1.11 \cdot 10^{-3}$ M AgNO_3 aqueous solution.⁵¹ After shaking thoroughly, the substrate was stored in the fridge and used within 4 weeks. Once a sample had been prepared with the SERS substrate, it needed to be measured immediately in order to prevent auto-oxidation of the silver nanoparticles which decreases the signal enhancement.



For each SERS substrate, the UV/Vis spectrum (1:10 dilution) was recorded (figure 97). The wavelength where maximum extinction is achieved is the one that should be used for Raman excitation in order to achieve maximum enhancement. Therefore, it would be worth adjusting the synthesis of the nanoparticles such, that the maximum of the UV/Vis absorption corresponds to the laser excitation wavelength.

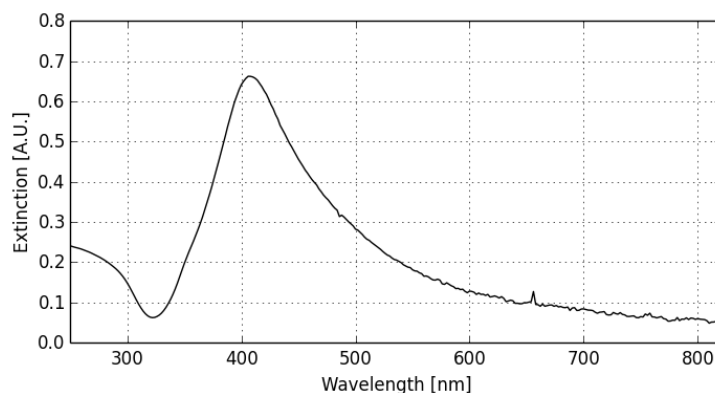


figure 97. UV/Vis spectrum of silver nanoparticles (1:10 dilution) with maximum at 407 nm

The prepared SERS substrate suspension had its extinction maximum at 407 nm. Based on FWHM (full width at half maximum) of 114 nm a polydisperse size distribution of the nanoparticles is indicated. A uniform shape and size of the SERS substrate is desirable as it affects the electromagnetic field and thus the enhancement effect. In order to obtain reproducible SERS spectra, the substrate must also be synthesized reproducibly which is still a

challenge for many applications. Although, there are some promising substrates on the market, none of them prevails due to its reliability, reproducibility and universal applicability.^{52,7,8,53,54}

The polydisperse size distribution of the silver nanoparticles is also mirrored in the AFM (atomic force microscopy; Agilent 5400) image recorded in contact mode and the according histogram (figure 98). If nanoparticles do not have a perfectly spherical shape, the equivalent radius can be calculated. Therefore, the area of elliptically shaped nanoparticles is determined by the software (Gwyddion 2.8). Then, the radius corresponding to a spherical particle of equivalent area is calculated. The histogram shows the distribution of the equivalent radius of our silver nanoparticles indicating that the majority of the particles have a radius between 50 nm and 100 nm.

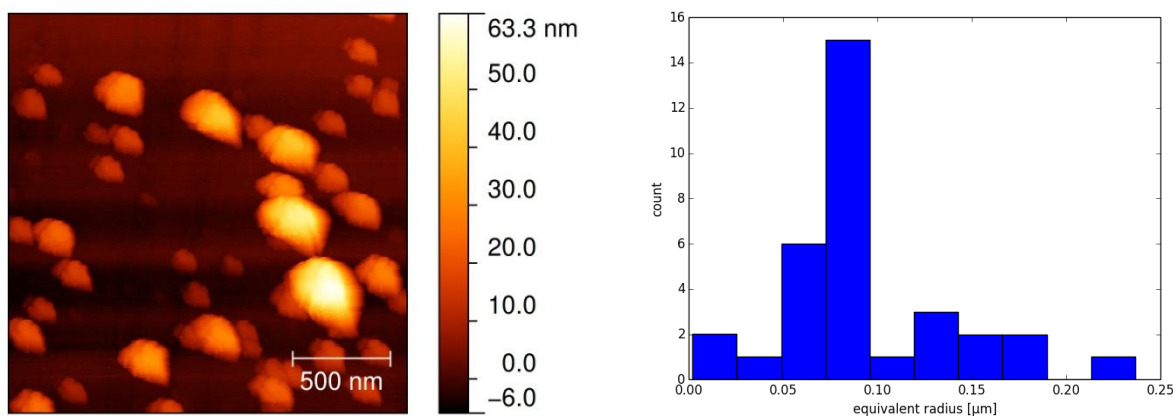


figure 98. AFM image of silver nanoparticles (left) and distribution of their equivalent radius (right)

A monodisperse size distribution as well as an extinction maximum around 532 nm would be favorable. This could be achieved by adjusting the synthesis of the nanoparticles accordingly in terms of mixing ratios, temperature, pH, mixing time etc. such, that the particles become uniform in shape and size. The described improvements of the SERS substrate, however, were beyond the scope of this work.

VII.3.2. Device settings

SERS measurements were performed with the confocal hole and the entrance slit set to 1000 μm in order to obtain maximum number of photons collected at the CCD detector. The laser power of the 532 nm Raman laser was set to 0.01 % to prevent carbonization of the organic material. In order to achieve maximum spatial resolution, the 100x objective was used. To obtain a sample evenly covered with SERS substrate three different sample preparation methods were investigated. In the first procedure, sample and SERS substrate were mixed in a

1:1 ratio prior to pipetting one droplet of the mixture onto the sample carrier (method A). As a second approach, SERS substrate was put onto the sample carrier and dried at room temperature. The mixture (sample:SERS substrate 1:1) was subsequently put onto the dried substrate (method B). Thirdly, the sample was pipetted onto the microscope slide and dried before an equivalent amount of silver nanoparticle solution was added (method C).⁵⁵ The results of this investigation are shown in chapter VII.3.4.

A SERS spectrum recorded in the middle of a spore of *P. chrysogenum* is displayed below (figure 99) with the according band assignments (table 11). According to the tentative band assignment by Szehalmi et al.⁵⁶ and Chao et al.⁵⁵ several Raman bands such as the amide III band, CH₃ deformation vibration or the amide I band are visible in the spectral fingerprint region. For the first time, Raman bands are seen in the spectrum of spores due to signal enhancement by silver nanoparticles. Using this enhancement effect makes it possible to apply very low laser power (0.01 %) and thus prevents sample damage by carbonization while recording a Raman spectrum.

table 11. Tentative band assignment for the SERS spectrum of a spore of *P. chrysogenum*

| Raman shift [cm ⁻¹] | Tentative band assignment ^{55,56} |
|---------------------------------|---------------------------------------------------------|
| 1099 | $\nu(\text{C-O}), \nu(\text{C-C}), \delta(\text{CC-H})$ |
| 1242 | Amide III |
| 1383 | $\delta(\text{CH}_2)$ |
| 1450 | $\delta(\text{CH}_2)$ lipids |
| 1501 | $\delta(\text{CH}_3)$ |
| 1612 | Amide I |

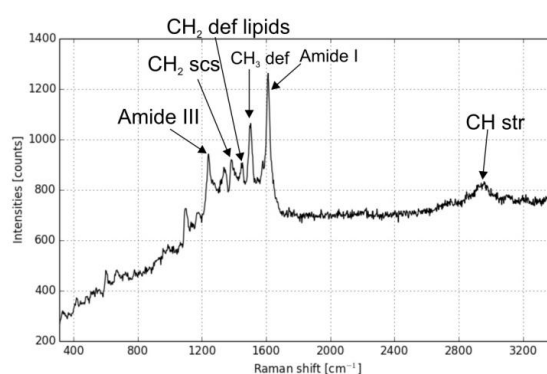


figure 99. SERS spectrum at 532nm excitation of a spore of *P. chrysogenum* (device settings see appendix)

VII.3.3. First SERS mapping of a spore

With the first SERS spectra being recorded, the next step was to obtain a Raman image of a spore in order to investigate different chemical compositions within the sample. Considering the size of a single spore with a diameter of approximately 4 μm , the number of spectra that can be collected from one spore is limited by the minimum step size that can be set without lateral overlap of the Raman photon collection area ($\approx 0.7 \mu\text{m}$ with 100x objective). For this, 100 μl of a washed spore sample were mixed with SERS substrate in a 1:1 ratio. One droplet of this mixture was dried at room temperature on a microscope slide and measured with 0.01 % laser power. The step size was set to 0.7 μm in x- and y-direction resulting in 72 spectra that were collected at an area of approximately 23 μm^2 (48 minutes of measurement time).

Having a look at the different focal planes of the measurement area, the spores seem to be well covered by the silver nanoparticles to ensure similar measurement conditions at every single measurement spot of the Raman image. As the enhancement effect decreases rapidly with the distance between nanoparticle and sample ($I_{\text{SERS}} \sim r^{-12}$ see chapter IV.1.1), a homogenous coverage of the measurement area with SERS substrate needs to be ensured. Otherwise, spectral changes between single spectra of the Raman image would primarily result from different contributions of the nanoparticles to the enhancement effect.

The distribution of the intensity of the CH stretch vibration (2933 cm^{-1}) matches the sample image (figure 101) in great parts. This vibration is mainly evoked by proteins and lipids, but also by sugars, amino acids, etc. and thus is present in every biological sample. Due to the small number of pixels (72), deviations in the shape of the CH intensity map and the spore image can be explained. Therefore, a smaller step size such as 0.5 μm or less would be more preferable for future measurements.

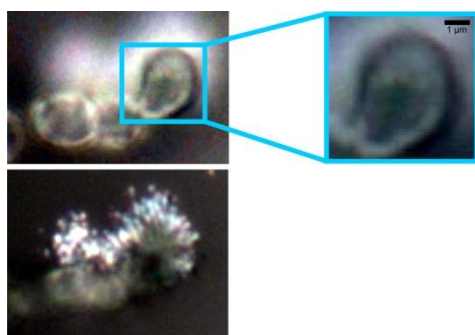


figure 100. Measurement area of SERS mapping of a single spore; images on the left represent different focal planes to show homogenous coverage of the sample with silver nanoparticles

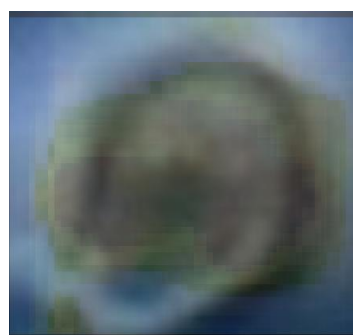


figure 101. Overlay of intensity map ($\nu(\text{CH})$ at 2933 cm^{-1}) and sample image

All in all, SERS imaging of spores of *P. chrysogenum* requires careful interpretation of the complex data, especially without knowing the reproducibility of the recorded SERS spectra. Repeated measurements at the same measurement spot are required to answer this question.

VII.3.4. Reproducibility of the SERS signal

With the SERS signal being very much affected by the size, shape and distribution of the nanoparticles, there are a lot of factors besides the sample itself influencing the enhanced Raman spectrum. Also, oxidation of the SERS substrate negatively influences the enhancement effect. Thus, measurements need to be performed as soon as possible after sample preparation. The reproducibility of Raman spectra recorded with silver nanoparticles as SERS substrate was investigated by recording time dependant spectra. Therefore, 21 spectra were recorded at the same measurement spot. 5x10 s were set as integration time for each spectrum, resulting in a total of 33 minutes that the sample is exposed to the laser and thus thermal stress. However, even with a very low laser power (0.01 %), changes in the integrity of the sample cannot be excluded.

As mentioned earlier (see VII.3.2), three different sample preparation methods were investigated in order to achieve optimized results in terms of reproducibility. Changes over time are outlined in the contour plot underneath the single spectra (figure 102 - figure 104). At first glance, none of the different preparation methods indicates a satisfying result. The intensity of single SERS bands seems very unstable from one spectrum to the next while it should remain identical since every set of measurements represents spectra recorded on the exact same measurement spot. The second sample preparation method (method B) seems the least promising compared to the other two as changes in the band intensities are in particular visually noticeable. Meanwhile, the third preparation method (method C) seems most promising for accomplishing more stable SERS spectra.

Considering the average radius of the nanoparticles with 0.075 μm (see chapter VII.3.1) and the diameter of a spore with 4 μm , the nanoparticle is significantly smaller than the sample. Thus, homogenous coverage of the sample with the SERS substrate is crucially important especially when taking the laser spot size of 0.72 μm in diameter (100x objective) and the stage allowing a lateral resolution of 0.5 μm into consideration. However, the precision of the x,y,z-stage is below 0.1 μm which means that the r^{-12} with which the enhancement effect decreases around the nanoparticle is not within the precision of the stage. Furthermore, the spectrometer

VII. Spores of *P. chrysogenum* - VII.3. SERS of spores

is not placed on a vibration-damped, but a granite table which definitely affects the precision and reproducibility of recording a Raman spectrum at exactly the same measurement spot.

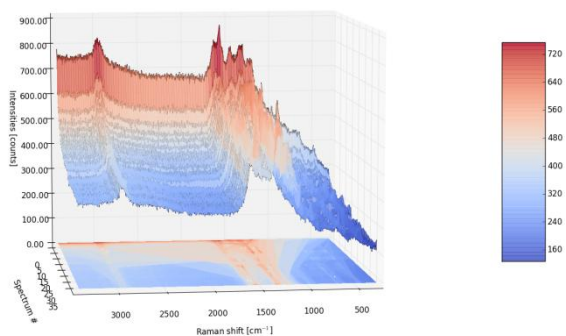


figure 102. Time dependant SERS spectra of spore sample prepared with method A (device settings see appendix)

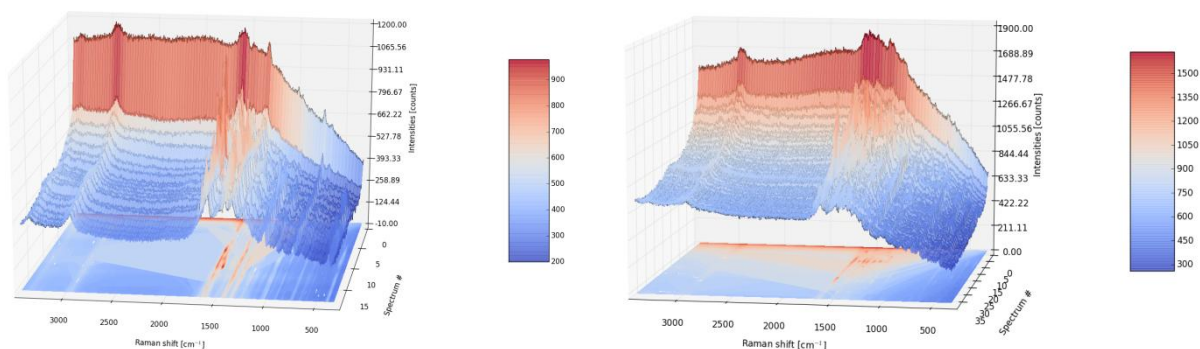


figure 103. Time dependant SERS spectra of spore sample prepared with method B (B1 left, B2 right; device settings see appendix)

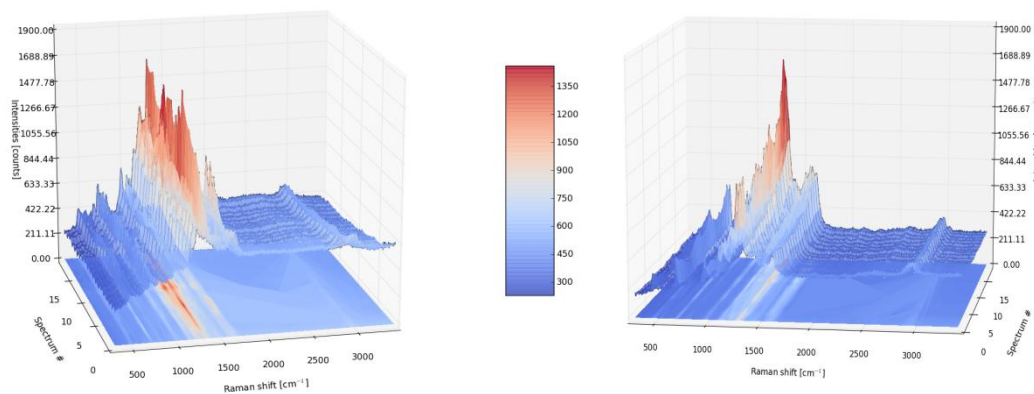


figure 104. Time dependant SERS spectra of spore sample prepared with method C (C1 left, C2 right; device settings see appendix)

Statements made so far were based on visual examination of the contour plot only. A more detailed insight can be gained by selecting certain Raman bands and following the change in intensity between single spectra over time. Therefore, the normalized intensity of the baseline

corrected spectra (see appendix) was investigated over time for the amide III band (1241 cm^{-1}) and the CH_2 wagging vibration (1318 cm^{-1} , see figure 105).

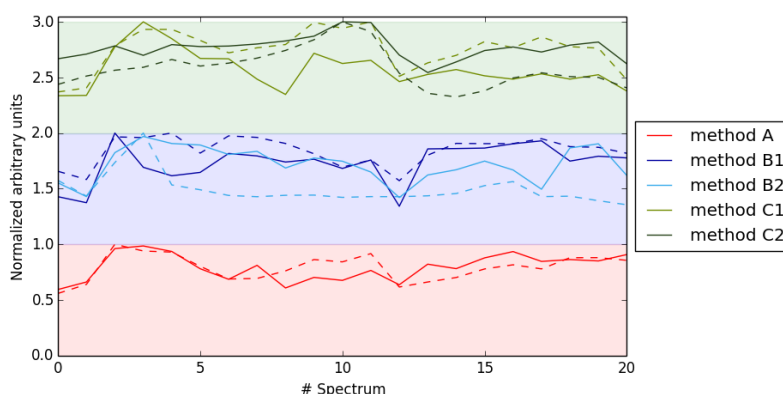


figure 105. Changes of normalized intensity of amide III band ('-') and $\omega(\text{CH}_2)$ ('--') over time using three different sample preparation methods (method A, B, C); shift introduced for clarity

Following the intensity change of two Raman bands in particular, differences in the sample preparation and their influence on obtaining reproducible SERS spectra get clearer. While the intensity of both bands changes by more than 50 % for method B and C, a more stable signal is achieved with method A (mixing sample and SERS substrate in a 1:1 ratio). However, changes are still massive with method A but the values seem to get more stable after the 15th measurement which corresponds to approximately 13 minutes of measurement time. This trend towards a more stable SERS signal cannot be observed for method B and C.

It can be concluded, that difficulties were faced in generating reproducible SERS spectra. To examine this, three different sample preparation methods were investigated yielding for optimized signal reproducibility with the employed silver nanoparticles. In doing so, mixing the sample with the SERS substrate in a 1:1 ratio turned out to be the most efficient method. Here, stabilization of the signal could be observed after approximately 13 minutes of measurement time. However, further optimization is required which primarily will need to be done by producing SERS substrate with monodisperse size distribution. Also, improvements in the reproducibility may be achieved by varying the mixing ratio between sample and SERS substrate.

VII.3.5. Dead/alive study

In order to investigate whether or not there are spectral differences detectable between living and dead spores of *P. chrysogenum* 5 ml of a fresh spore sample (stored for approximately one

VII. Spores of *P. chrysogenum* - VII.3. SERS of spores

month at 8°C in the fridge) was diluted in a 1:5 ratio with PBS buffer and microwaved for 30 s at approx. 940 W. This thermal stress had been proven to kill the spores (Ehgartner). Before one droplet of a dead and a living spore sample was put on a CaF₂ slide, the samples had been washed three times with deionized water. After the sample solution had been dried at room temperature, an equivalent amount of SERS substrate was added onto the sample carrier (preparation method C). Better results could probably have been achieved by using preparation method A. However, at the time these measurements were taken, the reproducibility study had not been evaluated yet.

In order to obtain a representative result, 11 different measurement spots of each sample were investigated recording ten Raman spectra at each position. Then, the average spectrum and the standard deviation of the baseline corrected data were calculated. As can be derived from the reproducibility study in chapter VII.3.4 the band intensities are changing by more than 50 % between single spectra for sample preparation method C. Although more than 100 spectra were averaged for each sample, high variability in the SERS spectra is reflected in a high standard deviation (figure 106). Therefore, it might be more convenient to see differences between spectra of living and dead spores without displaying the standard deviation (figure 107). However, quantitative interpretation of band intensities is not possible.

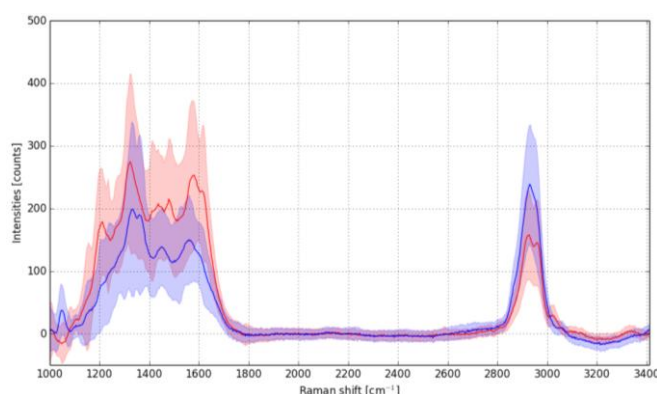


figure 106. Average SERS spectrum of living (red) and dead spores (blue) with standard deviation (device settings see appendix)

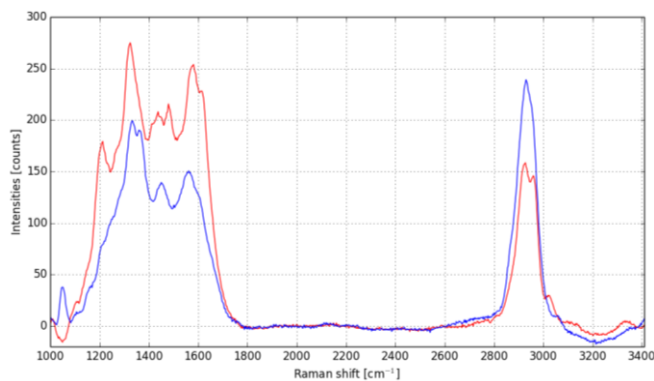


figure 107. Average SERS spectrum of living (red) and dead spores (blue) without standard deviation (device settings see appendix)

Several distinct differences can be observed between SERS spectra of living and dead spores which can be identified based on tentative band assignments by Chao et al.⁵⁵ and Szeghalmi et al.⁵⁶ (see table 12.) The microwave treatment leads to thermal stress and protein denaturation leading to loss of secondary structure (hence also the tertiary structure) due to breaking of chemical bonds and thus resulting in loss of function and subsequent cell death. These chemical differences are most definitely related to different Raman bands visible in the SERS spectra. The spectral features might be different when the spores are not killed in the microwave (i.e. without external intervention targeting cell death).

Two distinct vibrations are more intense in the SERS spectra of living spores compared to the ones of dead spectra: the amide I band which is a characteristic protein marker band mainly consisting of the C=O stretch vibration (1213 cm^{-1}) and the ring stretch vibration (1613 cm^{-1}) which can result from various components such as amino acids or carbohydrates (glucose, chitin, etc.). The decrease of these two bands in the SERS spectrum of dead spores indicates damage of the spore's integrity due to thermal stress leading to protein degradation.

table 12. Tentative band assignment of the SERS spectra of dead and living spores of *P. chrysogenum*

| Raman shift [cm ⁻¹] | Tentative band assignment ^{55,56} |
|---------------------------------|----------------------------------------------------------------------------------|
| 1050 | $\nu(\text{C-O})$, $\nu(\text{C-O})$ sugar, lipid, $\delta(\text{C-H})$, AgNPs |
| 1213 | Ring str, $\delta(\text{CC-H})$ |
| 1324 | $\delta(\text{C-H})$ protein |
| 1334 | $\delta(\text{CH}_3)$ |
| 1360 | $\delta(\text{CH}_3)$, $\delta(\text{C-H})$ protein |
| 1437 | CH_2 , $\delta(\text{CH}_3)$ |
| 1450 | $\delta(\text{CH}_2)$ lipid |
| 1479 | $\delta(\text{CH}_3)$ |
| 1562, 1581 | $\nu_{\text{as}}(\text{COO}^-)$ |
| 1613 | Amide I |

Although there are some interesting changes going on in the region of the CH stretch vibration around 2930 cm⁻¹, they were not investigated in detail as no band assignment is available for this spectral area. There is one distinct band at 1050 cm⁻¹ which is present in the spectrum of dead spores but absent in the one of living spores. While Szeghalmi et al. assigns C-O and C-C stretch vibrations from sugars and C-H deformation vibrations (table 12), Chao et al. claims this as the Raman band of the silver nanoparticles. It seems unlikely that a dead spore would have sugars and lipids that seem to be absent in the living spore. However, chemical double bonds can be broken as a result of the higher temperature due to the microwave's heat impact. This means that a C=C bands might result in a C-C stretch vibration which is now seen in the SERS spectrum of dead spores. Furthermore, the asymmetric COO⁻ stretch vibration decreases from living to dead spores while the C-O stretch vibration increases which might also result from breaking up double bonds. However, Chao et al. might have a point in claiming that band at 1050 cm⁻¹ does not result from the sample but from the SERS substrate. Measuring SERS substrate on a glass slide without sample (figure 108) outlines the presence of a band at 1060 cm⁻¹. Taking the spectral resolution of 6 cm⁻¹ into consideration, the band in the sample spectrum might actually be the same as in the spectrum of the SERS substrate. Silver nitrate is reduced to silver in the process of marking silver nanoparticles based on the Leopold-Lendl method.⁸ If AgNO₃ is not entirely reduced (e.g. due to a stoichiometric surplus of AgNO₃), it remains in the SERS solution which is subsequently mixed with the sample. Thus, the band in the SERS spectrum might result from AgNO₃^{57,58}. One might argue that, if the band results from SERS substrate, it should also be seen in the spectrum of living spores. However, rupture of the cell wall of the spores killed in the microwave might lead to cell leakage and subsequent

decrease of protein content in the spore. Thus, the overall distribution of the spore content on the sample carrier changes including the local ratio between sample and SERS substrate. Therefore, a band of the SERS substrate might now become visible in the SERS spectrum.

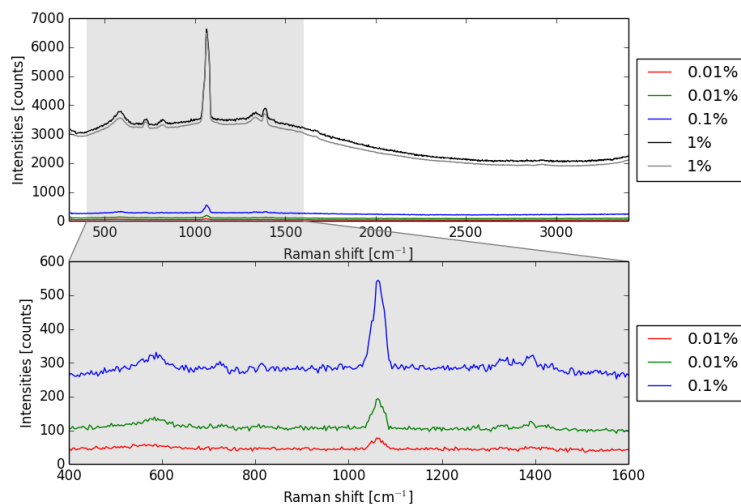


figure 108. Raman spectrum of SERS substrate on a glass slide (device settings see appendix)

To conclude, spectral differences in the SERS spectra of living and dead spores can be observed. However, in future investigations it needs to be determined if these differences can also be seen once the spores have not deliberately been killed in the microwave. Furthermore, poor reproducibility of the SERS signal needs to be considered for any interpretation of the resulting spectra. To overcome this problem and get a more significant result, the average spectrum of more than 100 spectra was calculated for each sample. Nevertheless, reproducibility needs to be improved.

VII.4. Dead/alive study with 785 nm laser

Similar experiments as with the SERS substrate were performed using a NIR Raman laser (785 nm) which was provided by Martin Kraft at the Carinthian Tech Research (CTR) in Villach. Samples were prepared similarly as described in the previous chapter (VII.3.5). One droplet of the living spore solution and one of the solution containing spores killed in the microwave were each put onto a glass slide and dried at room temperature. The samples were prepared in Vienna before measurements were performed during the following three days in Carinthia while it cannot be excluded that the spores were dying on the sample carrier due to dehydration and a lack of oxygen and nutrients (C- source, N- source). Three spectra were collected at each measurement spot. Considering 26 different measurement positions for dead

spores and 20 for living spores, this means that all in all 78 spectra of dead spores and 60 of living ones were recorded. Differences in the average spectra (baseline correction see appendix) between living and dead spores are mainly noticed by the band intensities which are weaker for dead spores (figure 109). However, there is one band around 1450 cm^{-1} particularly noticeable as it is visible in the spectrum of living spores but disappears underneath the fluorescence of glass for dead ones. According to Huang et al.² this band is evoked by lipids (see table 13). This means that either the amount of lipids is higher for living spores or the lipid bilayer in fungal membranes has been destroyed. The latter possibility mentioned would be the result of denaturation leading to unfolding of proteins or cell disruption evoked in the microwave when the membrane and thus the lipid bilayer are destroyed.

The amount of phenylalanine is also higher in living spores which might be explained by the following hypothesis: Phenylalanine is an aromatic amino acid synthesized via the shikimic acid pathway in plants and fungi (essential amino acid in mammals) and is part of the natural synthesis of penicillin G. Furthermore, the amino acid can be metabolized in various ways such as phenylpyruvate, phenylacetate or trans-cinnamate synthesis (see phenylalanine metabolism in *P. chrysogenum* in the appendix for more detailed information). It can also be used as carbon and nitrogen source by *P. chrysogenum*.^{59,60} Since metabolic activity stops once spores have been killed in the microwave, phenylalanine is neither produced nor metabolized anymore. Therefore, the concentration of this amino acid is significantly lower in dead spores than in living ones where the metabolic activity is still intact. However, considering the ratio of phenylalanine (1607 cm^{-1}) and tyrosine (1620 cm^{-1}), it seems that the tyrosine content is higher in dead spores than in living ones. As tyrosine is synthesized from phenylalanine, this might indicate that in dead/dying spores phenylalanine is metabolized to tyrosine. However, subsequent metabolization of tyrosine (e.g. degradation via homogentisate pathway⁶⁰) does not happen as effectively as in living spores.

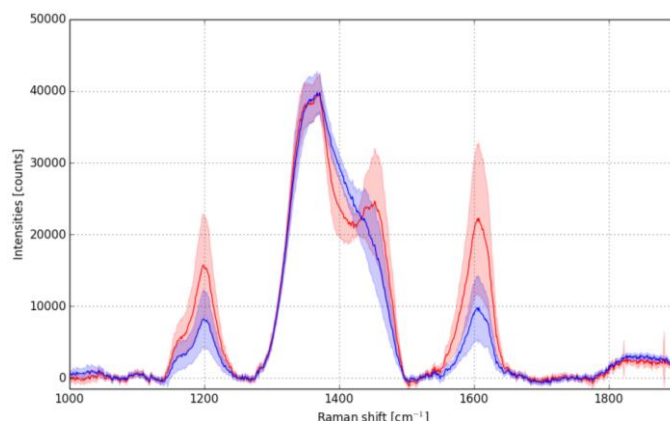


figure 109. Average spectra with according standard deviation of living (red) and dead (blue) spores (device settings see appendix)

table 13. Band assignment of the Raman spectra of dead and living spores of *P. chrysogenum*

| Raman shift [cm ⁻¹] | Band assignment ^{2,61} |
|---------------------------------|---------------------------------------------|
| 1620 | Tyrosine |
| 1607 | Phenylalanine |
| 1454 | Lipids |
| 1368 | Glass slide |
| 1355 | Phenylalanine |
| 1200 | Tyrosine, phenylalanine, protein, amide III |
| 1163 | $\nu(\text{C-C})$ |

The data was additionally investigated applying PCA on the baseline corrected and mean centered spectra. A few spectra containing cosmic rays were excluded from analysis. Furthermore, one measurement triplet (three Raman spectra recorded at the same measurement spot) recorded of dead spores was marked as bad pixels as they looked different from the average Raman spectra of dead spores. The difference is also seen in the score plot of the PCA with three dots being isolated in one corner of the score plot indicating great influence on the second principal component (figure 110). The spectra look more similar to those of living spores which is especially outlined by the band at 1454 cm⁻¹ evoked by lipids (figure 111). Maybe a few spores survived the microwave treatment and one of them was investigated in this study. As spectra of dead and living spores were recorded on two different days, unintentional mixing of the sample files can be excluded. Nonetheless, those three spectra were excluded from future investigations.

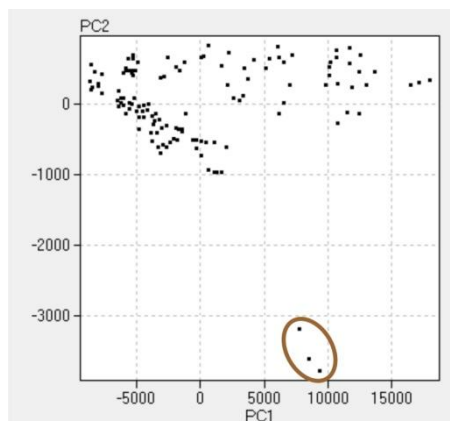


figure 110. Score plot with three spectra standing out from the remaining data

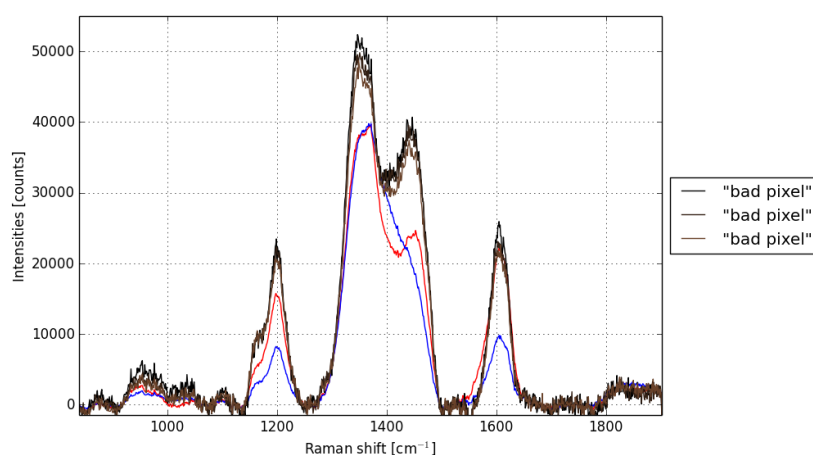


figure 111. Average spectra of dead (blue) and living spores (red) in comparison to the three single spectra ("bad pixel") recorded at the same measurement spot of a dead spore sample

In the resulting score plot (PC1 vs. PC2) the Raman spectra of dead and living spores can be very well differentiated (figure 112). Most of the spectra recorded from dead spores have moderate impact on PC1 while spectra of living spores tend to have bigger impact on PC1. On the contrary, spectra of dead spores show more influence on principal component two.

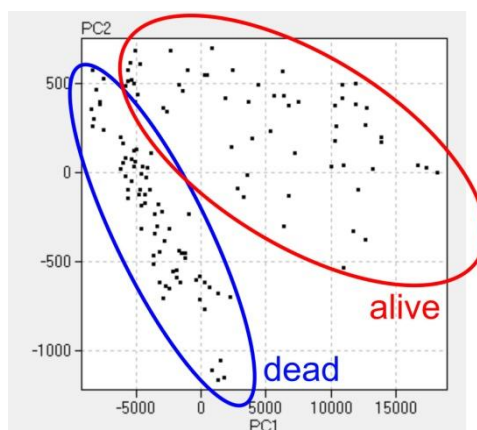


figure 112. Score plot showing a clear differentiation between Raman spectra of living and dead spores

All in all, Raman measurements with the 785 nm laser were successful in differentiation between living spores and dead spores which were killed in the microwave prior to analysis. The spectral difference could be seen in the average spectra and were also clearly outlined in the score plot of the PCA performed with the same data consisting of 60 spectra recorded from living spores and 75 spectra recorded from dead ones. However, it needs to be clarified in future experiments if the observed spectral differences are indeed characteristic for dead spores excluding any influence due to intentionally induced death in the microwave.

VII.5. Discussion and conclusion

Spores of *P. chrysogenum* are more thermolabile than hyphae and additionally negatively influence the Raman spectra with autofluorescence. Therefore, Raman measurements employing the 532 nm laser were not possible without carbonization of the sample. Various attempts such as using objectives with smaller magnification, different sample carriers or adding a green laser pointer as external light source to decrease the laser power per area and dissipate the heat did not lead to Raman spectra without graphite bands. As an alternative, silver nanoparticles prepared according to the Leopold-Lendl method were used to enhance the Raman signal and enable measurements with 0.01 % laser power. SERS mapping of a single spore as well as a live/dead study could be performed of spore samples. However, interpretation of the spectra is complex as there are only a few tentative band assignments available so far and the quality of the SERS spectra suffers from poor reproducibility. In case of spores the method of choice was to use a 785 nm laser because excitation of chromophores and carbonization of the sample can be widely excluded due to the higher laser wavelength. Using the NIR laser at the CTR in Carinthia, a dead/alive study of spores was conducted with promising results. Differences in

the recorded spectra could be observed and were further outlined with PCA. However, the investigated spores were killed in the microwave. Therefore, future investigations need to focus on the question to what extent the influence of the microwave is mirrored in the Raman spectra of spores compared to the ones that died due to “natural causes”.

VIII. Outlook

Raman imaging of hyphae of *P. chrysogenum* was successfully performed and investigated with non-supervised classification algorithms. Thus, for future prospects, it would be interesting to analyze the data using supervised algorithms such as MCR-ALS (multivariate curve resolution alternant least square)⁶². Therefore, reference spectra of proteins such as glucose, chitin, trehalose, phenylalanine and other components of fungal spores would be recorded and subsequently assigned to the according sample areas. Also VCA (vertex component analysis) as non-supervised classification algorithm would be an interesting approach for investigating single components of the hyphal Raman images.

Also, the combination of Raman microspectroscopy and fluorescence as reference method needs to be optimized in terms of avoiding leakage of the fluorescent dye during the washing steps. Furthermore, an alternative to propidium iodide as fluorescent dye staining dead fungi would be required for recording Raman measurements with the 532 nm laser. Another possibility would be using a different excitation wavelength. However, Raman spectra of hyphae recorded with the 633 nm laser are dominated by autofluorescence while spectra with the NIR laser mostly contain fluorescence from the glass slide. For future measurements, changing the sample carrier from glass to CaF₂ would be advisable to avoid interfering Raman bands in the spectral fingerprint region from 400 cm⁻¹ to 1900 cm⁻¹ where important protein marker bands, lipids, carbohydrates and other sample constituents are found.

SERS spectra of spores using the 532 nm laser enabled measurements with 0.01 % laser power. However, reproducibility of the SERS signal needs to be improved. For this, either the synthesis of the silver nanoparticles should be optimized for more stable results and a monodisperse size distribution or a different SERS substrate such as gold nanoparticles used in combination with the 633 nm laser can be investigated. As there are many SERS substrates commercially available, performing measurements with a purchased substrate might increase the reproducibility.

Marker-free Raman measurements of spores could be performed with the 785 nm laser providing promising results for the differentiation between living and dead spores based on the spectral data. Future investigations should focus on generating Raman spectra of dead spores which were not killed in the microwave to exclude the possibility that the killing method influences the according Raman spectrum. Additionally, the sample preparation could be improved. The sample on the glass carrier is dried at room temperature and therefore slowly

dying even before the Raman measurement is performed. Measuring the sample without drying step would be desirable. Thus, a portable Raman probe that can be directly used for in-situ analysis of spores in the production area could be developed. Once it is shown that spectral differences are observable between living spores and the ones that died from natural causes, a bigger data set for the live/dead study can be generated. Therefore, in the next step samples of unknown morphological state can be identified by comparison to a stable data matrix. Then, an automated screening method for spores can be established using single spore recognition software to scan great sample areas and perform measurements of a certain sample percentage.

IX. Appendix

IX.1. Device settings

FDA (Horiba LabRAM HR 800; figure 11)

| Spectrum | Laser power [%] | Slit [μm] | Confocal hole diameter [μm] | Acquisition time [s] | Number of accumulations |
|--------------|-----------------|------------------------|------------------------------------------|----------------------|-------------------------|
| 633 nm (i) | 100 | 500 | 600 | 2 | 120 |
| 633 nm (ii) | 100 | 500 | 600 | 2 | 120 |
| 633 nm (iii) | 100 | 500 | 600 | 2 | 120 |
| 532 nm | 100 | 500 | 600 | 2 | 120 |

Spectrograph positions: (i) 1500 cm^{-1} (ii) 2000 cm^{-1} (iii) 2500 cm^{-1}

PI (Thermo Scientific; figure 16)

| Laser wavelength [nm] | Laser power [mW] | Acquisition time [s] | Number of accumulations | Objective |
|-----------------------|------------------|----------------------|-------------------------|-----------|
| 780 | 9.0 | 2 | 300 | 100x |

DAPI (Horiba LabRAM HR 800; figure 20- figure 21)

Once again, the 100x objective and the 300 gr/mm grating were used.

| Laser | Laser power [%] | Entrance slit [μm] | Confocal hole [μm] | Acquisition time [s] | Number of accumulations |
|-------|-----------------|---------------------------------|---------------------------------|----------------------|-------------------------|
| 633 | 10 | 1000 | 1000 | 2 | 120 |
| 532 | 1 | 500 | 300 | 3 | 120 |

Hyphae of *P. chrysogenum*

Different objectives (figure 28)

| Laser | Laser power [%] | Entrance slit [μm] | Confocal hole [μm] | Acquisition time [s] | Number of accumulations |
|-------|-----------------|---------------------------------|---------------------------------|----------------------|-------------------------|
| 532 | 50 | 150 | 300 | 2 | 60 |

IX. Appendix - IX.1. Device settings

Carbonization of hypha: 100x objective (figure 29)



| Laser | Laser power [%] | Entrance slit [μm] | Confocal hole [μm] | Acquisition time [s] | Number of accumulations |
|-------|-----------------|---------------------------------|---------------------------------|----------------------|-------------------------|
| 532 | 100 | 150 | 300 | 3 | 60 |













Spectrum of hypha: 100x objective (figure 30)





| Laser | Laser power [%] | Entrance slit [μm] | Confocal hole [μm] | Acquisition time [s] | Number of accumulations |
|-------|-----------------|---------------------------------|---------------------------------|----------------------|-------------------------|
| 532 | 50 | 150 | 300 | 2 | 60 |

Small scale mapping: descriptor list HCA (figure 36, figure 39)

The spectral descriptor list for HCA is shown below. Two different methods were chosen to calculate the area of the selected peak:

- Area within range, with baseline subtraction 
- Correlation with a triangle template  (advantageous for bands sitting on another Raman band)

| Descriptor type | Integration range |
|-------------------------------------------------------------------------------------|-------------------|
|  | 712-781 |
|  | 953-1017 |
|  | 1039-1114 |
|  | 1100-1161 |
|  | 1193-1283 |
|  | 1279-1329 |
|  | 1311-1405 |
|  | 1247-1283 |
|  | 1189-1247 |
|  | 1279-1323 |
|  | 1411-1509 |
|  | 1519-1626 |

| | |
|-----------------------------------------------------------------------------------|-----------|
|  | 1620-1715 |
|  | 2812-3029 |
|  | 3034-3094 |
|  | 3034-3094 |

Large scale mapping: 100x objective; 50% laser power (chapter VI.3.2)






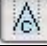

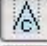
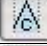
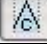
| Grating [lines/mm] | Entrance slit [μm] | Confocal hole [μm] | Acquisition time [s] | Number of accumulations | X,Y-step [μm] |
|-----------------------|------------------------------------|------------------------------------|-------------------------|----------------------------|-------------------------------|
| 300 | 300 | 1000 | 2 | 3 | 1 |

Pivots for baseline correction of 24h 2d mapping (chapter VI.3.2)

| # of pivot | Wavenumber [cm^{-1}] |
|------------|---------------------------------|
| 1 | 310.9 |
| 2 | 745.0 |
| 3 | 1212.6 |
| 4 | 1860.3 |
| 5 | 2081.7 |
| 6 | 2303.0 |
| 7 | 2646.8 |
| 8 | 2745.7 |
| 9 | 3188.4 |
| 10 | 3409.7 |

IX. Appendix - IX.1. Device settings

Spectral descriptors for HCA of large scale mapping (figure 54, figure 57)

| Descriptor type | Integration range |
|-----------------------------------------------------------------------------------|-------------------|
|  | 488-714 |
|  | 722-793 |
|  | 896-1193 |
|  | 1193-1273 |
|  | 1273-1376 |
|  | 1391-1502 |
|  | 1506-1637 |
|  | 1637-1716 |
|  | 2801-3033 |
|  | 3029-3093 |

Spectrum of FDA stained hyphae: 100x objective (figure 67)

| Spectrum | Laser power [%] | Slit [μm] | Confocal hole diameter [μm] | Acquisition time [s] | Number of accumulations |
|----------|-----------------|------------------------|------------------------------------------|----------------------|-------------------------|
| 10 % 0 | 10 | 150 | 200 | 2 | 20 |
| 10 % 1 | 10 | 150 | 200 | 2 | 20 |
| 10 % 2 | 10 | 150 | 200 | 2 | 20 |
| 25 % | 25 | 150 | 200 | 2 | 20 |
| 50 % | 50 | 150 | 200 | 2 | 20 |

Comparison of FDA stained fungus, unstained fungus and FDA: 100x objective (figure 68)

| Spectrum | Laser power [%] | Slit [μm] | Confocal hole diameter [μm] | Acquisition time [s] | Number of accumulations | Excitation wavelength [nm] |
|--------------------|-----------------|------------------------|------------------------------------------|----------------------|-------------------------|----------------------------|
| FDA stained fungus | 10 | 150 | 200 | 2 | 20 | 532 |
| Unstained fungus | 10 | 150 | 300 | 4 | 60 | 532 |
| FDA | 100 | 500 | 600 | 2 | 120 | 633 |

Spectrum of washed FDA stained fungus: 100x objective (figure 69)

| Spectrum | Laser power [%] | Slit [μm] | Confocal hole diameter [μm] | Acquisition time [s] | Number of accumulations |
|----------|-----------------|------------------------|------------------------------------------|----------------------|-------------------------|
| 10 % 4 | 10 | 150 | 600 | 2 | 120 |

Comparison of FDA stained washed fungus, unstained fungus and FDA: 100x objective (figure 70)

| Spectrum | Laser power [%] | Slit [μm] | Confocal hole diameter [μm] | Acquisition time [s] | Number of acc. | excitation wavelength [nm] |
|---------------------------|-----------------|------------------------|------------------------------------------|----------------------|----------------|----------------------------|
| Washed FDA stained fungus | 10 | 150 | 600 | 2 | 120 | 532 |
| Unstained fungus | 10 | 150 | 300 | 4 | 60 | 532 |
| FDA | 100 | 500 | 600 | 2 | 120 | 633 |

IX. Appendix - IX.1. Device settings

Spectrum of PI (Thermo Scientific; figure 71)

| Laser wavelength [nm] | Laser power [mW] | Pinhole [μm] | Acquisition time [s] | Number of accumulations | Objective |
|-----------------------|------------------|---------------------------|----------------------|-------------------------|-----------|
| 780 | 9.0 | 50 | 2 | 20 | 100x |

Spectra of hyphae stained with FDA, PI and DAPI: varying the laser power (figure 72)

| Laser wavelength [nm] | Slit [μm] | Pinhole [μm] | Acquisition time [s] | Number of accumulations | Objective |
|-----------------------|------------------------|---------------------------|----------------------|-------------------------|-----------|
| 532 | 150 | 300 | 2 | 20 | 50x |

Spectra of hyphae stained with FDA, PI and DAPI and washed: 100x objective (figure 73)

| Laser | Laserpower [%] | Entrance slit [μm] | Confocal hole [μm] | Acquisition time [s] | Number of accumulations |
|-------|----------------|---------------------------------|---------------------------------|----------------------|-------------------------|
| 532 | 10 | 100 | 200 | 2 | 60 |

Spore spectra: 100x objective (figure 74)

| Laser | Laser power [%] | Entrance slit [μm] | Confocal hole [μm] | Acquisition time [s] | Number of accumulations |
|-------|-----------------|---------------------------------|---------------------------------|----------------------|-------------------------|
| 532 | 0.01 | 900 | 1000 | 2 | 10 |
| 532 | 0.1 | 900 | 1000 | 2 | 10 |
| 532 | 1 | 900 | 1000 | 2 | 10 |

Spectra without sample with lights switched on and off (figure 75)

| Laser | Laser power [%] | Entrance slit [μm] | Confocal hole [μm] | Acquisition time [s] | Number of accumulations |
|-------|-----------------|---------------------------------|---------------------------------|----------------------|-------------------------|
| 532 | 0.01 | 900 | 1000 | 2 | 10 |

Spore spectra with WIO 100x (figure 78)

| Laser | Laser power [%] | Entrance slit [μm] | Confocal hole [μm] | Acquisition time [s] | Number of accumulations |
|-------|-----------------|---------------------------------|---------------------------------|----------------------|-------------------------|
| 532 | 0.1 | 900 | 1000 | 2 | 10 |
| 532 | 0.01 | 900 | 1000 | 2 | 10 |

Spores on aluminum foil (figure 80)

| Laser | Laser power [%] | Entrance slit [μm] | Confocal hole [μm] | Acquisition time [s] | Number of accumulations |
|-------|-----------------|---------------------------------|---------------------------------|----------------------|-------------------------|
| 532 | 0.1 | 900 | 1000 | 10/30* | 10 |

*see legend of figure 80

Spores on cryo-stage (figure 84)

| Laser | Laser power [%] | Entrance slit [μm] | Confocal hole [μm] | Acquisition time [s] | Number of accumulations |
|-------|-----------------|---------------------------------|---------------------------------|----------------------|-------------------------|
| 532 | 0.1 | 1000 | 1000 | 30 | 12 |
| 532 | 1 | 1000 | 1000 | 2 | 15 |
| 532 | 1 | 1000 | 1000 | 2 | 10 |
| 532 | 1 | 1000 | 1000 | 2 | 50 |

Spores on cryo-stage: spectrograph at 2100 cm^{-1} (figure 86)

| Laser | Laser power [%] | Entrance slit [μm] | Confocal hole [μm] | Acquisition time [s] | Number of accumulations |
|-------|-----------------|---------------------------------|---------------------------------|----------------------|-------------------------|
| 633 | 0.01 | 500 | 1000 | 60 | 12 |
| 633 | 0.01 | 500 | 1000 | 60 | 30 |
| 633 | 0.1 | 500 | 1000 | 20 | 30 |
| 633 | 0.01 | 500 | 1000 | 90 | 30 |

Spores: 20x objective (figure 88)

| Laser | Laser power [%] | Entrance slit [μm] | Confocal hole [μm] |
|-------|-----------------|---------------------------------|---------------------------------|
| 532 | 0.01 | 900 | 1000 |

IX. Appendix - IX.1. Device settings

Toluene spectra: 532 nm laser, 20x objective (figure 90)

| Light source | Laser power [%] | Entrance slit [μm] | Confocal hole [μm] | Acquisition time [s] | Number of accumulations |
|---------------|-----------------|---------------------------------|---------------------------------|----------------------|-------------------------|
| Laser pointer | 100 | 1000 | 1000 | 50 | 10 |
| laser | 10 | 1000 | 1000 | 0.5 | 5 |

Spore: Raman laser (100x objective) vs. laser pointer (20x objective); figure 91

| Light source | Laser power [%] | Entrance slit [μm] | Confocal hole [μm] | Acquisition time [s] | Number of accumulations |
|---------------|-----------------|---------------------------------|---------------------------------|----------------------|-------------------------|
| Laser pointer | 100 | 1000 | 1000 | 30 | 12 |
| Laser | 50 | 150 | 300 | 3 | 60 |

Spores: 100x objective; spectrograph at 2100 cm^{-1} (figure 92)

| Laser | Laser power [%] | Entrance slit [μm] | Confocal hole [μm] | Acquisition time [s] | Number of accumulations |
|-------|-----------------|---------------------------------|---------------------------------|----------------------|-------------------------|
| 633 | Varied | 1000 | 1000 | 2 | 10 |

Glass: 532 vs 785 nm laser (figure 94)

| Laser | Laser power [%] | Entrance slit [μm] | Confocal hole [μm] | Acquisition time [s] | Number of accumulations |
|-------|-----------------|---------------------------------|---------------------------------|----------------------|-------------------------|
| 785 | 100 | 100 | 1000 | 5 | 1 |
| 532 | 100 | 500 | 600 | 2 | 60 |

Spores: Thermo Scientific vs. Renishaw (figure 96)

| Laser | Laser power [%] | Objective | Grating [lines/mm] | Acquisition time [s] | Number of accumulations |
|-------|-----------------|-----------|--------------------|----------------------|-------------------------|
| 780 | 9.0 mW | 100x | 400 | 2 | 20 |
| 785 | 0.1 % | 50x | 1200 | 10 | 12 |

SERS single spectrum (entrance slit and confocal hole: 1000 μm ; figure 99)

| Laser | Laser power [%] | Objective | Grating [lines/mm] | Acquisition time [s] | Number of accumulations |
|-------|-----------------|-----------|--------------------|----------------------|-------------------------|
| 532 | 0.01 | 100 | 300 | 5 | 10 |

SERS mapping of a spore: 0.7 μm step size in x- and y-direction (entrance slit and confocal hole: 1000 μm ; figure 100, figure 101)

| Laser | Laser power [%] | Objective | Grating [lines/mm] | Acquisition time [s] | Number of accumulations |
|-------|-----------------|-----------|--------------------|----------------------|-------------------------|
| 532 | 0.01 | 100 | 300 | 2 | 20 |

3d plot method A,B,C (entrance slit and confocal hole: 1000 μm , figure 102- figure 104)

| Laser | Laser power [%] | Objective | Grating [lines/mm] | Acquisition time [s] | Number of accumulations |
|-------|-----------------|-----------|--------------------|----------------------|-------------------------|
| 532 | 0.01 | 100 | 300 | 5 | 10 |

Baseline correction of time dependant SERS spectra (figure 105)

| # of pivot | Wavenumber [cm^{-1}] |
|------------|---------------------------------|
| 1 | 310.6 |
| 2 | 595.4 |
| 3 | 753.3 |
| 4 | 896.2 |
| 5 | 1065.8 |
| 6 | 1829.2 |
| 7 | 2081.4 |
| 8 | 2302.8 |
| 9 | 2524.1 |
| 10 | 2745.5 |
| 11 | 3188.2 |
| 12 | 3409.5 |

IX. Appendix - IX.1. Device settings

SERS average dead alive (entrance slit: 500 μm , confocal hole: 600 μm ; figure 106, figure 107)

| Laser | Laser power [%] | Objective | Grating [lines/mm] | Acquisition time [s] | Number of accumulations |
|-------|-----------------|-----------|--------------------|----------------------|-------------------------|
| 532 | 0.01 | 100 | 300 | 5 | 10 |

SERS substrate on glass slide (entrance slit and confocal hole: 1000 μm , figure 108)

| Laser | Laser power [%] | Objective | Grating [lines/mm] | Acquisition time [s] | Number of accumulations |
|-------|-----------------|-----------|--------------------|----------------------|-------------------------|
| 532 | 0.01 | 100 | 300 | 10 | 10 |










Baseline correction of spore spectra dead/alive with 785 nm laser (CTR Villach; figure 109)

| # of pivot | Wavenumber [cm^{-1}] |
|------------|---------------------------------|
| 1 | 838.6 |
| 2 | 914.6 |
| 3 | 1066.5 |
| 4 | 1124.3 |
| 5 | 1256.6 |
| 6 | 1497.5 |
| 7 | 1522.4 |
| 8 | 1674.3 |
| 9 | 1750.3 |
| 10 | 1902.3 |

Spore spectra dead/alive (CTR Villach; figure 109)

| Laser | Laser power [%] | Objective | Grating [lines/mm] | Acquisition time [s] | Number of accumulations |
|-------|-----------------|-----------|--------------------|----------------------|-------------------------|
| 785 | 0.1 | 50x | 1200 | 10 | 6 |

Dead/alive study: spectral descriptors for PCA (figure 112)

| Descriptor type | Integration range |
|-----------------------------------------------------------------------------------|-------------------|
|  | 1176-1145 |
|  | 1247-1172 |
|  | 1361-1304 |
|  | 1499-1417 |
|  | 1615-1569 |
|  | 1637-1611 |
|  | 1394-1358 |
|  | 1253-1134 |
|  | 1662-1552 |

IX.3. Bibliography

1. C. V. Raman, K. S. K. A New Type of Secondary Radiation. *Nature* **121**, 501–502 (1928).
2. Huang, W. E., Li, M., Jarvis, R. M., Goodacre, R. & Banwart, S. a. *Shining light on the microbial world the application of Raman microspectroscopy*. *Adv. Appl. Microbiol.* **70**, 153–86 (Elsevier Inc., 2010).
3. Dietzek, B., Cialla, D., Schmitt, M. & Popp, J. in *Confocal Raman Microsc.* (Dieing, T., Hollricher, O. & Toporski, J.) 21–37 (Springer-Verlag, 2010).
4. Dieing, T., Hollricher, O. & Toporski, J. *Confocal Raman Microscopy*. (Springer-Verlag Berlin Heidelberg, 2010).
5. Wilson, T., To, P., Science, E., Road, P. & Ox, O. The effect of detector size on the signal-to-noise ratio in confocal polarized light microscopy. **189**, 12–14 (1998).
6. Nie, S. Probing Single Molecules and Single Nanoparticles by Surface-Enhanced Raman Scattering. *Science (80-.)*. **275**, 1102–1106 (1997).
7. Lee, C. & Meisel, D. Adsorption and Surface-Enhanced Raman of Dyes on Silver and Gold Sols'. *Phys. Chem.* **60439**, 3391–3395 (1982).
8. Leopold, N. & Lendl, B. A New Method for Fast Preparation of Highly Surface-Enhanced Raman Scattering (SERS) Active Silver Colloids at Room Temperature by Reduction of Silver Nitrate with Hydroxylamine Hydrochloride. *J. Phys. Chem. B* **107**, 5723–5727 (2003).
9. Schlücker, S. Surface-enhanced Raman spectroscopy: concepts and chemical applications. *Angew. Chem. Int. Ed. Engl.* **53**, 4756–95 (2014).
10. Rivera, V. A. G., Ferri, F. A. & Jr, E. M. Localized Surface Plasmon Resonances : Noble Metal Nanoparticle Interaction with Rare-Earth Ions. (2012).
11. *Surface Enhanced Raman Spectroscopy*. (WILEY-VCH, 2011).
12. Valley, N., Greeneltch, N., Van Duyne, R. P. & Schatz, G. C. A Look at the Origin and Magnitude of the Chemical Contribution to the Enhancement Mechanism of Surface-Enhanced Raman Spectroscopy (SERS): Theory and Experiment. *J. Phys. Chem. Lett.* **4**, 2599–2604 (2013).

13. Krause, M., Rösch, P., Radt, B. & Popp, J. Localizing and identifying living bacteria in an abiotic environment by a combination of Raman and fluorescence microscopy. *Anal. Chem.* **80**, 8568–75 (2008).
14. *The Molecular Probes® Handbook*. (Life Technologies Corporation, 2010).
15. Vitecek, J. *et al.* A Fluorimetric Sensor for Detection of One Living Cell. *Sensors* **7**, 222–238 (2007).
16. Life Technologies FDA Ex/Em. at http://www.lifetechnologies.com/content/dam/LifeTech/Documents/spectra/images/2761old_2.jpg
17. Life Technologies PI. at <http://www.lifetechnologies.com/content/dam/LifeTech/Documents/chemstructures/images/919.jpg>
18. Life Technologies PI Ex/Em. at <http://www.lifetechnologies.com/content/dam/LifeTech/Documents/spectra/images/1304dna.jpg>
19. Life Technologies DAPI Ex/Em. at <http://www.lifetechnologies.com/order/catalog/product/D3571>
20. Life Technologies DAPI. at <http://www.lifetechnologies.com/content/dam/LifeTech/Documents/chemstructures/images/1701>
21. Ulrich Kück, Minou Nowrousian, Birgit Hoff, I. E. *Schimmelpilze*. (2009).
22. Botany P. chrysogenum. at http://botit.botany.wisc.edu/toms_fungi/nov2003.html
23. Fleming, A. On the antibacterial action of cultures of a *Penicillium*, with special reference to their use in the isolation of *B. influenza*. *Br. J. Exp. Pathol.* **10**, (1929).
24. Houbraken, J., Frisvad, J. C. & Samson, R. a. Fleming’s penicillin producing strain is not *Penicillium chrysogenum* but *P. rubens*. *IMA Fungus* **2**, 87–95 (2011).
25. Böhm, J. *et al.* Sexual reproduction and mating-type – mediated strain development in the penicillin-producing fungus *Penicillium chrysogenum*. (2012). doi:10.1073/pnas.1217943110/-/DCSupplemental.www.pnas.org/cgi/doi/10.1073/pnas.1217943110
26. Rizza, V. & Kornfeld, J. M. Components of Conidial and Hyphal Walls of *Penicillium chrysogenum*. 307–315 (1969).

27. Lohninger, H. *Fundamentals of Statistics*. (Epina GmbH, 2012). at <www.epina.at>
28. Cytospec multivar. at <http://www.cytospec.com/multivar.php>
29. Lee, E. in *Raman Imaging* (Zoubir, A.) 10–13 (Springer-Verlag, 2012).
30. Olympus. at <http://www.olympus-ims.com/de/microscope/mpln/>
31. Lohninger, H. ImageLab. (2014). at <www.epina.at>
32. Hamasha, K. Raman Spectroscopy for the Microbiological Characterization and Identification of Medically Relevant Bacteria. (2011).
33. Schuster, K. C., Reese, I., Urlaub, E., Gapes, J. R. & Lendl, B. Multidimensional information on the chemical composition of single bacterial cells by confocal Raman microspectroscopy. *Anal. Chem.* **72**, 5529–34 (2000).
34. Petry, R., Schmitt, M. & Popp, J. Raman spectroscopy--a prospective tool in the life sciences. *Chemphyschem* **4**, 14–30 (2003).
35. Maquelin, K. *et al.* Raman spectroscopic method for identification of clinically relevant microorganisms growing on solid culture medium. *Anal. Chem.* **72**, 12–9 (2000).
36. Ro, P. *et al.* Chemotaxonomic Identification of Single Bacteria by Micro-Raman Spectroscopy : Application to Clean-Room-Relevant Biological Contaminations. **71**, 1626–1637 (2005).
37. Isenor, M., Kaminskyj, S. G. W., Rodriguez, R. J., Redman, R. S. & Gough, K. M. Characterization of mannitol in *Curvularia protuberata* hyphae by FTIR and Raman spectromicroscopy. *Analyst* **135**, 3249–54 (2010).
38. Walter, A. *et al.* Analysis of the cytochrome distribution via linear and nonlinear Raman spectroscopy. *Analyst* **135**, 908–17 (2010).
39. Do, H. *et al.* Ectomycorrhizas from a Lower Eocene angiosperm. 988–996 (2011).
40. Clarke, S. J., Littleford, R. E., Smith, W. E. & Goodacre, R. Rapid monitoring of antibiotics using Raman and surface enhanced Raman spectroscopy. *Analyst* **130**, 1019–26 (2005).
41. Wang, R. *et al.* Raman spectral study of silicon nanowires: High-order scattering and phonon confinement effects. *Phys. Rev. B* **61**, 16827–16832 (2000).
42. Bauer, M. Raman spectroscopy of laser induced material alterations. (2010).

43. Scattering, R. Raman Scattering by Silicon and Germanium. **155**, (1966).
44. Zhang, Y.-H. & Chan, C. K. Understanding the Hygroscopic Properties of Supersaturated Droplets of Metal and Ammonium Sulfate Solutions Using Raman Spectroscopy. *J. Phys. Chem. A* **106**, 285–292 (2002).
45. Wang, L., Roitberg, a, Meuse, C. & Gaigalas, a K. Raman and FTIR spectroscopies of fluorescein in solutions. *Spectrochim. Acta. A. Mol. Biomol. Spectrosc.* **57**, 1781–91 (2001).
46. Ghosal, S., Macher, J. M. & Ahmed, K. Raman Microspectroscopy-Based Identification of Individual Fungal Spores as Potential Indicators of Indoor Contamination and Moisture-Related Building Damage. (2012).
47. De Gussem, K., Vandenabeele, P., Verbeken, A. & Moens, L. Raman spectroscopic study of Lactarius spores (Russulales, Fungi). *Spectrochim. Acta. A. Mol. Biomol. Spectrosc.* **61**, 2896–908 (2005).
48. Mohacek-Grosev, V., Bozac, R. & Puppels, G. J. Vibrational spectroscopic characterization of wild growing mushrooms and toadstools. *Spectrochim. Acta. A. Mol. Biomol. Spectrosc.* **57**, 2815–29 (2001).
49. Kong, L., Zhang, P., Yu, J., Setlow, P. & Li, Y. Rapid confocal Raman imaging using a synchro multifoci-scan scheme for dynamic monitoring of single living cells. *Appl. Phys. Lett.* **98**, 213703 (2011).
50. Albertorio, F., Chapa, V. A., Chen, X., Diaz, A. J. & Cremer, P. S. The α , α - (1 \rightarrow 1) Linkage of Trehalose Is Key to Anhydrobiotic Preservation. *Langmuir* 10567–10574 (2007).
51. Cañamares, M. V, Garcia-Ramos, J. V, Gómez-Varga, J. D., Domingo, C. & Sanchez-Cortes, S. Comparative study of the morphology, aggregation, adherence to glass, and surface-enhanced Raman scattering activity of silver nanoparticles prepared by chemical reduction of Ag⁺ using citrate and hydroxylamine. *Langmuir* **21**, 8546–53 (2005).
52. Huang, H. *et al.* Silver nanoparticle based surface enhanced Raman scattering spectroscopy of diabetic and normal rat pancreatic tissue under near-infrared laser excitation. *Laser Phys. Lett.* **10**, 045603 (2013).
53. Su, Q., Ma, X., Dong, J., Jiang, C. & Qian, W. A reproducible SERS substrate based on electrostatically assisted APTES-functionalized surface-assembly of gold nanostars. *ACS Appl. Mater. Interfaces* **3**, 1873–9 (2011).

54. Fan, M., Andrade, G. F. S. & Brolo, A. G. A review on the fabrication of substrates for surface enhanced Raman spectroscopy and their applications in analytical chemistry. *Anal. Chim. Acta* **693**, 7–25 (2011).
55. Chao, Y. & Zhang, T. Surface-enhanced Raman scattering (SERS) revealing chemical variation during biofilm formation: from initial attachment to mature biofilm. *Anal. Bioanal. Chem.* **404**, 1465–75 (2012).
56. Szeghalmi, A., Kaminskyj, S., Rösch, P., Popp, J. & Gough, K. M. Time fluctuations and imaging in the SERS spectra of fungal hypha grown on nanostructured substrates. *J. Phys. Chem. B* **111**, 12916–24 (2007).
57. Balasubrahmanyam, K. Raman Spectra and Structure of Solid AgNO₃ and TlNO₃ at High Temperatures. *J. Chem. Phys.* **57**, 4084 (1972).
58. Martina, I., Wiesinger, R. & Schreiner, M. MICRO-RAMAN CHARACTERISATION OF SILVER CORROSION PRODUCTS : INSTRUMENTAL SET UP AND REFERENCE. 1–8 (2012).
59. Hyun, M. W., Yun, Y. H., Kim, J. Y. & Kim, S. H. Fungal and Plant Phenylalanine Ammonia-lyase. *Mycobiology* **39**, 257–65 (2011).
60. Veiga, T. *et al.* Resolving phenylalanine metabolism sheds light on natural synthesis of penicillin G in *Penicillium chrysogenum*. *Eukaryot. Cell* **11**, 238–49 (2012).
61. Gelder, J. De, Gussem, K. De, Vandenabeele, P. & Moens, L. Reference database of Raman spectra of biological molecules. 1133–1147 (2007). doi:10.1002/jrs
62. Zhang, X. & Tauler, R. Application of multivariate curve resolution alternating least squares (MCR-ALS) to remote sensing hyperspectral imaging. *Anal. Chim. Acta* **762**, 25–38 (2013).
63. Genome pathway *P. chrysogenum*. at <http://www.genome.jp/kegg-bin/show_pathway?pcs00360>

IX.4. List of Figures

| | |
|---------------------------------------------------------------------------------------------------------------------------------------------------------------------------------------------------------------------------------------------------------------------------------|----|
| figure 1. Energy and intensity sketch of Rayleigh scattering, Raman (Stokes and anti-Stokes) scattering and fluorescence | 17 |
| figure 2. Optical path of a confocal Raman spectroscopy set-up (Bernd Bleistein, Jobin Yvon) | 18 |
| figure 3. SERS principle: additional signal enhancement in the hotspots between two nanoparticles..... | 20 |
| figure 4. Induced dipole of a metal nanoparticle (Au) by excitation of a dipolar localized surface plasmon resonance (LSPR) ⁹ | 21 |
| figure 5. Electrochemical enhancement of both fields: incident field ω_{inc} and outgoing field ($\omega_{inc} - \omega_{vib}$); pyridine as example molecule ⁹ | 21 |
| figure 6. Real and imaginary part of $\epsilon(\lambda)$ of Ag and Au ¹¹ | 23 |
| figure 7. Effect of a decreasing gap between two nanoparticles on the plasmon resonance and the enhancement factor ¹¹ | 24 |
| figure 8. Intensity distribution of the enhancement factor (a) and LIEF as a function of θ (b) ¹¹ | 24 |
| figure 9. Hydrolization of FDA to fluorescein in the presence of esterases ¹⁵ | 27 |
| figure 10. FDA dissolved in acetone on CaF ₂ | 28 |
| figure 11. Raman spectrum of FDA recorded with the 532 nm laser (blue spectrum) and the 633 nm laser (green, red and black spectrum, each recorded at a different spectrograph position: (i) 1500 cm ⁻¹ (ii) 2000 cm ⁻¹ (iii) 2500 cm ⁻¹ | 28 |
| figure 12. Excitation/Emission spectrum of FDA ¹⁶ | 28 |
| figure 13. Chemical structure of PI ¹⁷ | 29 |
| figure 14. Excitation/Emission spectrum of PI ¹⁸ | 29 |
| figure 15. PI (2 mM) dissolved in PBS buffer..... | 29 |
| figure 16. Raman spectrum of PI recorded with the 780 nm Raman laser..... | 29 |
| figure 17. Excitation/Emission spectrum of DAPI bound to DNA ¹⁹ | 30 |
| figure 18. Chemical structure of 4',6-diamidino-2-phenylindole (DAPI) ²⁰ | 30 |
| figure 19. DAPI dried on CaF ₂ | 30 |
| figure 20. Raman spectra of DAPI recorded with the 532 nm laser and the 633 nm- laser (spectrograph position: (i) 1500 cm ⁻¹ (ii) 2000 cm ⁻¹ (iii) 2500 cm ⁻¹ | 31 |
| figure 21. Raman spectra of DAPI with the 633 nm laser at three different spectrograph positions: (i) 1500 cm ⁻¹ (ii) 2000 cm ⁻¹ (iii) 2500 cm ⁻¹ | 31 |
| figure 22. Sketch showing the principle of PCA..... | 34 |
| figure 23. Correlation between set and measured laser power (532 nm- laser)..... | 37 |
| figure 24. Transmittance curves of Olympus objectives (left: 10x; middle: 50x, right: 100x magnification) ³⁰ | 38 |

| | |
|------------------------------------------------------------------------------------------------------------------------------------------------------------------------------------------------------------------------------------------------|----|
| figure 25. Actual laser power on the sample surface using the 10x, 50x and 100x objective (Olympus) with $\lambda=532$ nm..... | 39 |
| figure 26. Fungal hyphae on microscope slide recorded with 20x magnification (left) and 100x magnification (right)..... | 42 |
| figure 27. Raman spectra of <i>P. chrysogenum</i> recorded with 532 nm and 633 nm excitation wavelength..... | 43 |
| figure 28. Single spectra of hyphae of <i>P. chrysogenum</i> generated with 50 % laser power using different objectives (device settings see appendix)..... | 44 |
| figure 29. Picture of the sample before (A) and after (B) the measurement with 100 % laser power (device settings see appendix)..... | 45 |
| figure 30. Raman spectrum of a hypha of <i>P. chrysogenum</i> (device settings see appendix)..... | 45 |
| figure 31. Sketch of a hyperspectral data cube..... | 47 |
| figure 32. Spectra of fungal parts burned by the laser beam which were excluded as bad pixels and replaced by averaged neighboring spectra, and spectrum of a fungal hypha for comparison (Spectra 0-7 represent carbonized sample parts)..... | 48 |
| figure 33. Raman spectrum recorded in the middle of a hypha of <i>Penicillium chrysogenum</i> (blue), next to the hypha (green) and at the edge of the hypha (red); measurement position see figure 34 (left)..... | 48 |
| figure 34. Picture of the sample (left) and overlay with the intensity map based on the intensity of the CH stretch vibration (right)..... | 49 |
| figure 35. Intensity map of the amide I band at 1656 cm^{-1} (left) and the band at 2933 cm^{-1} evoked by CH stretch vibrations (right); maximum intensity value of each wavelength as set to 100..... | 50 |
| figure 36. Overlay of cluster image and sample image (left); average spectra of each cluster (right)..... | 51 |
| figure 37. Dendrogram of HCA with three clusters..... | 51 |
| figure 38. Dendrogram of HCA showing further subdivisions of one component..... | 51 |
| figure 39. Overlay of cluster image (subdivision of cluster with highest protein content) and sample image (left); average spectra of the three subdivision of the hypha-cluster (right)..... | 52 |
| figure 40. Dendrogram and overlay of cluster image and sample image of the second HCA covering the spectral region from 400 cm^{-1} to 1900 cm^{-1} | 53 |
| figure 41. Average spectra of each cluster from the second HCA (cluster image see figure 40); double bands with changing intensity ratio are marked in grey..... | 53 |
| figure 42. Intensity ratios of three double bands of the average spectra from the first to the third cluster..... | 54 |
| figure 43. Bi-plot of first PCA..... | 55 |

| | |
|-------------------------------------------------------------------------------------------------------------------------------------------------------------------------------------------|----|
| figure 44. Score plot of the first PCA: standardized data (1 st plot) and mean centered data (2 nd plot); Score plot of the second PCA (3 rd plot) | 56 |
| figure 45. Bi-plot of second PCA..... | 56 |
| figure 46. Score plot PC1 vs PC2..... | 57 |
| figure 47. 300x300 μm^2 sample image with the mapping area (1052x124 μm^2 ; intensity map of CH str. vibration) | 58 |
| figure 48. Comparison of the Raman spectra evoked by hyphae (red) and glass background (green)..... | 59 |
| figure 49. Intensity map of the CH stretch vibration (left) and the amid I band (right)..... | 59 |
| figure 50. Overlay of intensity map and sample image (left) of the CH str. vibration (right).. | 60 |
| figure 51. Overlay of intensity map and sample image (left) of the Amide I band (right)..... | 60 |
| figure 52. Overlay of intensity map and sample image (left) of lipids (right)..... | 61 |
| figure 53. Overlay of intensity map and sample image (left) of the band mainly evoked by purine bases (right)..... | 61 |
| figure 54. Overlay of cluster image and sample image (left) with the according average spectra and the standard deviation (right)..... | 62 |
| figure 55. Dendrogram of HCA with 3 clusters | 62 |
| figure 56. Dendrogram of HCA showing subdivisions of the sample branch | 62 |
| figure 57. Overlay of cluster image and sample image (left) with the according average spectra and the standard deviation (right)..... | 63 |
| figure 58. Average spectra of HCA: intensity ratios are calculated of bands pairs A and B marked in grey | 63 |
| figure 59. Intensity ratios of three double bands of the average spectra from the first to the third cluster | 64 |
| figure 60. Scree plot..... | 65 |
| figure 61. Bi-plot | 65 |
| figure 62. Scores of PC1 vs PC2..... | 65 |
| figure 63. Score plot of PCA representing the glass background..... | 66 |
| figure 64. Score plot of PCA representing the sample..... | 67 |
| figure 65. Bi-plot of second PCA (mean centered data; spectral descriptor 1,3 and 9 excluded) | 68 |
| figure 66. Score plot of the second PCA (mean centered data; spectra descriptor 1,3 and 9 excluded)..... | 68 |
| figure 67. Raman spectra (left) and sample image (right) of hyphae stained with FDA (device settings see appendix) | 69 |
| figure 68. Comparison of the Raman spectra of FDA stained hyphae, unstained hyphae and FDA (device settings see appendix)..... | 70 |
| figure 69. Raman spectrum of washed FDA stained hyphae (device settings see appendix)..... | 70 |

| | |
|---------------------------------------------------------------------------------------------------------------------------------------------------------------------------------------------------------------------------|----|
| figure 70. Comparison of the Raman spectra of FDA stained and washed hyphae, unstained hyphae and FDA (device settings see appendix) | 71 |
| figure 71. Raman spectra of PI stained and washed hyphae (device settings see appendix) | 72 |
| figure 72. Raman spectra of hyphae stained with FDA, PI and DAPI (device settings see appendix) | 73 |
| figure 73. Raman spectrum (left) and sample image (right) of a stained (FDA, PI and DAPI) and washed hypha (device settings see appendix) | 74 |
| figure 74. Raman spectra of spores of <i>P. chrysogenum</i> (device settings see appendix) | 79 |
| figure 75. Raman spectra recorded without a sample with the room lights switched on and off (device settings see appendix) | 79 |
| figure 76. Measurement position (red cross) before (left) and after (right) the Raman laser (532 nm) hits the sample | 80 |
| figure 77. Spore sample on microscope slide in aqueous environment in the petri dish | 80 |
| figure 78. Raman spectrum of spore sample in aqueous environment (device settings see appendix) | 80 |
| figure 79. Three different measurement spots for collecting Raman spectra of spores on aluminum foil | 81 |
| figure 80. Raman spectra of spores on aluminum foil recorded at three different measurement spots; the set integration times are indicated in the legend on the right (see figure 79; device settings see appendix) | 82 |
| figure 81. Schematic representation of the cryo-stage | 82 |
| figure 82. Photograph of the set-up consisting of the Raman spectrometer (Horiba LabRAM 800HR), the cryo-stage fixed onto the XYZ-stage and the vacuum pump | 83 |
| figure 83. Cryo-stage with the cooled Dewar vessel (left); the laser beam is focused with a 20x objective through a quartz window onto the sample on the gold surface (right) | 84 |
| figure 84. Raman spectra of spores on the cryo-stage with the set integration time in the legend on the right: blue spectrum = 0.1 % laser power, green spectra = 1 % laser power (device settings see appendix) | 84 |
| figure 85. Three different measurement spots (I-III) of the Raman spectra in figure 86 | 85 |
| figure 86. Raman spectra of spores the cryo-stage with the set integration time in the legend on the right (device settings see table 9) | 86 |
| figure 87. Three different measurement spots were investigated to record Raman spectra of spores with smaller magnification (20x) | 87 |
| figure 88. Raman spectra of spores recorded with 20x objective; the integration time is listed up in the legend on the right (device settings see appendix) | 87 |
| figure 89. Measurement with laser pointer (left) and Raman laser (right) | 88 |
| figure 90. Raman spectra of toluene with the green Raman laser and the laser pointer as light source (device settings see appendix) | 89 |

| | |
|--------------------------------------------------------------------------------------------------------------------------------------------------------------------------------------------------------------------------------------------------------------------------------|-----|
| figure 91. Raman spectra of spores (532 nm laser pointer) compared to a Raman spectrum of a hypha (532 nm- laser)..... | 90 |
| figure 92. Raman spectra of spores recorded with the 633 nm Raman laser (device settings see appendix)..... | 91 |
| figure 93. Zoom of figure 92 showing spore spectra recorded with 0.01 % and 0.1 % laser power | 91 |
| figure 94. Raman spectra of glass recorded with the 532 nm Raman laser and the 785 nm Raman laser (device settings see appendix)..... | 92 |
| figure 95. Fluorescence spectrum of a glass slide using 532 nm (blue) and 785 nm (red) as excitation wavelength; green and grey shaded areas indicate the spectral region covered by the recorded Raman shift evoked by 532 nm and 785 nm laser excitation, respectively | 93 |
| figure 96. Spores spectra recorded with an NIR-Raman laser (Thermo Scientific: 780 nm laser; Renishaw: 785 nm laser; device settings see appendix)..... | 93 |
| figure 97. UV/Vis spectrum of silver nanoparticles (1:10 dilution) with maximum at 407 nm.. | 95 |
| figure 98. AFM image of silver nanoparticles (left) and distribution of their equivalent radius (right) | 96 |
| figure 99. SERS spectrum at 532nm excitation of a spore of <i>P. chrysogenum</i> (device settings see appendix)..... | 97 |
| figure 100. Measurement area of SERS mapping of a single spore; images on the left represent different focal planes to show homogenous coverage of the sample with silver nanoparticles..... | 98 |
| figure 101. Overlay of intensity map ($\nu(\text{CH})$ at 2933 cm^{-1}) and sample image..... | 98 |
| figure 102. Time dependant SERS spectra of spore sample prepared with method A (device settings see appendix)..... | 100 |
| figure 103. Time dependant SERS spectra of spore sample prepared with method B (B1 left, B2 right; device settings see appendix) | 100 |
| figure 104. Time dependant SERS spectra of spore sample prepared with method C (C1 left, C2 right; device settings see appendix)..... | 100 |
| figure 105. Changes of normalized intensity of amide III band ('-') and $\omega(\text{CH}_2)$ ('--') over time using three different sample preparation methods (method A, B, C); shift introduced for clarity | 101 |
| figure 106. Average SERS spectrum of living (red) and dead spores (blue) with standard deviation (device settings see appendix)..... | 102 |
| figure 107. Average SERS spectrum of living (red) and dead spores (blue) without standard deviation (device settings see appendix)..... | 103 |
| figure 108. Raman spectrum of SERS substrate on a glass slide (device settings see appendix) | 105 |

| | |
|----------------------------------------------------------------------------------------------------------------------------------------------------------------------------------------------|-----|
| figure 109. Average spectra with according standard deviation of living (red) and dead (blue) spores (device settings see appendix) | 107 |
| figure 110. Score plot with three spectra standing out from the remaining data | 108 |
| figure 111. Average spectra of dead (blue) and living spores (red) in comparison to the three single spectra (“bad pixel”) recorded at the same measurement spot of a dead spore sample..... | 108 |
| figure 112. Score plot showing a clear differentiation between Raman spectra of living and dead spores | 109 |

IX.5. List of Tables

| | |
|--------------------------------------------------------------------------------------------------------------------------------------|-----|
| table 1. Measured average laser power at 10 %, 25 %, 50 % and 100 % laser power set with Labspec 6 software | 36 |
| table 2. Laser spot size of the 532 nm Raman laser using different magnifications | 37 |
| table 3. Transmittance values for the Olympus objectives at 532 nm deduced from figure 24.. | 38 |
| table 4. Power per area [mW/ μm^2] for 10x (measured values), 50x and 100x Olympus objectives with $\lambda=532$ nm..... | 38 |
| table 5. Spatial resolution for different objectives with $\lambda=532$ nm..... | 40 |
| table 6. Device settings for both lasers..... | 43 |
| table 7. Band assignment: Hyphae of <i>P. chrysogenum</i> | 46 |
| table 8. List of spectral descriptors according to their impact on PC2; band assignment according to Huang et al. ² | 55 |
| table 9. Parameter settings for the spectra in figure 86 | 85 |
| table 10. Band assignment of spore spectra according to Huang et al. ² | 94 |
| table 11. Tentative band assignment for the SERS spectrum of a spore of <i>P. chrysogenum</i> | 97 |
| table 12. Tentative band assignment of the SERS spectra of dead and living spores of <i>P. chrysogenum</i> | 104 |
| table 13. Band assignment of the Raman spectra of dead and living spores of <i>P. chrysogenum</i> | 107 |